NTNU

Norwegian University of
Science and Technology

Effects of load histories on reliability analyses based on nonlinear finite element analyses of reinforced concrete structures

Vegard Joten Andersen

Civil and Environmental Engineering
Submission date: December 2017
Supervisor: Max Hendriks, KT
Co-supervisor: Morten Engen, Multiconsult

Norwegian University of Science and Technology
Department of Structural Engineering

Department of Structural Engineering
Faculty of Engineering Science and Technology
NTNU- Norwegian University of Science and Technology

ACCESSIBILITY

MASTER THESIS 2017

SUBJECT AREA:	DATE:	NO. OF PAGES:
Structural Design	30.12.2017	91

TITLE:

Effects of load histories on reliability analysis based on nonlinear finite element analysis of reinforced concrete structures

Påvirkinger av lasthistorier på pålitelighetsanalyser basert på ikke-lineære element analyser av betongkonstruksjoner

BY:

Vegard Joten Andersen

SUMMARY:
The effects of load histories on reliability analysis using nonlinear finite element analysis (NLFEA) of reinforced concrete (RC) structures was studied in this thesis. Using a finite element software, several NLFEA on an undetermined RC frame was performed with various combinations of a vertical and horizontal load. The global failure mode of the frame for all analyses was concrete in bending. Ultimate design capacities was calculated according to three safety format methods, the partial safety factor method (PSFm), the global resistance factor method (GRFm) and the method of estimation of a coefficient of variation of resistance (ECOV).

A solution strategy for NLFEA was developed based on NLFEA guidelines provided by the Rijkswaterstaat Ministry of Infrastructure and the Environment. The solution strategy was verified by comparing NLFEA predictions to predictions from a calibrated NLFEA solution strategy.

Results show that the load histories influenced the estimated design capacities of the safety format methods, and that the initial loading condition was found to be the greatest source of influence. The degree of influence varied between methods, with GRFm being most affected and PSFm the least. Furthermore, initial loading had an inverse influence on the GRFm compared to the influence on ECOV and PSFm.

The results of the thesis represent only a small population and further analyses are necessary to map the effects. Such analyses should include other failure modes, such as shear or punching shear failure.

Key words: Nonlinear finite element analysis, NLFEA, safety format, reinforced concrete, load history, design capacity, structural reliability

RESPONSIBLE TEACHER:

SUPERVISOR(S): Max Hendriks, Morten Engen

CARRIED OUT AT: Department of Structural Engineering

ABSTRACT

The effects of load histories on reliability analysis using nonlinear finite element analysis (NLFEA) of reinforced concrete (RC) structures was studied in this thesis. Using a finite element software, several NLFEA on an undetermined RC frame was performed with various combinations of a vertical and horizontal load. The global failure mode of the frame for all analyses was concrete in bending. Ultimate design capacities was calculated according to three safety format methods, the partial safety factor method (PSFm), the global resistance factor method (GRFm) and the method of estimation of a coefficient of variation of resistance (ECOV).

A solution strategy for NLFEA was developed based on NLFEA guidelines provided by the Rijkswaterstaat Ministry of Infrastructure and the Environment. The solution strategy was verified by comparing NLFEA predictions to predictions from a calibrated NLFEA solution strategy.

Results show that the load histories influenced the estimated design capacities of the safety format methods, and that the initial loading condition was found to be the greatest source of influence. The degree of influence varied between methods, with GRFm being most affected and PSFm the least. Furthermore, initial loading had an inverse influence on the GRFm compared to the influence on ECOV and PSFm.

The results of the thesis represent only a small population and further analyses are necessary to map the effects. Such analyses should include other failure modes, such as shear or punching shear failure.

Key words: Nonlinear finite element analysis, NLFEA, safety format, reinforced concrete, load history, design capacity, structural reliability

Sammendrag

I denne oppgaven ble påvirkningen av lasthistorier på pålitelighets analyser undersøkt ved bruk av ikke-lineære element analyser (NLFEA) på en statisk ubestemt armert betongramme. Det ble brukt programvare for element analyser og lasthistoriene inkluderte ulike kombinasjoner av en horisontal og en vertikal last. Alle analysene av rammen førte til kollaps på grunn av bøyningsbrudd i betong. Dimensjonerende kapasitet ble beregnet ved bruk av tre sikkerhetsformat metoder, partiell sikkerhetsfaktor metoden (PSFm), global motstandsfaktor metoden (GRFm) og metoden ved å estimere en variasjonskoeffisient for motstand (ECOV).

En løsningsstrategi for NLFEA ble utviklet ved hjelp av retningslinjer utgitt av Rijkswaterstaat Ministry of Infrastructure and the Environment. Løsningsstrategien ble verifisert for nøyaktighet ved å sammenligne NLFEA forutsigelser basert på løsningsstrategien mot andre NLFEA forutsigelser som er basert på en kalibrert løsningsstrategi.

Resultater viser at lasthistoriene påvirker den dimensjonerende kapasiteten til sikkerhets metodene, og det er den initielle last tilstanden som påvirker mest. Påvirkningsgraden er noe ulik for de ulike metodene, hvor GRFm er mest påvirket og PSFm er minst påvirket. Videre er påvirkningen på kapasitetene til GRFm på grunn av den initielle last tilstanden omvendt av påvirkningen til ECOV og PSFm.

Resultatene fra denne oppgaven representerer bare et lite utvalg og videre analyser er nødvendig for å kartlegge effekten av lasthistorier på sikkerhetsformatene. Slike analyser bør inkludere andre bruddformer, slik som skjærbrudd eller gjennomlokking.

PREFACE

This MSc thesis is written as the final part of the masters program of Civil and Environmental Engineering at the Norwegian University of Science and Technology, NTNU, in Trondheim. The thesis was written for the Department of Structural Engineering in the period from August to December 2017.

The thesis concern assessment of nonlinear finite element analysis and load histories effects on safety formats used to determine design capacities of reinforced concrete structures. It has provided a great opportunity to increase my understanding of the complexity and challenges of using nonlinear computational methods to accurately and reliably describe the real behaviour of concrete structures.

The thesis supervisor have been Professor Max A. N. Hendriks from NTNU and Delft University of Technology in The Netherlands and co-supervisor PhD Morten Engen at Multiconsult AS. I would like to extend my gratitude and thank you both for your time and sharing your knowledge. I appreciate all the motivating discussions we have had and your guidance through these last few months. I wish you luck with your future endeavors.

I would also like to extend my gratitude to my brother, Kristian J. Andersen, for proofreading and useful support when writing this thesis.

Trondheim, December 2017

Vegard Joten Andersen

Contents

Notations

Acronyms

CDF	Cumulative density function
E.O.H.	Elements over the height
ECOV	Method of estimation of a coefficient of variation of resistance
FE	Finite element
FEA	Finite element analysis
FEM	Finite element method
GRFm	Global resistance factor method
LFEA	Linear finite element analysis
LH	Load history
NLFEA	Nonlinear finite element analysis
PD	Probability distribution
PDF	Probability density function
PSFm	Partial safety factor method
RC	Reinforced concrete
SLS	Serviceability limit state
ULS	Ultimate limit state

Roman upper case letters

$\mathbf{Q}$	Vector of applied loads
$\mathbf{Q}_D$	Vector of dead loads
$\mathbf{Q}_L$	Vector of live loads
$\mathbf{R}$	Vector of plastic resistance
$\mathbf{R}_R$	Vector of plastic resistances
$\mathbf{X}$	Vector of stochastic variables
E_{cd}	Design Young's modulus of concrete
E_{ck}	Characteristic Young's modulus of concrete
$E_{cm,GRF}$	Mean Young's modulus of concrete for GRFm
E_{cm}	Mean Young's modulus of concrete
E_{sd}	Design Young's modulus of reinforcement steel
E_{sk}	Characteristic Young's modulus of reinforcement steel
$E_{sm,GRF}$	Mean Young's modulus of reinforcement steel for GRFm
E_{sm}	Mean Young's modulus of reinforcement steel
F_d	Design load actions
F_H	Horizontal load on frame
F_V	Vertical load on frame
$F_X()$	Cumulative density function of random variable X
$G()$	Generalized limit state function
$G_R()$	Generalized resistance
$G_S()$	Generalized loading
G_{cd}	Design compressive fracture energy of concrete
G_{ck}	Characteristic compressive fracture energy of concrete

$G_{cm,GRF}$	Mean compressive fracture energy of concrete for GRFm
G_{cm}	Mean compressive fracture energy of concrete
G_{fd}	Design tensile fracture energy of concrete
G_{fk}	Characteristic tensile fracture energy of concrete
$G_{fm,GRF}$	Mean tensile fracture energy of concrete for GRFm
G_{fm}	Mean tensile fracture energy of concrete
LFS	Sequential load factor
$P()$	Probability
R	Resistance
R_d	Design resistance
R_i	Loading in load history i
R_K	Characteristic value of resistance
R_m	Mean value of resistance
R_{pi}	Plastic resistance
S	Load effect
V_R	Coefficient of variation of resistance
$W_Q()$	External work function
$W_R()$	Internal work function
F	Factor of safety

Roman lower case letters

$f_R()$	Probability density function of variable R
$f_RS()$	Joint density function
$f_{\mathbf{X}}(\mathbf{x})$	Joint probability density function of variables in $\mathbf{X}$
f_{cd}	Design compressive strength of concrete
f_{ck}	Characteristic concrete compressive strength
$f_{cm,GRF}$	Mean concrete compressive strength for GRFm
f_{cm}	Mean compressive strength of concrete
f_{ctd}	Design tensile strength of concrete
f_{ctk}	Characteristic tensile strength of concrete
$f_{ctm,GRF}$	Mean tensile strength of concret for GRFme
f_{ctm}	Mean tensile strength of concrete
f_{ud}	Design ultimate strength of reinforcement steel
f_{uk}	Characteristic ultimate strength of reinforcement steel
$f_{um,GRF}$	Mean ultimate strength of reinforcement steel for GRFm
f_{um}	Mean ultimate strength of reinforcement steel
f_{yd}	Design reinforcement yield stress
f_{yk}	Characteristic yield stress of reinforcement steel
$f_{ym,GRF}$	Mean yield stress of reinforcement steel for GRFm
f_{ym}	Mean reinforcement yield stress
p_f	Probability of failure

Greek lower case letters

α_R	Sensitivity factor for the resistance
β	Reliability index
γ_c	Partial safety factor for concrete

γ_D	Partial factor of dead load(s)
γ_G	Partial load factor for dead loads
γ_L	Partial factor of live load(s)
γ_M	Material partial factor
γ_m	Material partial factor, model uncertainty not included
γ_Q	Partial load factor for live loads
γ_R	Global safety factor for resistance uncertainty
γ_R^*	Global resistance safety factor
γ_s	Partial safety factor for reinforcement steel
γ_{Rd}	Model uncertainty factor
γ_{Rd}	Partial factor for resistance modeling
γ_{Sd}	Partial factor for load effect modeling
λ	Load factor
ν_G	Coefficient of variation of geometric uncertainty
ν_M	Coefficient of variation of material uncertainty
ν_R	Coefficient of variation of resistance
ν_θ	Coefficient of variance of modelling uncertainty
ϕ	Partial factor for resistance vector
ϕ_i	Partial factor for resistance of limit state i
σ_i	Stress due to load i
σ_{pi}	Permissible stress due to load i
σ_{ui}	Measure of strength of which σ_{pi} is derived
θ_M	Mean value of modelling uncertainty
ε_{ud}	Strain of reinforcement at design ultimate strength
ε_{uk}	Strain of reinforcement at characteristic ultimate strength
$\varepsilon_{um,GRF}$	Strain of reinforcement at mean ultimate strength for GRFm
ε_{um}	Strain of reinforcement at mean ultimate strength

Selected subscripts

d	Design material parameter, capacity, or load
H	Parameter of the horizontal acting load
k	Characteristic material parameter, capacity, or load
m	Mean material parameter, capacity, or load
V	Parameter of the vertical acting load
GRF	For material parameters used in GRFm analysis

1. Introduction

Large concrete structures, e.g. bridges, dams and offshore structures, must be designed to withstand the exposure of a variety of loads. Moreover, the design needs to meet a margin of safety predetermined by building codes and based on the structure's classification and lifespan.

1.1 Background

In engineering practice today, the design and verification of large concrete structures are done be using linear finite element analysis (LFEA) (Brekke et al., 1994). One advantage of LFEA is the ability to utilize the superposition principle which states that the effects of two or more loads can be found by adding the individual effects of each load. Individual load effects may also be scaled up or down in comparison to other loads. The addition of load effects is typically performed using a post processing software which can test for several load combinations using the results from an individual LFEA of each load. In addition, the post-processor may create the reinforcement layout.

1.2 Problem description

In order for a LFEA to be accurate, the material properties in the structure have to be linear as well, however, this is not the case of reinforced concrete (RC). Concrete cracks for even small loads and reinforcement steel yields before material failure which causes nonlinearities at increased loading. This behaviour can not be represented by a LFEA; therefore, LFEA is unsuited for estimating the true behaviour and capacity of RC structures.

An analysis that recognize the nonlinear behaviour of RC should be considered as an alternative to LFEA when designing large complex structures, e.g. a nonlinear finite element analysis (NLFEA). A NLFEA can accurately represent the strain-stress situation in concrete and estimate the true capacity of concrete structures. However, NLFEA is more demanding of the user compared to LFEA due to the large influence modelling have on the results. Consequently, for a NLFEA to be performed, there usually have to be a financial or environmental gain. This may come in the form of reduced material use (and cost) or a more accurate evaluation of remaining service life of existing structures.

There exists some guidelines on performing NLFEA (Hendriks et al., 2017a) and efforts have been put towards creating a stable, robust solution strategy for conducting NLFEA (Engen, 2017; Engen et al., 2014). The common design principle when using LFEA involves a local control of structural members in design sections to ensure safety. Furthermore, material properties are scaled down while loads effects are scaled up using predetermined safety factors to obtain design values. In contrast, global NLFEA obtains the total response of the structure where all members contribute to the capacity.

Due to the nonlinear behaviour of reinforced concrete, the principle of superposition can not be used to evaluate different load combinations when performing NLFEA. Every load combination and load history requires its own analysis which makes the use of a post processor not feasible.

1.3 Aim

The aim of this thesis, through a case study on a complex RC frame, will be to examine the effect of different load histories on the safety formats used in NLFEA. The safety formats to be examined are those given in fib Model Code 2010 (fib, 2013).

1.4 Limitations

There will be no physical experiments performed for this thesis. Furthermore, the aim is to compare existing safety formats, so there will be no attempt to develop a new format which would require both time and experience.

1.5 Method

First, a short literature review is performed to gain knowledge of the safety formats to be examined as well as any guidelines for conducting NLFEA, prioritizing the most recent guidelines.

Next, a finite element (FE) model of a RC frame is modelled based on the frame designed in the master's thesis of Blomfors (2014). A solution strategy for NLFEA is developed based on the guidelines given in Hendriks et al. (2017a) and from strategy choices made by Blomfors (2014). The solution strategy is verified for accuracy by comparing analysis predictions to predictions from Blomfors (2014), and not by comparing against physical experiments as this was performed by Blomfors (2014).

In order to provide a basis on which any conclusions can be made, several new load histories are developed in addition to the two load histories studied in Blomfors (2014). Furthermore, the material properties for concrete and reinforcement steel is recalculated based on guidelines given in Hendriks et al. (2017a). This adjustment provides material properties for NLFEA as recommended in Model Code 2010 (fib, 2013).

Nonlinear analyses are performed on the model frame for every load history and every safety format using a nonlinear finite element software, and the results for global capacity, load-displacement and yielding are presented. These results serve as a basis for examining the effects of load histories on the selected safety formats.

2. Theory

This chapter will provide a theoretical basis for assessment of safety formats in global nonlinear finite element analyses. First, a brief summary of finite element analysis and solution strategy. This is followed by some background on structural reliability, and lastly, the safety formats for NLFEA from Model Code 2010 (fib, 2013) are described.

2.1 Finite element analysis

Finite element analysis (FEA), also called the finite element method (FEM), is a method for numerical solution of field problems (Cook et al., 2002). Some of the advantages of FEA is the applicability to any field problem (e.g. stress analysis and heat transfer), there are also no geometric restrictions, and there are no restrictions to boundary conditions or loading. Furthermore, material properties are not restricted to isotropy and may change from element to element or within the element itself. Consequently, this makes FEM ideal for solving the load effects on complex concrete structures. A real structural problem contains an infinite number of degrees of freedom which would be impossible to represent in a computational model. Instead, in FEM, the problem is discretized into finite elements and connected by nodes, each node containing a finite number of degrees of freedom. FEM solves for the displacements in the nodes and approximates the stresses in the elements. The displacements and stresses satisfies the weak solution of the differential equations; therefore, FEM does not provide an exact solution. However, the approximated solution is accurate enough for engineering purposes.

As mentioned above, the material properties does not have to be isotropic. For an accurate result, material models should be as representing of reality as possible within a reasonable extent. RC has material properties that are very an-isotropic compared to regular construction steel, and a accurate structural model of a steel frame may give inaccurate results if run on a RC frame if the concrete material properties are not sufficiently defined. The following sections will present an overview of LFEA, NLFEA and a strategy for structural modeling.

2.1.1 Linear finite element analysis

A linear finite element analysis is based on the assumptions that the materials have a linear elastic behaviour and that deformations are small as to not create nonlinear loading effects (Hinton, 1992). LFEA is a one-step calculation as material properties, boundary conditions and geometry are assumed to be unchanging with load level. Influences due to boundary conditions and different loads may be scaled and superimposed post analysis, and linear solutions may be obtained with considerable ease and less computational cost when compared to nonlinear solutions (Reddy, 2004). In many instances, assumptions of linearity lead to reasonable idealization of the behaviour of the system; however, in some cases assumption of linearity may result in an unrealistic approximation of the response, and the only option left to ensure an accurate response is a nonlinear analysis (Reddy, 2004).

2.1.2 Nonlinear finite element analysis

A nonlinear finite element analysis is needed to describe the true behaviour of a structure with nonlinear properties. To identify behaviour as nonlinear is only to say what the behaviour is not, precisely not linear (Cook et al., 2002). In structural mechanics the most common nonlinearities are material, contact and geometric nonlinearity. Cracking of concrete is one example of a material nonlinearity. Opening or closing gaps between adjacent structures is easily a contact nonlinearity, and larger deformations of slender structures at increased loading adds to geometrical nonlinearity when it altars the structural resistance. In contrast to LFEA, a nonlinear analysis involves a multi-step calculation where structural stiffness is constantly updated throughout the analysis. Notable features of nonlinear analysis are (Reddy, 2004):

- The principle of superposition does not hold.
- Analysis can be carried out for one "load" case at a time.
- The history of "loading" influences the response.
- The initial state of the system may be important.

2.1.3 Strategy for finite element modeling

This section will present a short summary of the strategy for modeling a structure using finite element analysis. It is based on the guidelines given in Hendriks et al. (2017a) and Engen (2017) and separated into three parts as can be seen in Fig. 2.1.

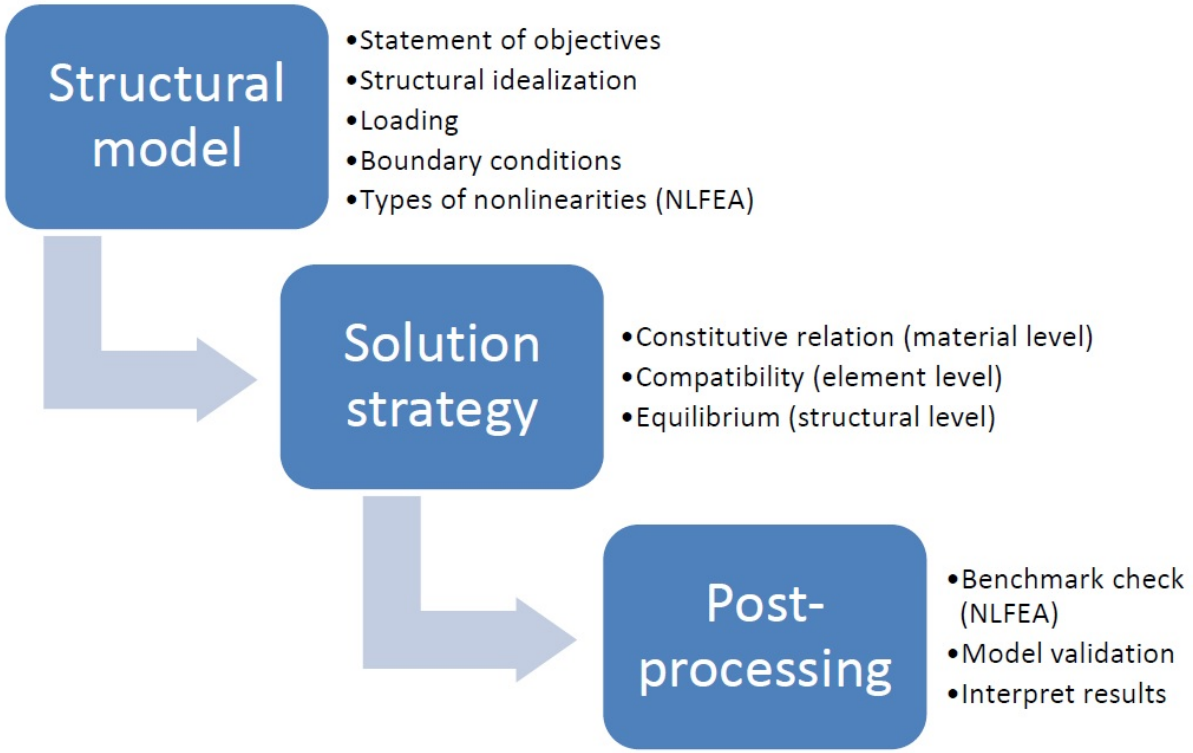

Figure 2.1: Strategy for modelling using NLFEA, by Blomfors (2014).

2.1.3.1 Structural model

The first step is to create a FE-model that can represent the physical structure. Assumptions and simplifications have to be made regarding to which extent and to which detail the structure has to be modelled, how the boundaries of the model are described, which loads on the structure are significant and how they are described (Hendriks et al., 2017a). This includes decisions like what elements to use (i.e. 1-D, 2-D or 3-D elements), or if symmetries in the structure allows for a reduced model to save computation time. However, if the modeller is not careful, simplifications may cause unforeseen failure modes to disappear from the NLFEA.

2.1.3.2 Solution strategy

A solution strategy for NLFEA consists of making choices regarding kinematic compatibility, material models and equilibrium (Engen, 2017), as can be seen in Table 2.1. Material models are often pre-programmed into analysis software which may allow for the combination of several material models and element types. Furthermore, choices of kinematic compatibility, e.g. boundary conditions, may influence the performance of the solution strategy if combined with sensitive material models. For example, a boundary condition that induces artificial tensile forces at a support may lead to reduced compressive strength, and thereby reducing the estimated capacity leading to increased construction expenses due to larger cross sections. Engineers are typically left with two options, either design a solution strategy themselves, or use a NLFEA strategy developed by others that are compatible to the problem at hand, e.g. Hendriks et al. (2017a).

By designing their own strategy, engineers should take care to choose a strategy that does not include too many variables that must be calibrated. This is to ensure the model is not being overfitted to any baseline experiments. The chosen strategy should then be verified against a baseline experiment. It is important to assess if the model works as expected and to assess the sensitivity to variations in model strategy (i.e. changes in mesh size). Next, the model should be validated against similar experiments to the verification, does it predict

Table 2.1: Examples of the content of a solution strategy for NLFEA, from Engen (2017).

Kinematic compatibility	• Finite element types for concrete and reinforcement, including order of numerical integration. • Finite element sizes. • Idealization of geometry. • Idealization of boundary conditions.
Material models	• Material models for concrete and reinforcement. • Material models for possible interfaces and boundary conditions.
Equilibrium	• Iterative methods for the solution of the nonlinear equilibrium equations. • Convergence criteria and suitable tolerances. • Method for determining if the capacity was reached or not.

the real structural behaviour. This is to get a quantifiable measurement of uncertainty. Lastly, the solution strategy should demonstrate applicability on realistic cases similar to the practical problem it is designed for. This is to check if it can capture the expected important phenomena at a level of detail sufficient to be used as a basis for decisions (Engen, 2017).

2.2 Structural probability

This section will provide some background of structural probability and reliability assessment. It begins with a short review of limit state design and continues with the description of basic engineering variables. This is followed by both deterministic and probabilistic measures of limit state violation, and lastly, the handling of uncertainties.

2.2.1 Limit state design

As a structure is subjected to loading, it will respond in terms of deformations and internal stresses. The response is restricted by building codes such as Eurocode 1990 (CEN, 2002) to ensure functionality through the lifespan of the structure. Requirements of the structure are typically governed by the two main limit states, the serviceability and ultimate limit state.

2.2.1.1 Serviceability limit state

The serviceability limit state (SLS) corresponds to the requirements of a structure in service (i.e. expected mean loading). Such requirements include, but are not restricted to (Norwegian Standard, 2016):

- Deformations affecting the structures appearance or the users comfort.
- Vibrations that may cause discomfort for the user.
- Structural damage that may affect the structures overall durability.

Some violations of the SLS may be reversible, for example large deformations, as long as they do not cause permanent damage to the structure. Other violations, like fatigue cracking is typically irreversible but is still covered by SLS.

2.2.1.2 Ultimate limit state

The ultimate limit state (ULS) corresponds to requirements for 1) peoples safety and/or 2) the structural safety (Norwegian Standard, 2016). Typically, damage done to the structure is irreversible; however, sometimes ULS may involve requirements of functionality after exposure to the design loads (i.e. hospitals).

Safety assessment of structures aims at finding the probability of violating the limit states over the course of a structures lifetime. Consequently, building codes are defining requirements for the limit states based on a socially accepted risk of such a violation (e.g. probability of failure). Of course, these risks vary from structure to structure depending on the structures

functional role. In terms of a reliability based approach the structural risk corresponds to a required minimum reliability often referred to as the target reliability (JCSS, 2001).

2.2.2 Basic variables

A model describing the behavior of a structure should contain a specified set of basic variables. These variables may be physical properties such as material strengths, dimensions, loading and environmental influences, as well as model parameters and structural requirements (JCSS, 2001). Many of these are random of nature, so to assess their effect on structures, they need to be modelled as random variables.

It is almost impossible to create an exact model for a basic random variable, instead, the variables are simplified to variables with a suitable probability distribution with a few characteristic parameters, i.e. mean, standard deviation etc. JCSS (2001). Which distribution to assign a variable is often chosen based on experience and on an accumulation of recorded measurements, e.g. concrete compressive strength.

2.2.3 Deterministic measures of limit state violation

Deterministic design control is a simplified check of the reliability of a structure, where random variables are given a determined value based on parameters from their probability distributions. Three deterministic measures are presented below.

2.2.3.1 Factor of safety

Factor of safety, or factor of safety method, is a traditional method to define structural safety and is usually connected to the use of linear elastic analysis. The applied stress, σ_i, due to a load effect, i, is restricted to a permissible stress, σ_{pi} derived from a measure of strength, σ_{ui}, (e.g. ultimate strength) by a factor, F, (Melchers, 1999):

$$\sigma_i \leq \sigma_{pi} \tag{2.1}$$

$$\sigma_{pi} = \frac{\sigma_{ui}}{F} \tag{2.2}$$

The factor F may be chosen based on experimental results, practical experience, and economic and/or political considerations, though it should be noted it is usually selected by a code committee (Melchers, 1999).

The occurring stresses in a structure rarely correspond with the stresses resulting from a linear elastic analysis. This is because of stress redistribution and concentration, size effects, and boundary effects all contributes to discrepancies. In addition, the permissible stresses are usually obtained by scaling down the ultimate strengths from well into the plastic regions. However, the latter is not at much concern provided that Eq. (2.1) is a conservative safety measure (Melchers, 1999).

2.2.3.2 Load factor

The load factor, λ, is a safety factor originally used in plastic theory of structures. It is the theoretical factor of which the loads on a structure need to be multiplied in order to cause structural failure (e.g. collapse) (Melchers, 1999). Load factors are determined for a collapse mode, which need to be pre described. The structure is considered to have collapsed for the given mode when the plastic resistance R_{pi} is related to the factored loads λQ_i by

$$W_R(\mathbf{R}_R) \leq W_Q(\lambda \mathbf{Q}), \tag{2.3}$$

where $\mathbf{R}_R$ is all the plastic resistances, $\mathbf{Q}$ is the vector of all applied loads, $W_R(\,)$ is the internal work function for the given collapse mode, while $W_Q(\,)$ is the external work function for the same collapse mode.

There are similarities between the factor of safety method and the load factor method, specially in formulation, however, the reference levels at which they operate are different. The factor of safety method operate at a 'member level', while the load factor method operate at a 'structure level' (Melchers, 1999).

2.2.3.3 Partial factor

The partial factor approach is a further development of the above mentioned measures. For a limit state i it can be expressed as

$$\phi_i R_i \leq \gamma_{Di} S_{Di} + \gamma_{Li} S_{Li} + ..., \tag{2.4}$$

where R is member resistance, ϕ is the partial factor on R and S_D and S_L are dead and live loads respectively, each with their own associated partial factor λ_D and λ_L (Melchers, 1999). It was developed during the 1960s for use in reinforced concrete codes, and it enabled engineers to better account for uncertainties when designing structures. For example, live loads were able to have greater partial factors compared to dead loads due to the former having a greater uncertainty. Additionally, variation in workmanship and modeling uncertainties could be associated with the structural resistance.

Similar to the load factor method, plastic collapse analysis could then be performed with the expression

$$W_R(\phi \mathbf{R}) \leq W_Q(\gamma_D \mathbf{Q}_D + \gamma_L \mathbf{Q}_L + ...), \tag{2.5}$$

where $\mathbf{R}$ and $\mathbf{Q}$ are vectors of resistance and loads respectively. Note that the partial factors in Eqs. (2.4) and (2.5) will be different as the partial factors of the latter expression has to take into account effects on a structural level.

2.2.4 Probabilistic measure of limit state violation

Probabilistic measurements are important for reliability assessments of structures, as it is not possible to use deterministic values to calculate the probability of failure. This is because deterministic load values are time invariant, thereby, it does not represent the fact that at any time, the actual loading is uncertain. The loading may be described in probabilistic terms by giving it a probability distribution (PD). As a load affects the structure, the load effects, S, (i.e. bending moments) may also be represented by a PD. The same goes for resistance, geometric and workmanship variability (Melchers, 1999).

Similar to the deterministic measures, the limit state will be violated if, at any point in time, the load effect is greater than the resistance, R. For a simplified case, with only one load and one resistance the limit state equation becomes

$$R \leq S \quad \text{or} \quad R - S \leq 0. \tag{2.6}$$

As R and S are probabilistic variables, they have a corresponding probability density function (PDF) $f_R(\,)$ and $f_S(\,)$ respectively. From Melchers (1999), if the variables are independent of each other, the joint density function, $f_{RS}(\,)$, becomes

$$f_{RS}(r,s) = f_R(r) f_S(s), \tag{2.7}$$

and the probability of failure, p_f, becomes

$$p_f = P(R - S \leq 0) = \int_{-\infty}^{\infty} \int_{-\infty}^{s \geq r} f_R(r) f_S(s) \mathrm{d}r \mathrm{d}s. \tag{2.8}$$

Knowing that the cumulative density function, CDF, for a random variable X is given by

$$F_X(x) = P(X \leq x) = \int_{-\infty}^{x} f_X(y) \mathrm{d}y, \tag{2.9}$$

provided that $x \geq y$, and R and S are independent, then the probability of failure can be written in single integral form

$$p_f = P(R - S \leq 0) = \int_{-\infty}^{\infty} F_R(x) f_S(x) \mathrm{d}x, \tag{2.10}$$

where $F_R(x)$ is the probability that $R \leq x$, or simply, that the resistance is less than a value x.

An illustration of the probability density functions for the variables R and S can be seen in Fig. 2.2. The failure density distribution (the contents of the integrand in Eq. (2.10)) is also depicted, with the area under the curve being the probability of failure, p_f.

When load effects and and resistances come from several sources, and some load effects like dead weight correspond to the geometry, thereby the resistance, the expression of structural failure becomes much more complicated. To simplify this, a generalized limit state function, $G(\,)$, is developed. In addition, all variables are placed into one vector, $\mathbf{X}$. Furthermore,

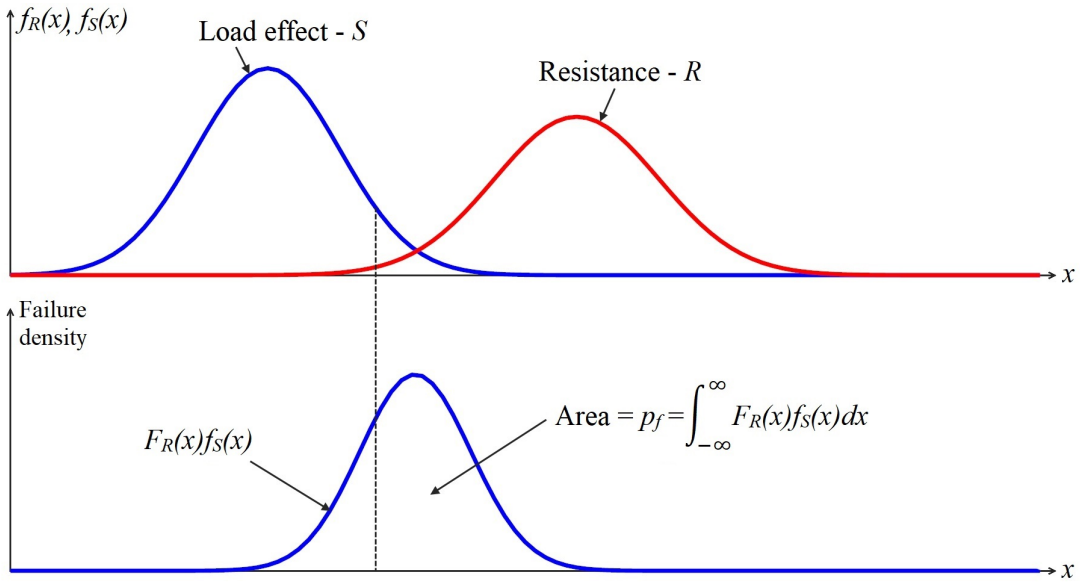

Figure 2.2: Basic $R - S \leq 0$ problem. Representation of probability density functions for resistance, $f_R(\,)$, and load effects, $f_S(\,)$, and the combined failure density. Modified from Melchers (1999).

the resistance and load effects may be generally represented as $R = G_R(\mathbf{X})$ and $S = G_S(\mathbf{X})$ respectively. Other aspects of the generalized limit function may also be represented in a similar fashion. The generalized limit state function can then be written as

$$G(\mathbf{X}) = G(G_R(\mathbf{X}),\, G_S(\mathbf{X}),\, \ldots). \tag{2.11}$$

The generalized function is defined such that $G(\mathbf{X}) > 0$ represents the safe domain, while $G(\mathbf{X}) < 0$ represents the domain of failure. Probability of failure of the generalized limit state function can be written as

$$p_f = P[G(\mathbf{X}) \leq 0] = \int_{G(\mathbf{X})\leq 0} f_{\mathbf{X}}(\mathbf{x})\mathrm{d}\mathbf{x}, \tag{2.12}$$

were $f_{\mathbf{X}}(\mathbf{x})$ is the joint (bivariate) probability density function of variables in $\mathbf{X}$. This probability is often solved by numerical integration (Melchers, 1999).

2.2.5 Uncertainties

Uncertainties with origin from essential sources must be evaluated and included in a basic variable model. The different types of uncertainties can be split into three categories (JCSS, 2001):

- Intrinsic physical or mechanical uncertainty
- Statistical uncertainty, when the design decicions are based on a small sample of observations or when there are other similar conditions
- Model uncertainties

All basic variables, based on the class of the structural problem, should also be given standardized types of probability distributions (JCSS, 2001).

In different model approaches, the uncertainties are often handled separately as this may simplify the design of new structures. Eurocodes, which rely on a semi-probabilistic approach, account for the model uncertainty of the resistance model with a partial factor γ_{Rd} on the resistance side while accounting for model uncertainties for action effect calculations with a factor γ_{Sd} on the loading side. In contrast, a nonlinear analysis is a one-step procedure that utilizes a nonlinear model that includes a global structural analysis. It is able to calculate the loading of a section and the sectional resistance at the same time which is one of the advantages of a one-step approach. However, this makes it difficult to separate the model uncertainties (Schlune, 2011).

2.3 Safety formats for NLFEA

In order to assess if a structure is adequately designed, one shall use a probability-based method to verify that the limit state function is satisfied, and the model describing the limit state function should include all relevant design parameters. This verification is commonly performed by using a safety format that is checking if a structure satisfy a minimum safety level rather than calculating the exact probability of failure. Safety formats recommended by Model Code 2010 (fib, 2013) for using in NLFEA include the:

- Partial factor format
- Global resistance format
- Probabilistic safety format

The probabilistic format is based on numerical simulations with random sampling. It formulates a numerical model and describes the resistance function for a given set of variables. Randomized input together with Monte Carlo-type sampling (i.e. Latin hypercube importance sampling) may give parameters such as mean resistance and standard deviation (fib, 2013). However, due to the random sampling nature of the method, it will not be implemented in this thesis and therefore not explained in further detail.

The general design principle of the formats consider the design condition with separated uncertainties for actions and resistance. The splitting of uncertainties between action and resistance uncertainties may prove itself problematic, or at least inaccurate. The general design principle can be written as

$$F_d \leq R_d \ , \quad R_d = \frac{R_m}{\gamma_R^* \, \gamma_{Rd}}, \tag{2.13}$$

where F_d is the design load actions, R_d is the design resistance, R_m is the mean value of resistance, γ_R^* is the global resistance safety factor, and γ_{Rd} is the model uncertainty factor.

The partial factor format and the global resistance format evaluates R_d in different ways and will be described in greater detail in the following sections.

2.3.1 Partial Safety factor method

The partial factor format consists of the partial safety factor method (PSFm) where the design resistance, R_d, is calculated by the means of a NLFEA by using the design values for input parameters f_d. The new design expression becomes

$$R_d = r(f_d, ...), \tag{2.14}$$

where $r(\,)$ represents the nonlinear analysis model. This analysis is based on extremely low material parameters at all locations in the structure, which does not correspond to the probabilistic concept of simulation. This may cause the structure to fail in a failure mode that deviates from the real behaviour. However, case studies show that the PSFm is practically applicable and can be used as a safe estimate when other methods are unavailable (fib, 2013).

The model uncertainty factor,γ_{Rd}, is not included in Eq. (2.14). Instead, the model uncertainty is included in the partial safety factors of materials, $\gamma_M = \gamma_m \cdot \gamma_{Rd}$, and should not be included a second time.

2.3.2 Global resistance methods

Model Code 2010 (fib, 2013) includes two methods for the global resistance format using NLFEA. Both methods include a simplified probabilistic approach for dealing with uncertainties.

2.3.2.1 Global resistance factor method

The global resistance factor method (GRFm) utilizes the mean material parameters while accounting for the different uncertainties of steel and concrete. The design resistance is calculated from

$$R_d = \frac{r(f_m, ...)}{\gamma_R \, \gamma_{Rd}}, \tag{2.15}$$

where function $r(\,)$ represents the nonlinear analysis with mean input material parameters. The global safety factors for resistance and model uncertainty γ_R and γ_{Rd} shall be set to the values 1.2 and 1.06 respectively (fib, 2013). The mean values to be used in the GRFm is found by

$$f_{ym,GRF} = 1.1 f_{yk}, \tag{2.16}$$

where $f_{ym,GRF}$ is the mean yield stress of steel for GRFm and f_{yk} is the characteristic yield stress of steel, and by

$$f_{cm,GRF} = 1.1 f_{ck} \frac{\gamma_s}{\gamma_c}, \tag{2.17}$$

where $f_{cm,GRF}$ is the reduced value of the concrete compressive strength for GRFm accounting for a reduction due to concrete uncertainty. f_{ck} is the characteristic concrete compressive strength. Eq. (2.17) can be simplified by inserting the values of the partial factor for reinforcement steel, $\gamma_s = 1.15$, and for concrete, $\gamma_c = 1.5$, resulting in

$$f_{cm,GRF} = 0.85 f_{ck}. \tag{2.18}$$

Mean values of the remaining material parameters are calculated from these two mean values using a set of equations for which a summary may be found in Annex A of Hendriks et al. (2017a).

2.3.2.2 Method of estimation of a coefficient of variation of resistance

Model Code 2010 states that the method of estimation of a coefficient of variation of resistance (ECOV) is based on probabilistic studies that have shown that the random distribution of resistance of reinforced concrete structures can be described by a two-parameter lognormal distribution. The two parameters are mean resistance, R_m, and coefficient of variation of resistance, V_R; in addition, the lower bound is set at origin (fib, 2013). It is further proposed that the coefficient of variation may be calculated from a approximated relation between the estimated mean and characteristic resistance, R_m and R_k respectively. Mean and characteristic resistance is estimated using mean and characteristic material parameters, and the coefficient is estimated by

$$V_R = \frac{1}{1.65} \ln\left(\frac{R_m}{R_k}\right). \tag{2.19}$$

Model Code 2010 further propose the global resistance factor γ_R to be determined from

$$\gamma_R = e^{\alpha_R \beta V_R}, \tag{2.20}$$

where α_R is a sensitivity factor for the resistance and β is a reliability index with respective values of 0.8 and 3.8 which corresponds to a probability of failure $p_f = 10^{-3}$. The design resistance is then calculated from

$$R_d = \frac{R_m}{\gamma_{Rd}\, \gamma_R}. \tag{2.21}$$

In the equation above, γ_{Rd} is the model uncertainty factor which needs to be included in the design value expression. However, Model Code 2010 does not provide a specific value to be used, but recommends the value 1.06 to be used for models based on a refined numerical analysis (i.e. NLFEA) with low mesh sensitivity.

Engen et al. (2017) describes an alternative way to treat the different uncertainties. They argue that geometrical and model uncertainties should be interpreted as uncertainties that propagate through the structure and influences the structural resistance. They propose a design resistance

$$R_d = \frac{R_m}{\gamma_R}, \tag{2.22}$$

where γ_R is a factor taking into account the uncertainties due to material, geometry and modelling. γ_R is to be calculated from

$$\gamma_R = \frac{1}{\theta_m} e^{\alpha_R \beta v_R}, \tag{2.23}$$

where

$$v_R = \sqrt{v_M^2 + v_G^2 + v_\theta^2}. \tag{2.24}$$

Here, α_R and β have the respective values 0.8 and 3.8 which coinsides with Model Code 2010. v_R is the new coefficient of variation of the resistance, and it is comprised of the coefficient of variation of material, geometry and modelling uncertainty v_M, v_G and v_θ respectively. Furthermore, θ_m is the mean value of modelling uncertainty which may be determined from calibration analyses. According to Pimentel et al. (2014), $v_G = 0.05$ is a reasonable assumption for large structures that are insensitive to 2nd order effects. v_M is estimated by substituting V_R in Eq. (2.19).

3. Case Study - results and comparison

This chapter presents the case study performed in order to compare the different safety format methods. First, a short description of the Blomfors (2014) case study will be provided. Second, information about the design of the frame and modelling considerations in DIANA will be given. This is followed by a validation of the solution strategy used in this thesis against the strategy of Blomfors (2014). Next, the additional load cases used in analyses are presented, and an update of the material parameters is performed. This is followed by a short study on the mesh sensitivity. In the end, the structural behaviour are given for all load history analyses that implement the updated material parameters, together with a summary of reinforcement yield and the estimated design capacities for the safety format methods.

3.1 Case study of Blomfors (2014)

The case study by Blomfors (2014) involved creating a solution strategy, setting up a FE model in accordance with Fig. 2.1 and do a benchmark analysis of a physical experiment to verify the model. The benchmark test was performed on the experiment by (Seraj et al., 1995), in which an indeterminate portal frame is loaded by a vertical and horizontal load until failure.

Blomfors (2014) used the FE-software DIANA v.9.4.4 developed by DIANA FEA (2014). The coarse element mesh consisted of 20-noded 3D quadratic hexahedron elements (CHX60, DIANA FEA (2017b)), 3 elements over the height (E.O.H.) of the cross sections and 2 over the thickness. The nodes at the frame foundation was modelled as fixed for all translation, and nodes located at the center of the frame was fixed against translation normal to the frame's major directions to reduce the possibility of spurious deformations. Furthermore, the load increment for each load step was set to 5% of the total increment for each load sequence.

Blomfors' solution strategy and analysis resulted in an ultimate capacity equal to 96% of the measured experimental capacity and load-displacement curves as seen in Fig. 3.1 (for more results, see Blomfors (2014)). Material models was chosen according to guidelines provided by the Dutch ministry of infrastructure, Rijkswaterstaat (2012). A total overview of Blomfors' solution strategy can be seen in Tables 3.5 - 3.7 in Blomfors (2014).

The final part in Blomfors (2014) case study was to design a similar frame using LFEA and partial factors according to Eurocode 2 (CEN, 2004), and run nonlinear analyses to determine the probability of failure of the designed frame using the developed solution strategy.

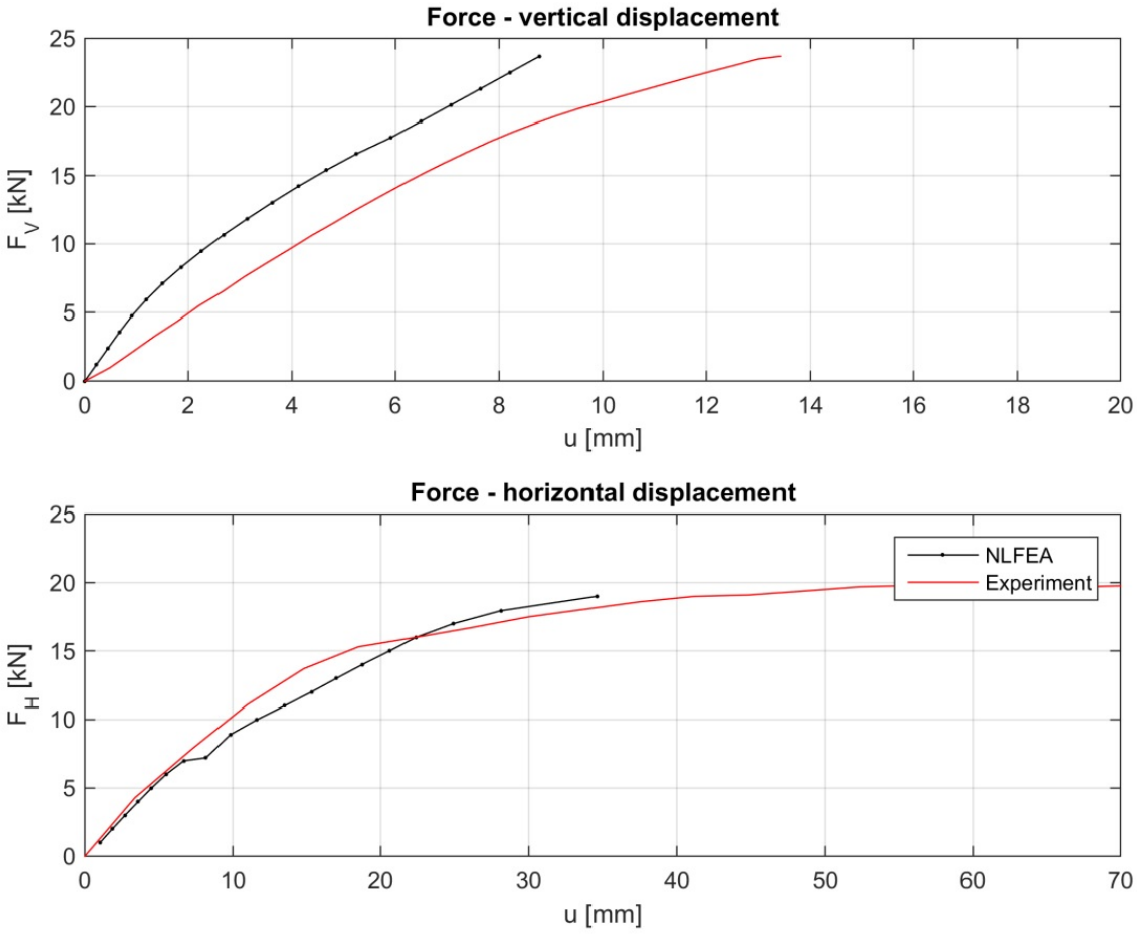

Figure 3.1: Benchmark study in Blomfors (2014). Load-displacement relations: (above) vertically at mid span of the top beam and (below) horizontally at upper right corner. Figure by Blomfors (2014).

3.2 Design and modelling of the concrete frame

This section will give a description of the frame designed by Blomfors (2014) and how it was adapted and modelled in DIANA for the use in NLFEA.

3.2.1 Design of frame

The concrete frame used in further analyses was designed by Blomfors (2014) using LFEA and the software ANSYS Mechanical 14.5 (ANSYS, 2014). The shape of the frame and the points at which it is loaded may be seen in Fig. 3.2. The frame is 6 m high and 10 m wide (outer dimensions) with cross sectional height 800 mm and 1000 mm for the columns and beam respectively. Common thickness is set to 500 mm. To put it into some perspective, Blomfors' goal was for the dimensions and loads to be realistic, and considered the frame to act as a bridge support in a location where an ordinary column support is not possible. The assumed design loads F_V and F_H act in vertical and horizontal direction respectively, with F_V considered as a dead load and F_H as a live load. Furthermore, it was assumed that F_V is to be applied first then F_H second. Characteristic load values are 800 kN dead load and 675 kN live load.

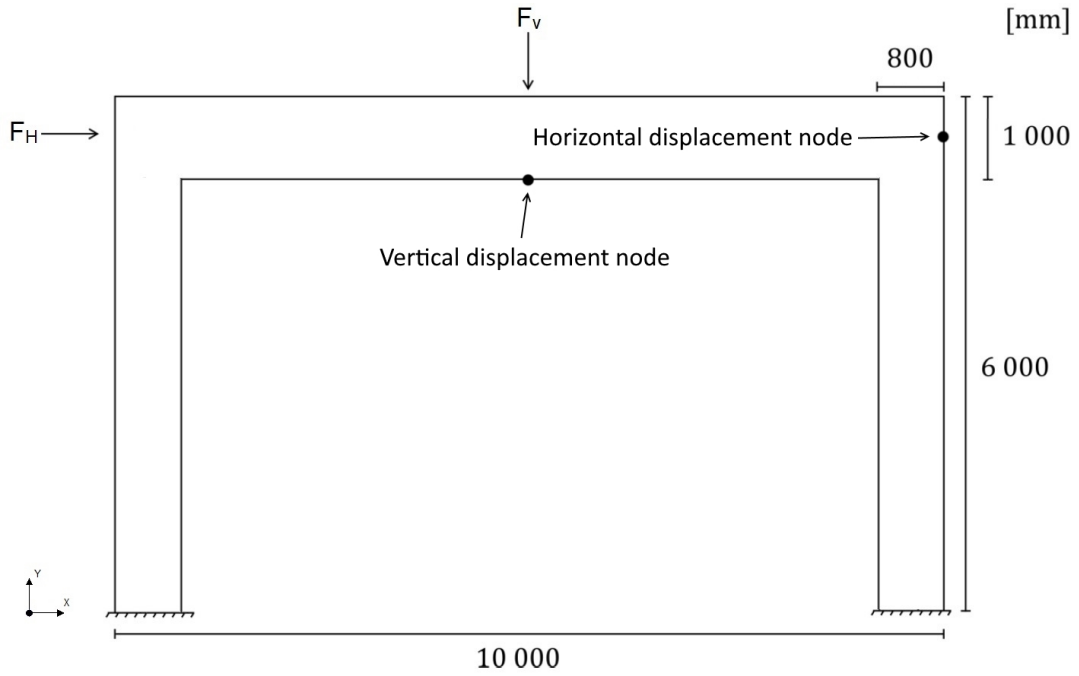

Figure 3.2: Dimensions and loading of the frame adopted from Blomfors (2014) including vertical load, F_V, and horizontal load, F_H. In addition, the figure shows the location of nodes used for recording displacements.

Blomfors (2014) used a software MultiCon (an in-house post-processor at Multiconsult AS) to design the reinforcement layout of the frame. Load effects and geometry were imported from ANSYS and designed for ultimate limit state according to the provisions of Eurocode 0 and Eurocode 2 (CEN, 2002, 2004). The concrete class used was C45/55 along with reinforcement class B500. The ULS load combination for a global design check are given by Eq. (6.10) in Eurocode 0, Table A1.2(A). This results in partial load factors for dead loads $\gamma_G = 1.35$ and live loads $\gamma_Q = 1.5$. Some specifications regarding the reinforcement layout parameters may be seen in Table 3.1 and the resulting layout scheme can be seen in Figs. 3.3 and 3.4.

Table 3.1: Some reinforcement layout parameters

Parameter	**Value**
Concrete cover	50 mm
Minimum clear distance between bars	32 mm
Minimum clear distance between parallel layers	32 mm

3.2.2 Modelling of frame in DIANA

An input file was written in a .py document consisting of python-code commands readable by DIANA v.10.1. (DIANA FEA, 2017a) as opposed to modeling directly in the user interface of DIANA. The choice for writing a script was justified by the possibility for effective changes in model properties and equilibrium parameters compared to performing the same changes in the user interface.

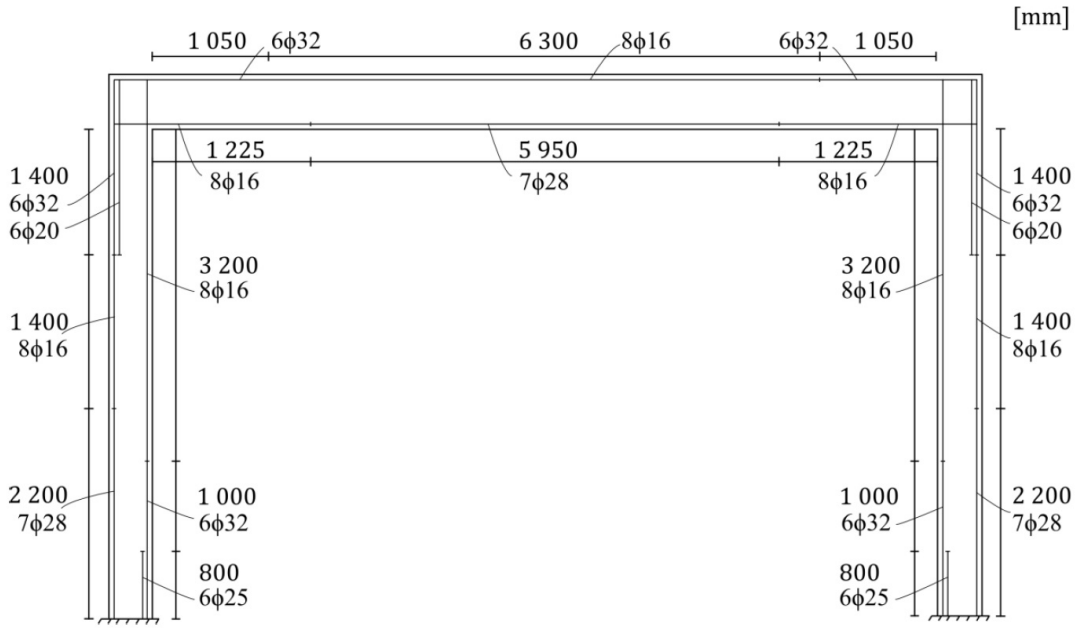

Figure 3.3: Longitudinal reinforcement scheme, by Blomfors (2014).

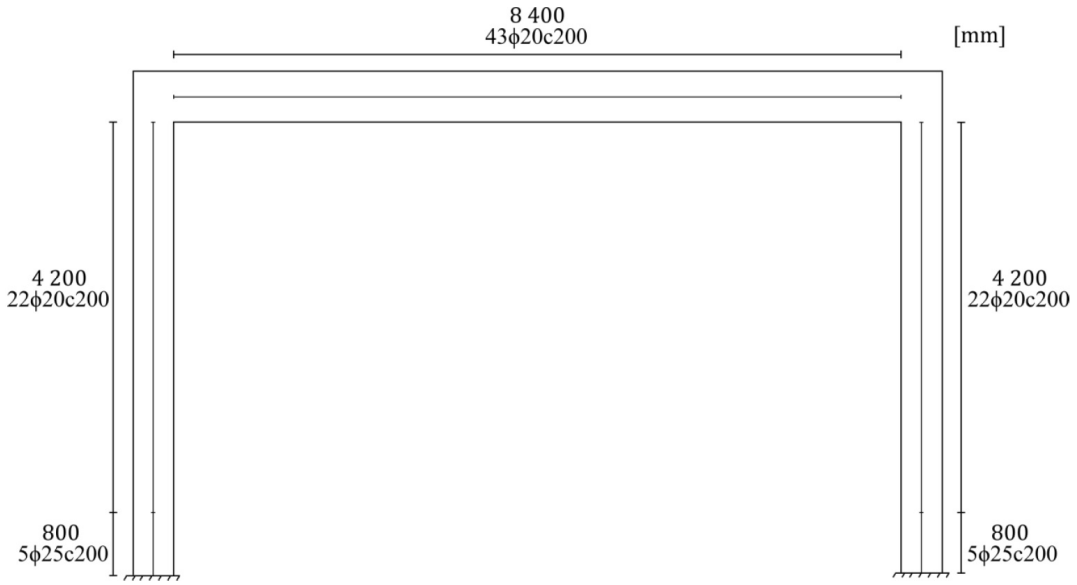

Figure 3.4: Shear reinforcement scheme, by Blomfors (2014).

The loads are modelled as pressure loads on the surface elements over an area of (0.5 x 0.5)m^2 and (1.0 x 0.5)m^2 for vertical and horizontal load respectively. The frame is modelled using 8 noded quadratic 2D sheet elements, with quadratic interpolation for concrete and embedded truss elements for reinforcement. The choice of 2D modelling will reduce computation time and due to symmetry and in plane forces, it is not expected to behave any differently compared to 3D modelling. In addition, this will eliminate any concern regarding spurious bending modes out of plane. The supports are modelled as fix against translation in all both x and y direction (see Fig. 3.2) and there are no slip surfaces in the structure.

The reinforcement was modelled according to measurements from Figs. 3.3 and 3.4 as well as parameters from Table 3.1. The reinforcement was placed with respect to the

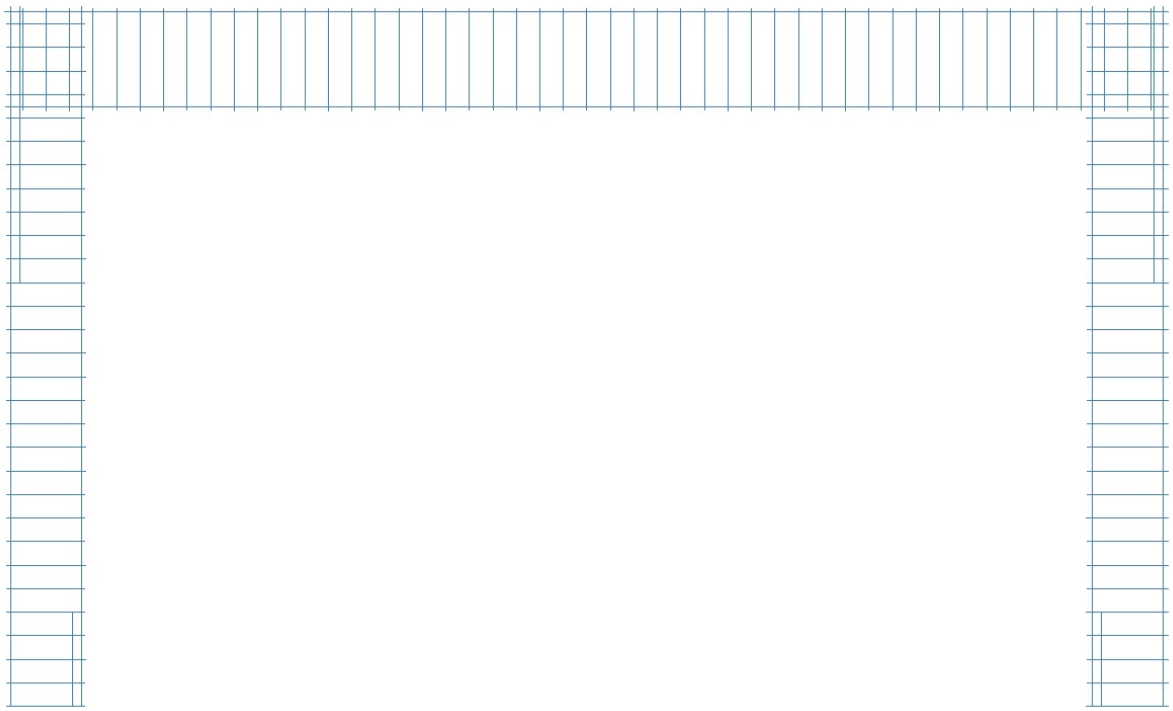

Figure 3.5: Reinforcement design in DIANA.

characteristic diameter of the reinforcement bars (the diameter including ribs), but the modelled reinforcement area is calculated from the nominal diameter. The outermost reinforcement, the stirrups, was placed with a concrete cover of 50 mm, the longitudinal reinforcement was placed on the inside of the stirrups with a clear distance of 50 mm between parallel layers. In contrast to Blomfors (2014), the longitudinal reinforcement was not placed as far out as possible at any point in the frame, instead, the center axis of bars in the same layer, but with different diameter, was placed at the effective depth of the largest diameter bar in each layer, placed according to Table 3.1. This results in a possible maximum difference of ±7 mm, or roughly ±1% of the cross sectional height. This is assumed acceptable as the generally allowed deviation in placement of reinforcement in relation to nominal concrete cover Δc_{dev} = 10 mm (CEN, 2004), and would probably not contribute to significant deviations in the frame's ultimate capacity. In addition, there have been no further precautions taken regarding reinforcement layout constructablity. The final reinforcement design in the DIANA model can be seen in Fig. 3.5.

3.3 Solution strategy

When creating a nonlinear FE model and solution strategy, there are several choices that needs to be made regarding material properties, and compatibility and equilibrium parameters. The purpose of this section is to create a solution strategy to be used in comparison of load histories effect on NLFEA safety formats. Furthermore, it is benchmarked against Blomfors' case study. A summary of the solution strategy is also provided.

3.3.1 Validation of strategy

The validation of the solution strategy was performed against the data from Blomfors (2014) case study. The FE-software used for the analyses was DIANA v.10.1 (DIANA FEA, 2017a). As Blomfors used a previous version of the same non-linear software (DIANA), it was expected that the results the strategies provide would be very similar.

3.3.1.1 Loading of the frame

The vertical and horizontal load are applied to the frame in what is called a load history (LH). Load histories apply forces at different times and the load sequences may vary between load histories. The LHs used in the validation are represented in Eqs. (3.1) and (3.2), where R_i is representing the loading in load history i. Note, each line of the two equations represents a separate load sequence. In load history 1 (LH1), the vertical force was applied first to its characteristic value in 20 load steps. Then the horizontal force was applied to characteristic value over 20 load steps. Finally, both loads were simultaneously increased at a rate relative to each other so that they both achieved design values after another 20 load steps. This relative loading continues until global failure occurs, where the load level is representative by a load factor, LFS, of the last sequence, from now on called sequential load factor, which increases its value by 1.0 for every 20 steps. To increase accuracy of the failure load, which also increases the accuracy of the global ECOV method, all analyses were run twice, with the second analysis reducing the last load steps before failure by a factor of 5 (LFS increases 0.01 instead of 0.05 per load step). Load history 2 (LH2) are almost identical to LH1 except it applies horizontal load before vertical load in the first two load sequences.

$$\begin{aligned} R_1 = {} & F_{Vk} \\ & + F_{Hk} \\ & + LFS \cdot \left[(\gamma_G - 1) F_{Vk} + (\gamma_Q - 1) F_{Hk} \right] \end{aligned} \tag{3.1}$$

$$\begin{aligned} R_2 = {} & F_{Hk} \\ & + F_{Vk} \\ & + LFS \cdot \left[(\gamma_G - 1) F_{Vk} + (\gamma_Q - 1) F_{Hk} \right] \end{aligned} \tag{3.2}$$

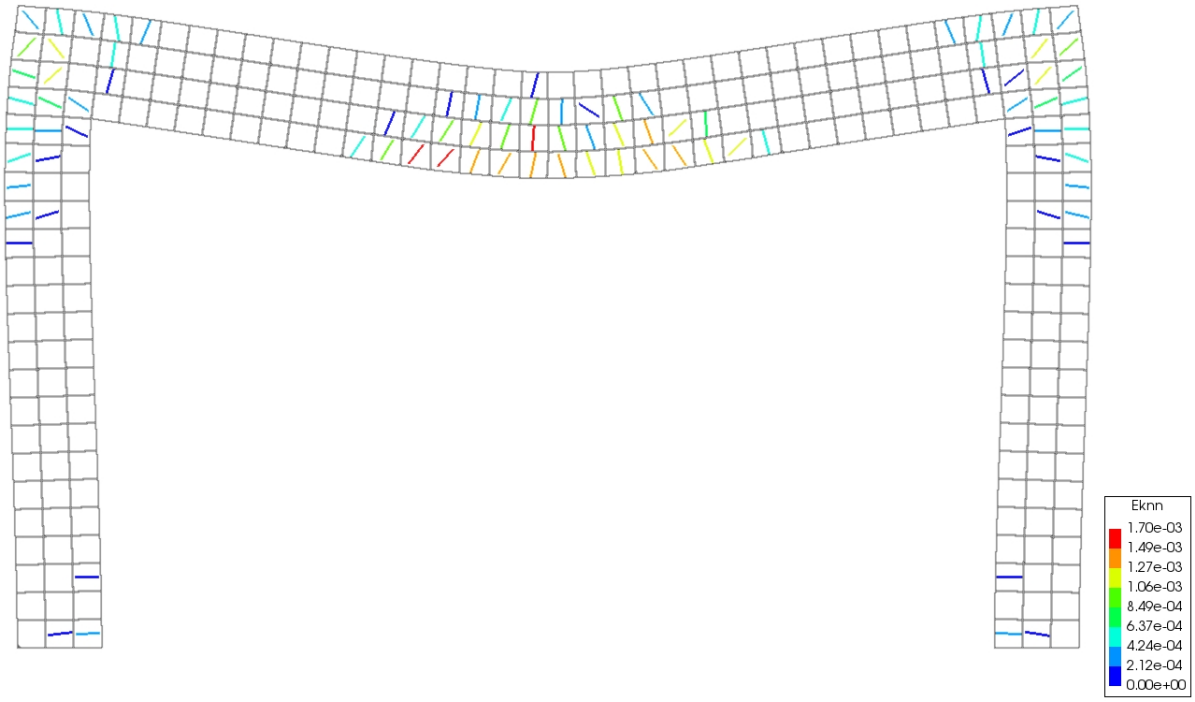

Figure 3.6: Crack pattern after application of the first load sequence of load history 1. From the verification of solution strategy and the mean ECOV analysis. Eknn is the crack strains perpendicular to the crack direction.

3.3.1.2 Structural response and behavior

The behavior of the frame for both load sequences behave as expected and are almost identical compared to the results of Blomfors (2014). For LH1, the first cracks appear in the underside of beam, directly beneath the vertical load, at approximately 25-35% of characteristic load level depending on the safety format method. Soon after, more cracks appear in the underside of the beam adjacent to the initial cracks, but also in the outer elements of the frame corners and on the inside of the columns at the supports. Fig. 3.6 gives an overview of the cracks after the first load sequence is applied. Note that the deformations are normalized and greatly exaggerated, which applies for all the illustrations of the frame in this thesis. This is to help visualize the bending of the loaded frame. Applying the horizontal load causes the cracks on the inside of the left-hand column support to close. Further appearance of new cracks are located at the inside of the right-hand column, with cracking propagating upwards, and in the lower left part of the beam propagating from the mid span towards the left corner. In addition, cracks start appearing on the outside of the left-hand column along its entire height. In the right column, cracking propagates upwards from the inside of the support and downwards on the outside from the corner. A picture of the crack pattern when loaded at full characteristic load can be seen in Fig. 3.7.

The crack pattern shows little change throughout the last load sequence and the frame fails in concrete compression on the inside of the right column adjacent to the corner. It should be noted that both principal stresses are in compression and that the greater of these exceeds the uni-axial compressive strength of concrete. This is not unexpected due to the modelled material property of increased strength due to lateral confinement. The failure caused divergence for the ECOV method for certain load histories while the others were able

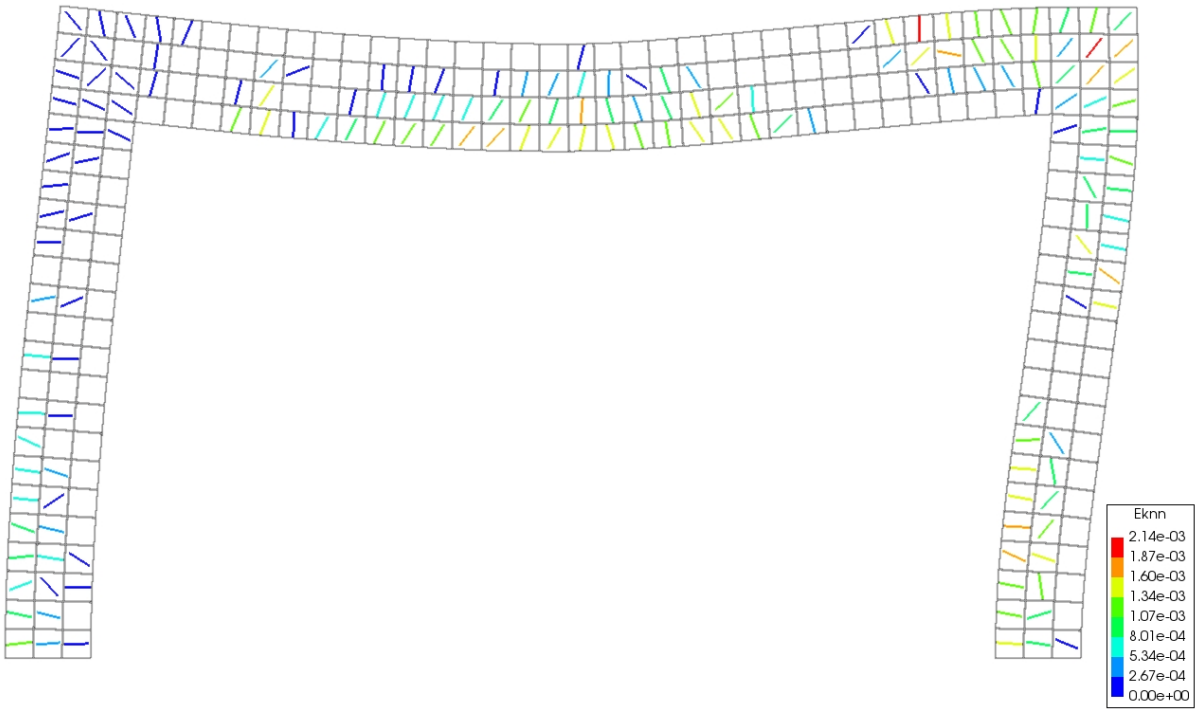

Figure 3.7: Crack pattern after application of the second load sequence of load history 1. From the verification of solution strategy and the mean ECOV analysis. Eknn is the crack strains perpendicular to the crack direction.

to gain some increased capacity due to a redistribution of forces from the corner into the beam and columns. This increase of capacity is further explained in Section 3.7.1.2. If an analysis survived the concrete failure in the right corner, it came to an ultimate capacity due to compressive failure either at the outside of the right column, just above the support, or in the mid span at the top of the beam. The longitudinal reinforcement is yielding in the failure regions before concrete failure, primarily in tension, however, concrete failure appears to happen soon after the longitudinal reinforcement in the interior of the right column yields in compression. The shear reinforcement is not yielding before failure though it is most utilized in the top right corner.

The crack pattern for LH2 is slightly different compared to LH1. The horizontal load causes the first cracks to appear simultaneously on the left side of both columns above the supports and at the inside of the left corner of the column. At increased loading, the cracking propagates upwards from the column supports and downwards from the left corner. Cracks appear soon on the outside of the right corner and propagate into the column and beam. The pattern after characteristic horizontal load is applied can be seen in Fig. 3.8.

When applying the vertical force in load sequence 2 of LH2, new cracks appear in the lower part of the beam at the left corner which propagate past the mid span by the end of load sequence 2. In addition, during load sequence 2, only a slight increase of cracks in the right column can be seen propagating downwards from the corner. The complete crack pattern for characteristic loading for LH2 can be seen in Fig. 3.9. The most notable differences between the load histories are the amount of cracks on the outer part of the left column, the lack of cracking on the outer part of the left corner for LH2, and the orientation of the cracks in the left corner.

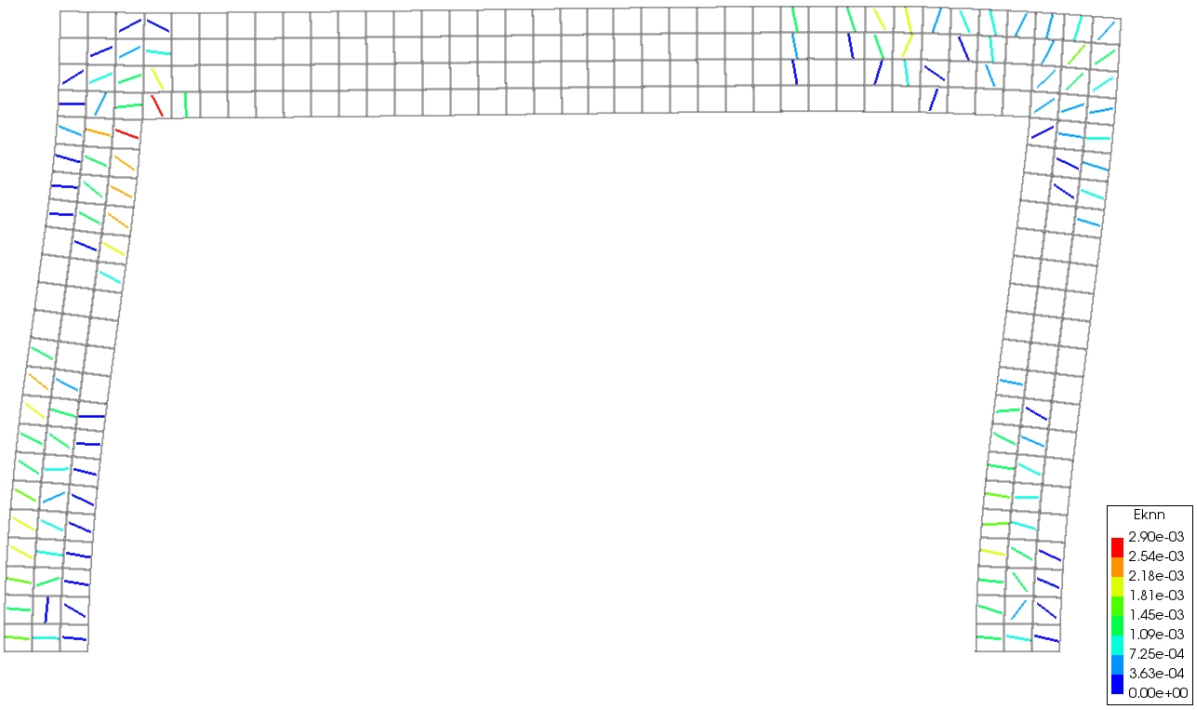

Figure 3.8: Crack pattern after application of the first load sequence of load history 2. From the verification of solution strategy and the mean ECOV analysis. Eknn is the crack strains perpendicular to the crack direction.

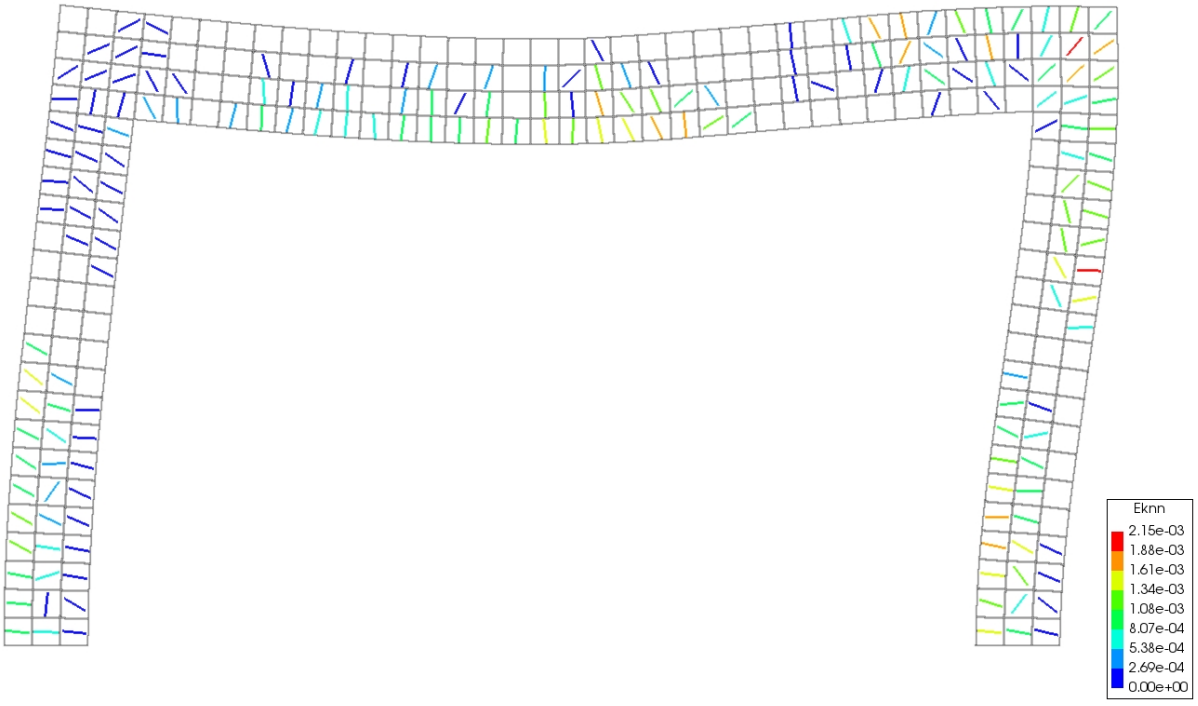

Figure 3.9: Crack pattern after application of the second load sequence of load history 2. From the verification of solution strategy and the mean ECOV analysis. Eknn is the crack strains perpendicular to the crack direction.

3.3.1.3 Verification analysis and comparison of results

In order to estimate the accuracy of the chosen solution strategy, the values of material parameters will be those given in Blomfors (2014). This is to better compare the uncertainties in the structural model and equilibrium calculations by reducing the uncertainty from the different estimations of material parameters. The material parameter values used for the three safety format methods can be found in Tables 3.2 to 3.4.

The results of the analyses are measured with the same categories used in Blomfors (2014). These are the total applied loading of the frame and the load-displacement relations of both vertical load vs. vertical displacement at mid span and horizontal load vs. horizontal displacement of the top right hand corner of the frame. Here, the loading is determined by a summation of the reaction forces at the support nodes. The displacements are measured at the node located at the bottom of the beam, directly below the center of the applied vertical force and at the node located to the far right end of the frame in the middle of the beam cross section (see Fig. 3.2). Note that in Figs. 3.10 to 3.15, load sequence 1 and 2 is left out of the horizontal and vertical force-displacement plots respectively to increase clarity as the

Table 3.2: Mean and characteristic material strength parameters used for ECOV analyses when verifying the solution strategy. Values from Blomfors (2014).

Steel					
Mean values			Characteristic values		
E_{sm}	200 000	MPa	E_{sk}	200 000	MPa
f_{ym}	533	MPa	f_{yk}	500	MPa
f_{um}	628	MPa	f_{uk}	600	MPa
ε_{um}	0.1171	[-]	ε_{uk}	0.1170	[-]
Concrete					
Mean values			Characteristic values		
E_{cm}	37 486	MPa	E_{ck}	35 496	MPa
f_{cm}	53.0	MPa	f_{ck}	45.0	MPa
f_{ctm}	3.80	MPa	f_{ctk}	3.33	MPa
G_{fm}	149.2	N/m	G_{fk}	144.8	N/m
G_{cm}	37 294	N/m	G_{ck}	36 211	N/m

Table 3.3: Mean material strength parameters used for GRFm analyses when verifying the solution strategy. Values from Blomfors (2014).

Steel		
$E_{sm,GRF}$	220 000	MPa
$f_{ym,GRF}$	550	MPa
$f_{um,GRF}$	660	MPa
$\varepsilon_{um,GRF}$	0.1170	[-]
Concrete		
$E_{cm,GRF}$	30 171	MPa
$f_{cm,GRF}$	31.5	MPa
$f_{ctm,GRF}$	2.83	MPa
$G_{fm,GRF}$	123.1	N/m
$G_{cm,GRF}$	30 779	N/m

Table 3.4: Design material strength parameters used for PSFm analyses when verifying the solution strategy. Values from Blomfors (2014).

Steel		
E_{sd}	173 913	MPa
f_{yd}	435	MPa
f_{ud}	522	MPa
ε_{ud}	0.1170	[-]
Concrete		
E_{cd}	23 664	MPa
f_{cd}	30.0	MPa
f_{ctd}	2.22	MPa
G_{fd}	96.6	N/m
G_{cd}	24 141	N/m

variation in recorded forces are negligible.

Tables 3.5 and 3.6 presents the ultimate limit capacity from load history analyses for the three safety format methods. They present both the analysis values and the calculated design values for the GRFm and ECOV methods. Note that the design capacity for ECOV is calculated as in Blomfors (2014) which is according to Eqs. (2.19), (2.20) and (2.21). The analyses give ultimate capacities averaging 96% of the corresponding analyses in Blomfors (2014). The results are described in greater detail below.

Table 3.5: Design resistances R_d for load history 1 calculated according to the three safety formats with the corresponding values from Blomfors (2014).

	R_m [kN]	R_k [kN]	V_R	γ_R	γ_{Rd}	R_d [kN]
ECOV*	2 864	2 614	0.055	1.18	1.06	2 284
ECOV	2 525	2 399	0.031	1.099	1.06	2 168
GRFm*	2 492	-	-	1.20	1.06	1 959
GRFm	2 258	-	-	1.20	1.06	1 775
PSFm*	-	-	-	-	-	1 967
PSFm	-	-	-	-	-	1 962

* values from Blomfors (2014).

Table 3.6: Design resistances R_d for load history 2 calculated according to the three safety formats with the corresponding values from Blomfors (2014).

	R_m [kN]	R_k [kN]	V_R	γ_R	γ_{Rd}	R_d [kN]
ECOV*	2 923	2 402	0.119	1.437	1.06	1 920
ECOV	2 617	2 330	0.070	1.239	1.06	1 993
GRFm*	2 491	-	-	1.20	1.06	1 959
GRFm	2 434	-	-	1.20	1.06	1 914
PSFm*	-	-	-	-	-	1 939
PSFm	-	-	-	-	-	1 703

* values from Blomfors (2014).

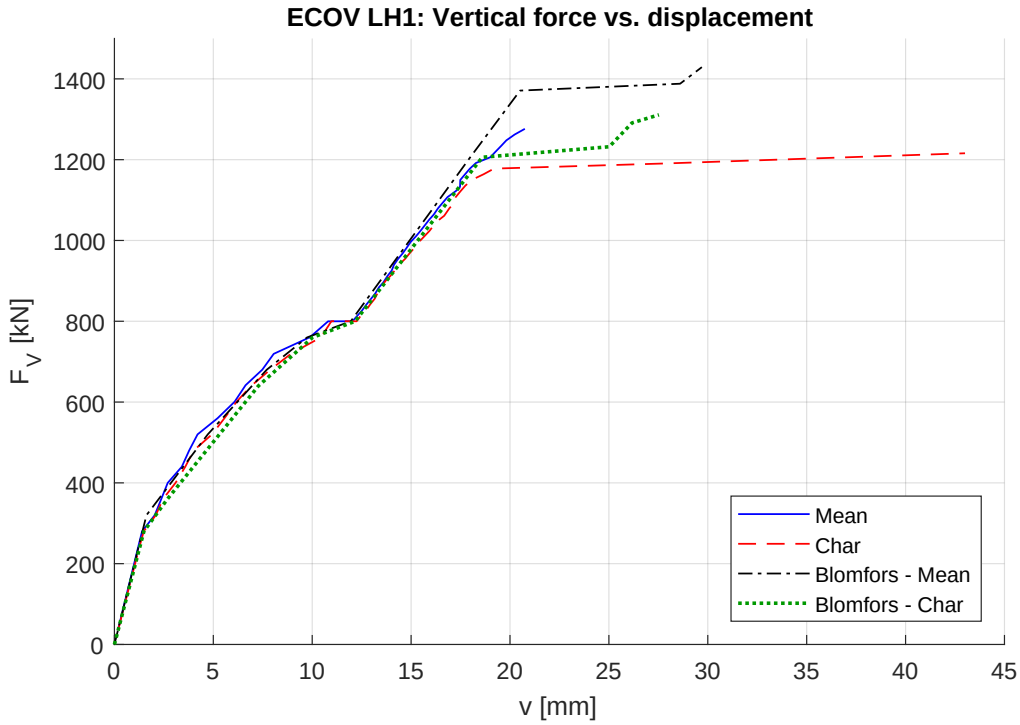

Figure 3.10: Vertical force, F_V, vs. vertical displacement, v, in mid span of the frame for ECOV analyses of load history 1 with reference curve from Blomfors (2014). Plots with both mean and characteristic material parameters. Load sequence 2 is left out for clarity which causes the horizontal shift at 800 kN.

ECOV results

The ECOV method requires two separate analyses for each load history, one analysis with mean and one with characteristic material properties. These properties are given in Table 3.2. In LH1, the two analyses behaved almost identical during the first two load sequences. For the third and last sequence, the mean analysis showed a slightly stiffer behaviour than the characteristic analysis. This is similar to what is seen in Blomfors (2014) which gives an almost identical behaviour. This behaviour can be seen in Figs. 3.10 and 3.11 for the vertical and horizontal load-displacements respectively.

Deviations from Blomfors (2014) are most notable at ultimate capacity. The analyses performed do not represent the same cause of global failure, as they diverge before load effects are redistributed. This can be seen in Figs. 3.10 and 3.11 where the mean analysis reaches ultimate strength at crushing, and the characteristic analysis yielded only a slight capacity increase before global failure. However, the failure loads have a smaller variation of resistance compared to the capacities in Blomfors (2014) which results in a design capacity only slightly smaller than in Blomfors (2014).

For LH2 there are no reference curves from Blomfors (2014), consequently, there are no load-displacement curves presented. The analyses show the same trend as for LH1, with the mean curve slightly stiffer than the characteristic curve as should be expected from material parameters. Meanwhile, the variation in global capacity is greater for LH2 than for LH1. This is the same observation as made in Blomfors (2014). The ultimate capacities measured in this work are smaller than for Blomfors (2014), however, the variation is smaller as well, which results in a greater design capacity of roughly 4%.

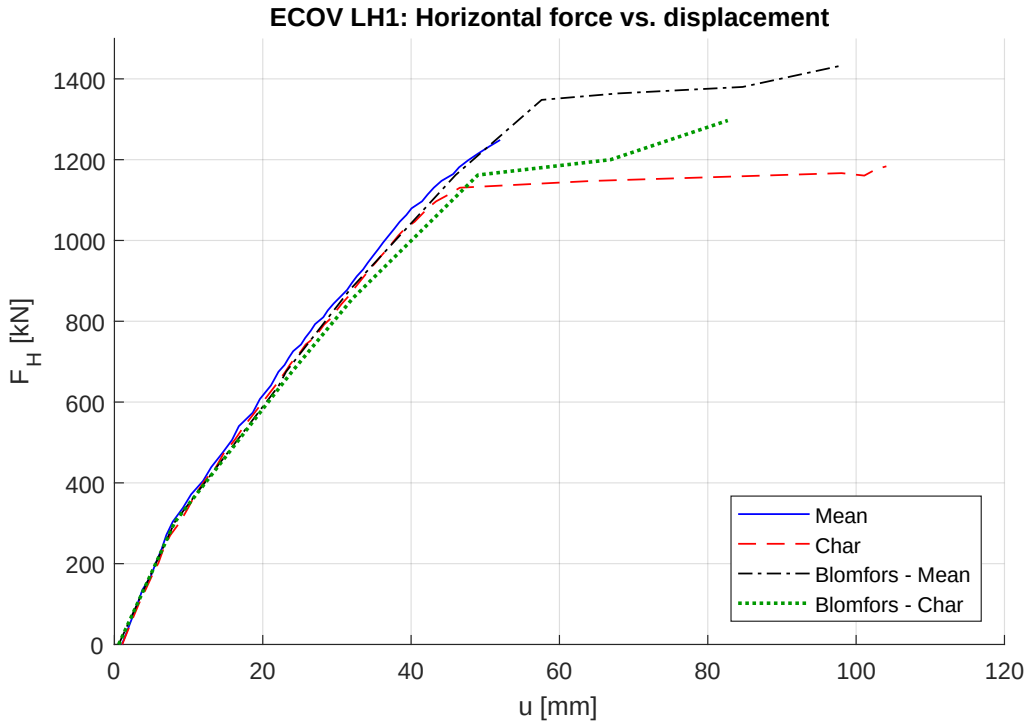

Figure 3.11: Horizontal force, F_H, vs. horizontal displacement, u, of the top right corner of frame for ECOV analyses of load history 1 with reference curve from Blomfors (2014). Plots with both mean and characteristic material parameters. Load sequence 1 is left out for clarity which causes the small initial shift from the origin.

GRFm results

The GRFm analysis for LH1 is identical to the reference analysis from Blomfors (2014) for loads below characteristic level as seen in Figs. 3.12 and 3.13. The first local failure occurs in the right column at the inside of the right corner, just as for Blomfors (2014), however, the load level is roughly 8% greater. The analysis gives some increase in capacity due to redistribution of forces from the right hand corner to the column bases of both columns, but the increase is not as great as the reference data and the global failure load is 9% smaller than in Blomfors (2014).

The analysis for LH2 results in a global ultimate capacity only 2% smaller than the reference capacity from Blomfors (2014). The first local concrete failure occurs at the same spot as for LH1 but for a smaller load. In contrast to LH1, the post failure strength increase is greater for LH2.

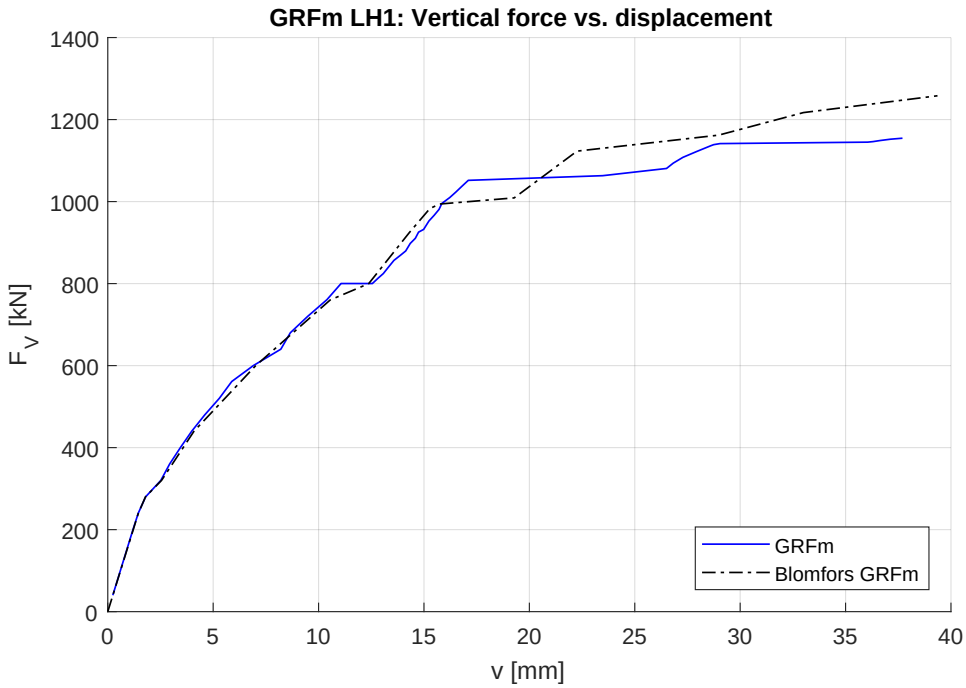

Figure 3.12: Vertical force, F_V, vs. vertical displacement, v, in mid span of the frame for GRFm analysis of load history 1 with reference curve from Blomfors (2014). Load sequence 2 is left out for clarity which causes the horizontal shift at 800 kN.

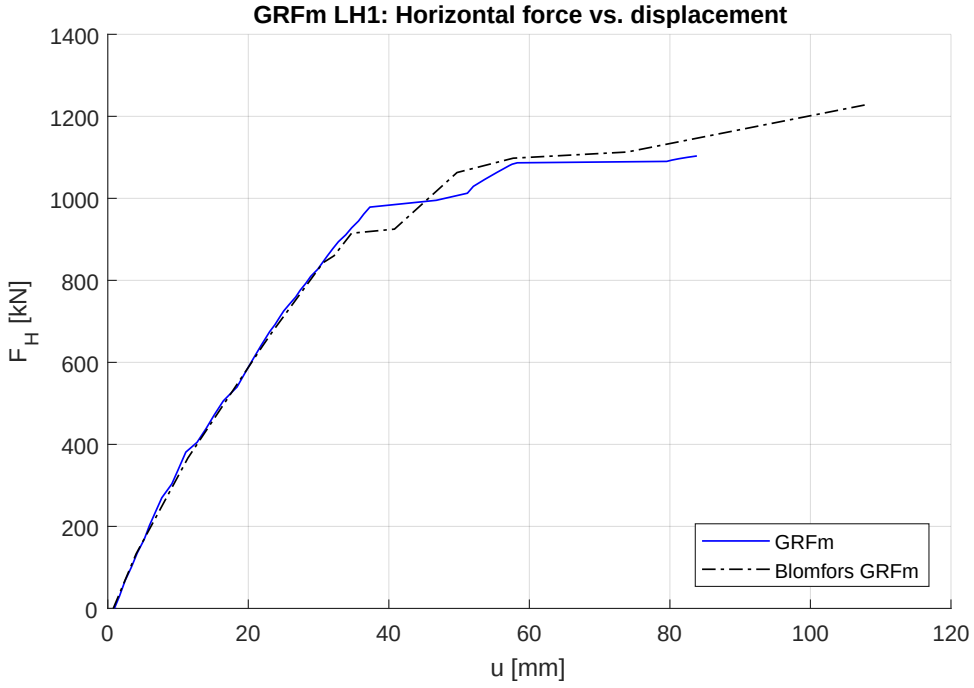

Figure 3.13: Horizontal force, F_H, vs. horizontal displacement, u, of the top right corner of the frame for GRFm analysis of load history 1 with reference curve from Blomfors (2014). Load sequence 1 is left out for clarity which causes the small initial shift from the origin.

PSFm results

The analysis for the partial safety factor method yields great results for LH1 while not so good for LH2. The results for LH1 can be seen in Figs. 3.14 and 3.15. They show identical behavior leading up to the local failure of the right corner which occurs at almost the exact same load level as in Blomfors (2014). As for the other methods, the structural stiffness post local failure is smaller in reference to Blomfors (2014). However, the capacity increase is the same and results in an almost equal design capacity for LH1.

In contrast, the analysis for LH2 behaves as expected for pre characteristic load levels, but it fails to give convergence after the local failure of the right corner and results in a significantly reduced capacity. The analysis struggles to find a deformed shape with crushing in the right corner and results in a shape giving large spurious compressive stresses in the mid span of the beam. The consequence of this is another failure in the preceding load step. The local failure occurs at the same load level for LH2 as for LH1. This is unfortunate as LH2 was expected to receive a capacity increase as for LH1 and both of the GRFm analyses. It is assumed that the divergence is an unfortunate result of numerical error and not a trait of the solution strategy. Therefore, the chosen solution strategy will not be changed as the other analyses provide good estimates compared to Blomfors (2014).

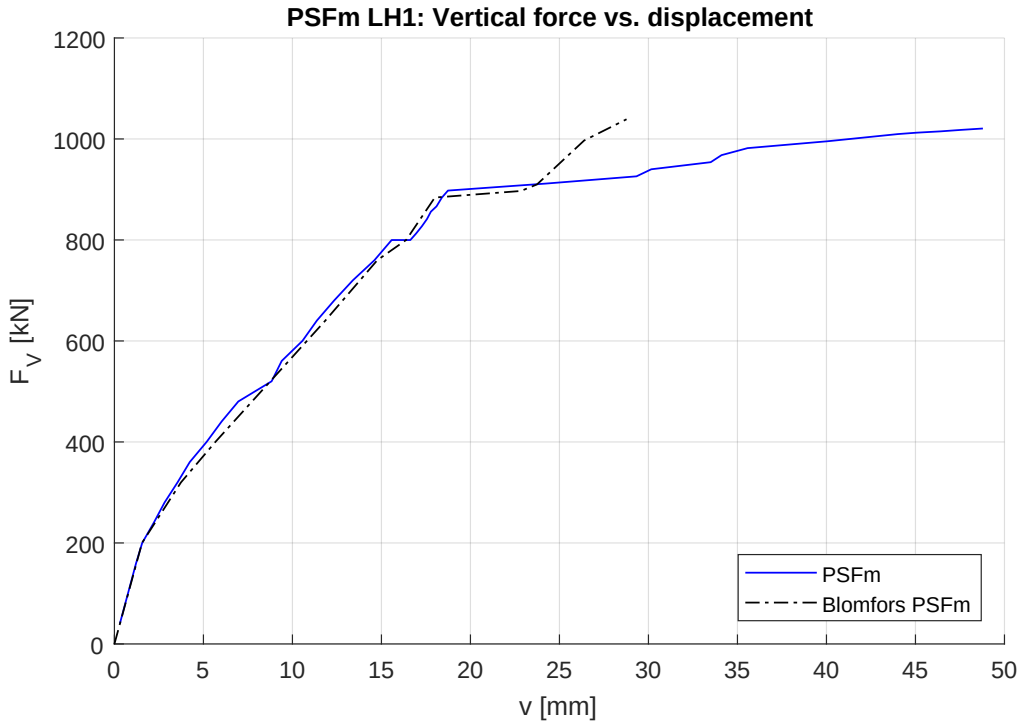

Figure 3.14: Vertical force, F_V, vs. vertical displacement, v, in mid span of the frame for PSFm analysis of load history 1 with reference curve from Blomfors (2014). Load sequence 2 is left out for clarity which causes the horizontal shift at 800 kN.

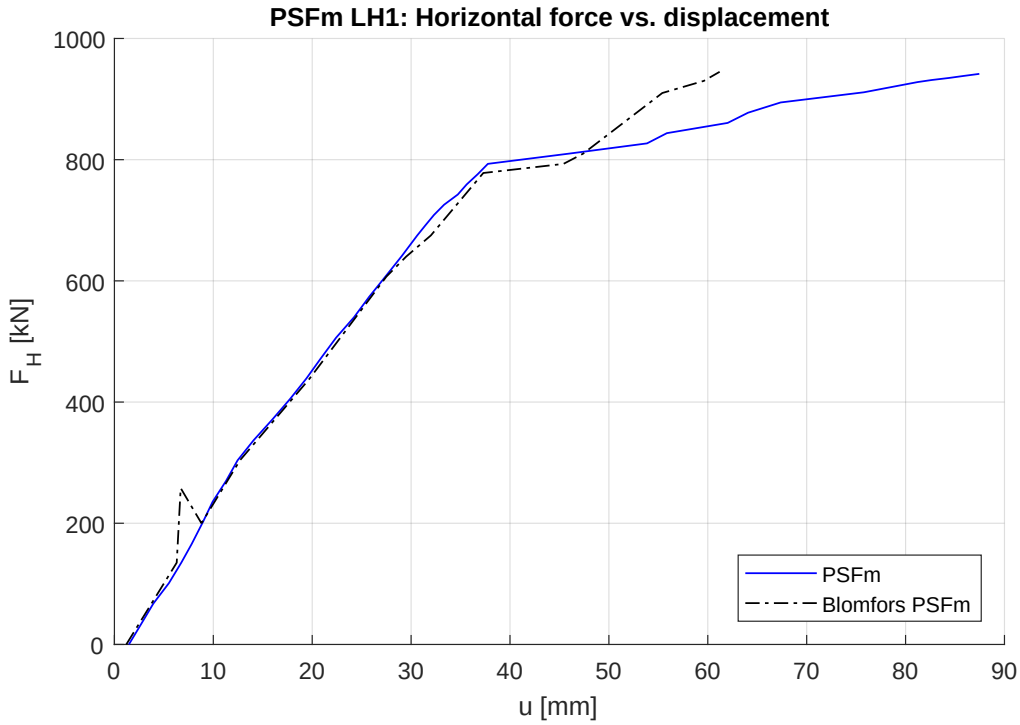

Figure 3.15: Horizontal force, F_H, vs. horizontal displacement, u, of the top right corner of the frame for PSFm analysis of load history 1 with reference curve from Blomfors (2014). Load sequence 1 is left out for clarity which causes the small initial shift from the origin.

3.3.2 Choice of solution strategy

The chosen solution strategy for further analyses is based on the guidelines given in Rijkswaterstaat Technical Document (RTD 1016-1:2017) by Hendriks et al. (2017a). No benchmark test of the solution strategy have been performed on a physical experiment, but as stated in section 3.3.1, the strategy is benchmarked against the analyses of Blomfors (2014) to obtain a model close to or equivalent to that of Blomfors.

The choices of model properties for reinforcement steel and concrete can be found in Table 3.7 while model properties for compatibility (e.g. element type) can be found in Table 3.8. Furthermore, the properties of the equilibrium iterations are presented in Table 3.9. Some of the property choices are determined by trial and error and some are determined by recommendations in Hendriks et al. (2017a). Properties chosen from the latter is indicated with a $^{\Delta}$ in the previous mentioned tables. More information about the chosen properties can be found in the DIANA v.10.1 Users's Manual (DIANA FEA, 2017b).

A notable difference between the chosen solution strategy and the strategy of Blomfors (2014) is the choice of modelling in 2D. This is done in order to reduce computation time by reducing the amount of modelled degrees of freedom to roughly one fourth that of 3D modelling. An argument for this is that the forces are acting in the frame's major plane and there are no significant constrains out of plane that may induce confinement.

The guidelines of Hendriks et al. (2017a) recommend using at least 6 elements over the height (E.O.H) of cross sections. The model does not comply with this, as it uses 3 to 4 E.O.H. This is because the finer mesh achieve significantly smaller design capacities compared to

Blomfors (2014). However, The choice of 4 E.O.H. for the beam is to reduce the distortion of the quadrilateral element in regard to aspect ratio. Maximum aspect ratio is 1.06, while for Blomfors (2014) it is 1.33.

Table 3.7: Constitutive material properties implemented in the solution strategy. Recommended properties are marked with $^{\Delta}$.

Property	**Choice in DIANA**	**Comments**
Concrete material model$^{\Delta}$	Total strain based crack model	Smeared cracking model for concrete.
Crack orientation$^{\Delta}$	Fixed	Physically appealing model, stress-strain relations are evaluated in a fixed coordinate system which is fixed upon cracking.
Tensile softening of concrete$^{\Delta}$	Exponential	The concrete softens exponentially after tensile strength is reached. Based on fracture energy and equivalent length.
Poisson's ratio reduction$^{\Delta}$	Damage	Poisson's ratio reduces after cracking.
Compression curve of concrete$^{\Delta}$	Parabolic	Parabolic diagram based on fracture energy and crack bandwidth.
Reduction model due to lateral cracking$^{\Delta}$	VC1993	Perpendicular tensile strains reduce the compressive strength of concrete. Reduction model by Vecchio and Collins (1993).
Influence of lateral confinement	VECCHI	Lateral confinement increases concrete compressive strength. Model by Selby and Vecchio (1997).
Shear retention model	Constant	A constant shear retention after cracking. reduction of shear stiffness by a factor β. factor chosen as 0.1 for computational stability.
Plasticity model for reinforcement steel	Von Mises	Von Mises plasticity model with isotropic stain hardening and a linear plastic strain-stress relation.

Table 3.8: Compatibility properties implemented in the solution strategy. Recommended properties are marked with $^{\Delta}$.

Property	Choice in DIANA	Comments
Concrete element type$^{\Delta}$	CQ16M	8-node quadrilateral isoparametric plane stress element with quadratic interpolation and Gauss integration.
Integration method$^{\Delta}$	3x3 Gauss integration	Full integration for quadratic interpolation to avoid possible spurious modes.
Reinforcement element type	Embedded bar element	No slip between reinforcement and concrete. reinforcement strains computed from the displacement field of the concrete element in which it is embedded.
Geometric nonlinearity	Total Lagrange	Strain and stress measures are defined with reference to the undeformed geometry.

Table 3.9: Equilibrium properties implemented in the solution strategy. Recommended properties are marked with $^{\Delta}$.

Property	Choice in DIANA	Comments
Convergence criteria$^{\Delta}$	1% tolerance for force norm - 0.1% tolerance for energy norm	Load increments in which at least one of the two norms is satisfied can be considered as converged.
Iteration method$^{\Delta}$	Regular Newton-Raphson, max. 200 iterations	Regular Newton-Raphson was found to give better convergence.
Load increments*	maximum 5% of target load for either vertical and horizontal load	The increments were found to be adequate from validation.
* General load increments of 5% of target load for every load sequence. Exception is made for load sequences applying design target loads in the first load sequence, here load increments are reduced by a factor 2/3. This is to equate the physical value of load increments between load histories. For improved accuracy, load increments are reduced by a factor of 5 to 1% when approaching divergence.		

3.4 Load histories

There can be many load histories to consider when trying to estimate an ultimate global capacity using NLFEA, such as the previously mentioned load history 1 and 2. In general, the self-weight of a structure should be applied first, followed by remaining permanent loads. Live loads are then applied until the characteristic load combination is achieved, where by permanent and live loads are increased until failure (Pimentel et al., 2014). This best describes LH1 as the vertical load is assumed a self-weight and the horizontal load is assumed a live load. However, these assumptions will not be emphasized in the choice of load histories due to the number of loads being only two. This opens for a more valid assumption of load history 2 and other LHs which applies the horizontal load first. Another possible load history can be seen in Engen et al. (2017) at which both self-weight and live loads are applied simultaneously although not during the first load sequence, noted there are more than two loads.

In order to compare results of different analyses, one must also choose a measure or measures to represent the resistance. In both Pimentel et al. (2014) and Engen et al. (2017) a load factor for the last load sequence is used as measurement. This is a clear representation of several load values in one measurement, however, these loads typically only act in the same direction. If all loads work in the same direction, and sometimes in the same point of application, then the origin of the total load should not matter, only the value of the loading. In the frame analysis of this thesis, the vertical and horizontal load act in orthogonal directions and in different application points. This makes the choice of measure not as trivial to make. Blomfors (2014) decided to choose the total applied load, and made sure that a total load level above characteristic values was obtainable by one load combination, thus eliminating the problem described above.

Another measure to consider is the load factor of one or both loads. Taking into account LH1 and LH2, either a load factor or the total load would be able to represent the loading at the exact same accuracy for load levels above characteristic loads. By using the load factor for the horizontal load as a measure, one can construct load histories in which the load factor of the vertical load can be fixed as a constant. This will result in a slightly different load situation at failure, but may at some times be of interest as we may control the self weight of a structure to a greater accuracy than live loads originating from nature, e.g. earthquakes, winds.

On the basis of the two measures described in the previous paragraphs, a set of new load histories are prepared. These histories are separated into two groups, one for a total load measure, and the other for a load factor measure. The first set consists of three load histories, of which two are the histories described in Blomfors (2014) (see Eqs. (3.1) and (3.2)). The third load history, LH3, considers simultaneous loading of the characteristic loads then follows load sequence 3 of LH1 and LH2. Following the structure of Eqs. (3.1) and (3.2), the loading in LH3 may be described as:

$$\begin{aligned} R_3 &= F_{Vk} + F_{Hk} \\ &\quad + LFS \cdot \left[(\gamma_G F_{Vk} - F_{Vk}) + (\gamma_Q F_{Hk} - f_{Hk}) \right]. \end{aligned} \tag{3.3}$$

The second set of load histories assumes a maximum value of the vertical force equal to its design load. Consequently, they increase only the horizontal load during the last load sequence to obtain global failure:

$$\begin{aligned} R_4 = {} & F_{Vk} \\ & + F_{Hk} \\ & + (\gamma_G - 1)F_{Vk} \\ & + (LF_H - 1)F_{Hk} \end{aligned} \tag{3.4}$$

$$\begin{aligned} R_5 = {} & F_{Hk} \\ & + F_{Vk} \\ & + (\gamma_G - 1)F_{Vk} \\ & + (LF_H - 1)F_{Hk} \end{aligned} \tag{3.5}$$

$$\begin{aligned} R_6 = {} & \gamma_G F_{Vk} + \gamma_Q F_{Hk} \\ & + (LF_H - \gamma_Q)F_{Hk} \end{aligned} \tag{3.6}$$

$$\begin{aligned} R_7 = {} & F_{Vk} \\ & + F_{Hk} \\ & + (\gamma_G - 1)F_{Vk} + (\gamma_Q - 1)F_{Hk} \\ & + (LF_H - \gamma_Q)F_{Hk} \end{aligned} \tag{3.7}$$

$$\begin{aligned} R_8 = {} & F_{Hk} \\ & + F_{Vk} \\ & + (\gamma_G - 1)F_{Vk} + (\gamma_Q - 1)F_{Hk} \\ & + (LF_H - \gamma_Q)F_{Hk} \end{aligned} \tag{3.8}$$

The load histories, LH4-LH8, are described in Eqs. (3.4) to (3.8) respectively, and a graphical illustration of all load histories may be seen in Fig. 3.16. Note that LH7 and LH8 are equal to LH1 and LH2 for the first three load sequences respectively, and that the sequential load factor LFS is substituted by the horizontal load factor LF_H which increases with the same general rate of 1.0 for every 20 load steps.

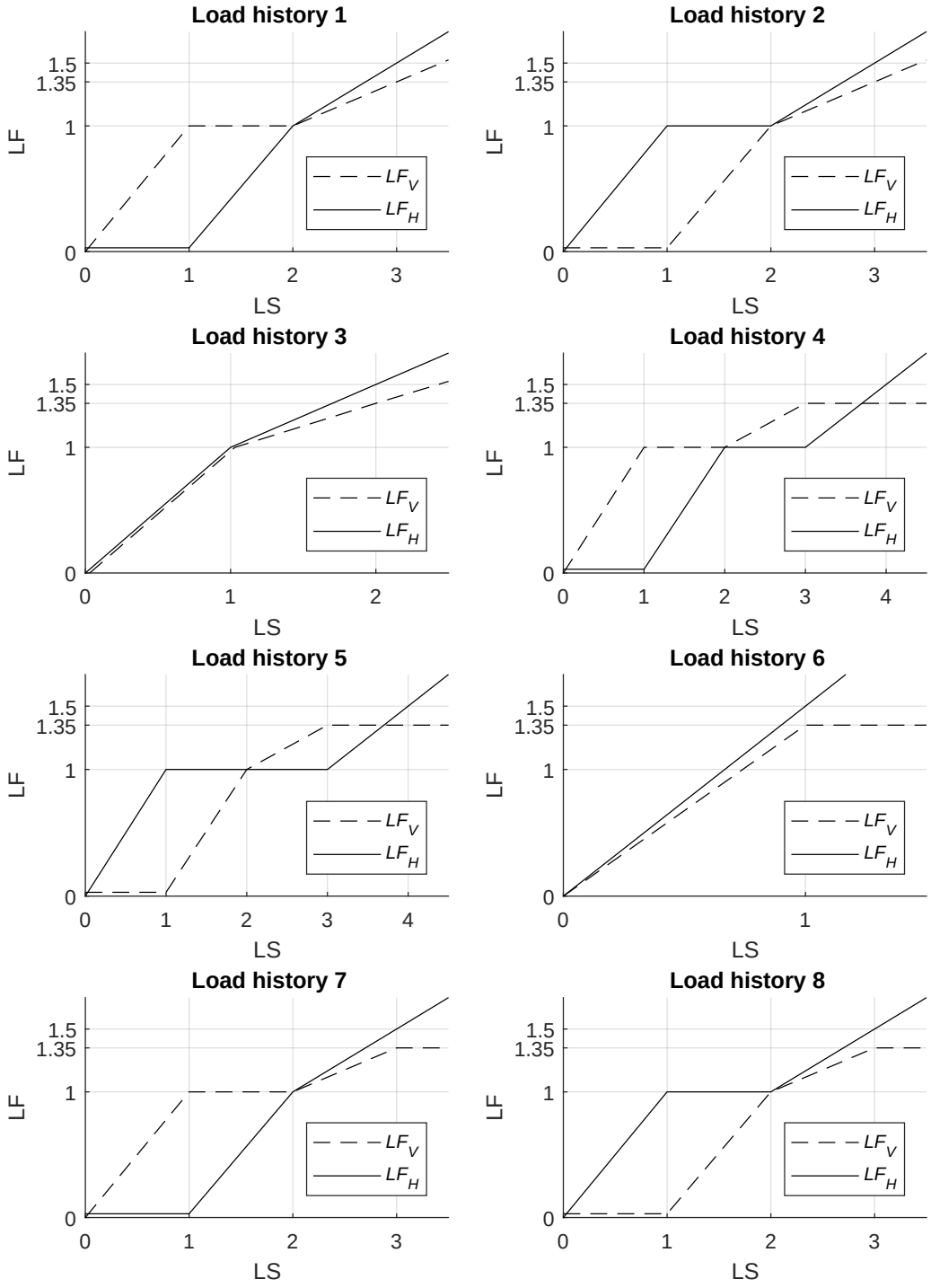

Figure 3.16: Illustration of the load histories used in analyses. LF_V and LF_H are the load factors for vertical and horizontal load respectively. Load factor (LF) values on the y-axis and load sequences (LS) on the x-axis.

3.5 Material parameters

Material parameters for NLFEA are calculated from Model Code 2010 by fib (2013). A summary of these calculations can be found in Annex A of Hendriks et al. (2017a). The assumed concrete strength class C45/55 gives an assumed characteristic compressive strength f_{ck} of 45 MPa, and reinforcement classification is assumed to be B500NC. Information about reinforcement parameters such as characteristic yield stress and characteristic ultimate strength for B500NC is given in NS 3576-3 (Norwegian Standard, 2012).

The Young's modulus for reinforcement steel is set as a constant 200 GPa for all safety formats as its variation is smaller than the strength variation and Model Code 2010 does not provide any calculations to assume otherwise. It should be noted that mean steel parameters are determined from the equations of Annex A (Hendriks et al., 2017a) and not from the minimum requirement listed in Norwegian Standard (2012). In addition, ultimate reinforcement strain for plasticity curves is determined as the strain at ultimate strength, i.e. not the failure strain. It is assumed that the ultimate strains for PSFm and GRFm are proportional to the ultimate stresses in relation to the characteristic parameters, even though this might not be as intuitive when compared to the mean ECOV value of ultimate stain and stress. A summary of all material parameters can be found in Tables 3.10 to 3.12.

Table 3.10: Mean and characteristic material strength parameters used in ECOV analyses.

Steel					
Mean values			Characteristic values		
E_{sm}	200 000	MPa	E_{sk}	200 000	MPa
f_{ym}	543	MPa	f_{yk}	500	MPa
f_{um}	652	MPa	f_{uk}	600	MPa
ε_{um}	0.094	[-]	ε_{uk}	0.080	[-]
Concrete					
Mean values			Characteristic values		
E_{cm}	37 486	MPa	E_{ck}	35 496	MPa
f_{cm}	53.0	MPa	f_{ck}	45.0	MPa
f_{ctm}	3.795	MPa	f_{ctk}	2.657	MPa
G_{fm}	149.2	N/m	G_{fk}	144.8	N/m
G_{cm}	37 294	N/m	G_{ck}	36 211	N/m

Table 3.11: Mean material strength parameters used in GRFm analyses.

Steel		
$E_{sm,GRF}$	200 000	MPa
$f_{ym,GRF}$	550	MPa
$f_{um,GRF}$	660	MPa
$\varepsilon_{um,GRF}$	0.088	[-]
Concrete		
$E_{cm,GRF}$	33 624	MPa
$f_{cm,GRF}$	38.25	MPa
$f_{ctm,GRF}$	3.406	MPa
$G_{fm,GRF}$	140.7	N/m
$G_{cm,GRF}$	35 167	N/m

Table 3.12: Design material strength parameters used in PSFm analyses.

Steel		
E_{sd}	200 000	MPa
f_{yd}	435	MPa
f_{ud}	522	MPa
ε_{ud}	0.070	[-]
Concrete		
E_{cd}	31 008	MPa
f_{cd}	30.0	MPa
f_{ctd}	1.771	MPa
G_{fd}	134.7	N/m
G_{cd}	33 662	N/m

3.6 Analysis of mesh sensitivity

According to the guidelines given in Hendriks et al. (2017a), the maximum element size should not exceed 1/6th of the cross sections height or 1/50th of the construction members length. This corresponds to roughly 133 mm and 120 mm respectively for the columns, and 166 mm and 200 mm for the beam of the frame. As the element model consists of element sizes equal to 1/3rd cross sectional height for columns and 1/4th of the beam, the mesh is rather coarse. The coarse mesh was selected based on the results from Blomfors (2014), however, it should be noted there is a possibility of the model being mesh sensitive.

In order to check if the model might be mesh sensitive, four analyses were run with an additional finer mesh. The mesh size was chosen as 6 E.O.H. for columns and 8 E.O.H. for the beam. The analyses that were rerun were PSFm of LH3 and LH7, GRFm of LH7 and ECOV of LH3. PSFm of LH7 and ECOV of LH3 had problems with divergence for the coarse mesh when the right concrete corner failed in concrete compression (this is presented in later sections).

The PSFm analysis of load history 3 with a finer mesh resulted in a more detailed behaviour and a noticeable small increase in ultimate capacity. Fig. 3.17 show the horizontal load - displacement curve from the analysis with a reference curve from the analysis with 3 E.O.H. The finer mesh show a behavior that is equally stiff, however, the local compressive failure of the right frame corner occurs at a lower load level. This is counter acted by a greater

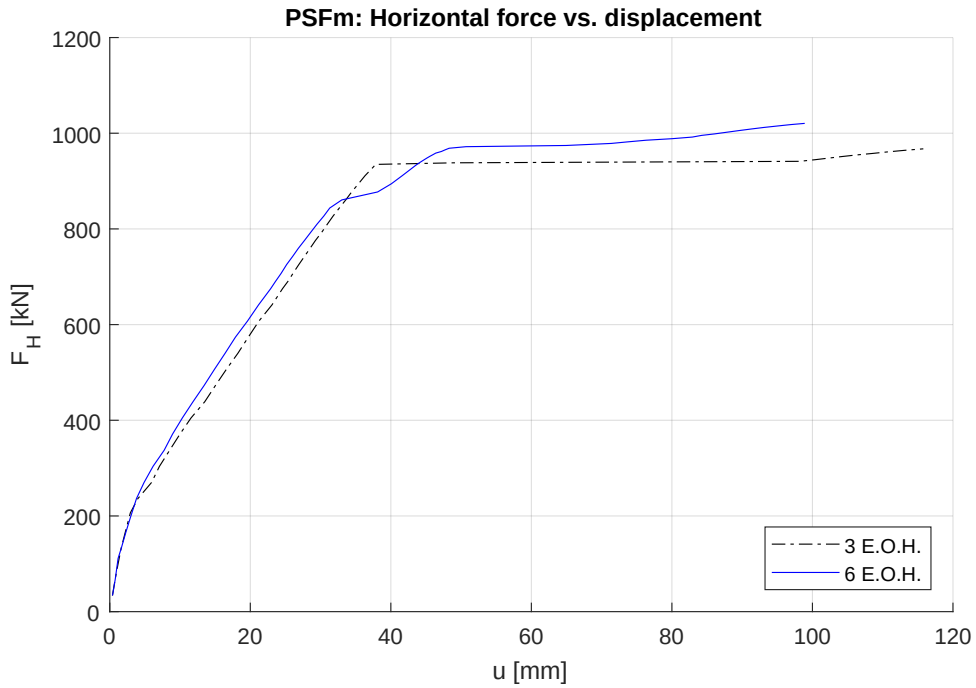

Figure 3.17: Horizontal force, F_H, vs. horizontal displacement, u, of the top right corner of the frame for PSFm analysis of load history 3. Includes the results from analyses with a mesh of 3 and 6 elements over the height (E.O.H.) of column cross sections.

strength increase post failure compared to the coarse mesh, and the final ultimate capacity is increased by roughly 5%.

The details of the PSFm analysis of load history 7 are improved by the finer mesh as for LH3. The behavior is slightly stiffer for smaller loads and have equal stiffness for higher loads. The first concrete failure occurs at a smaller load than for the coarse mesh as seen in Fig. 3.18, however, the analysis does not diverge as for the coarse mesh. The capacity increase post local failure is great enough to increase the global capacity to just reaching design loads.

In contrast to the PSFm analyses, the ECOV analyses of load history 3 with a finer mesh produced some unexpected results. The results seen in Fig. 3.19 show a similar behaviour for both meshes as loads remain below characteristic values. As the loading approaches design values, the characteristic analysis with fine meshing experiences local failure of the right corner without divergence of the analysis (coarse mesh diverged on the second load step after failure). The post strength increase is roughly 20%. Mean analysis with fine meshing experienced local failure shortly after design loads were reached (also this without divergence, while coarse mesh diverged). The strength increase was not as great as for the characteristic analysis, and the final global failure load was just shy of the characteristic capacity. These results are not optimal to use in an estimate of a coefficient of variation for material properties as it would result in a negative value using Eq. (2.19).

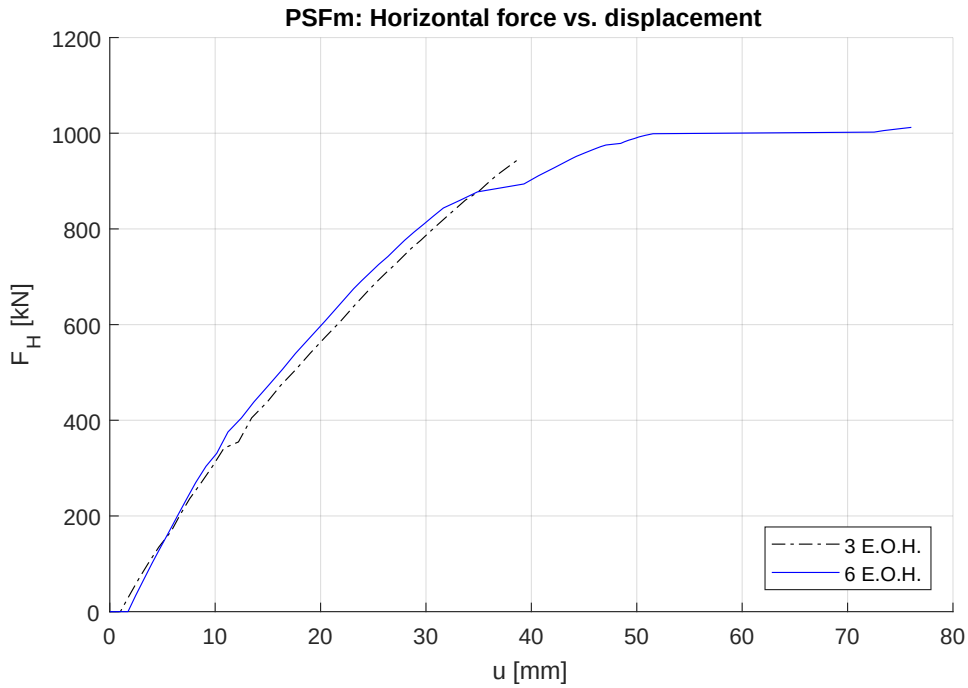

Figure 3.18: Horizontal force, F_H, vs. horizontal displacement, u, of the top right corner of the frame for PSFm analysis of load history 7. Includes the results from analyses with a mesh of 3 and 6 elements over the height (E.O.H.) of column cross sections. Load sequence 1 is left out for clarity which causes the small initial shift from the origin.

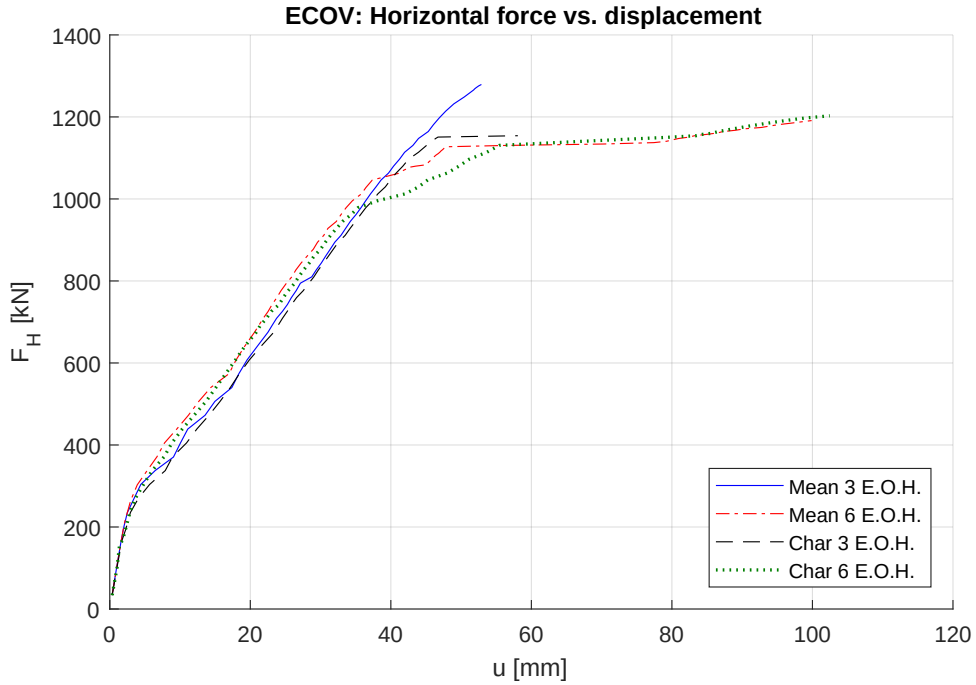

Figure 3.19: Horizontal force, F_H, vs. horizontal displacement, u, of the top right corner of the frame for ECOV analyses of load history 3. The plot includes the results from mean and characteristic (char) analyses for mesh with both 3 and 6 elements over the height (E.O.H.) of column cross sections.

In the GRFm analysis of LH7, the sensitivity is still highly visible, see Fig. 3.20. Like the other analyses with a fine mesh, the local concrete failure occurs for smaller loads. The structural stiffness post failure is equivalent to the stiffness pre failure, which is similar to the PSFm analysis of LH7. However, it is not as ductile as with the coarse mesh and diverges for a significantly smaller capacitty.

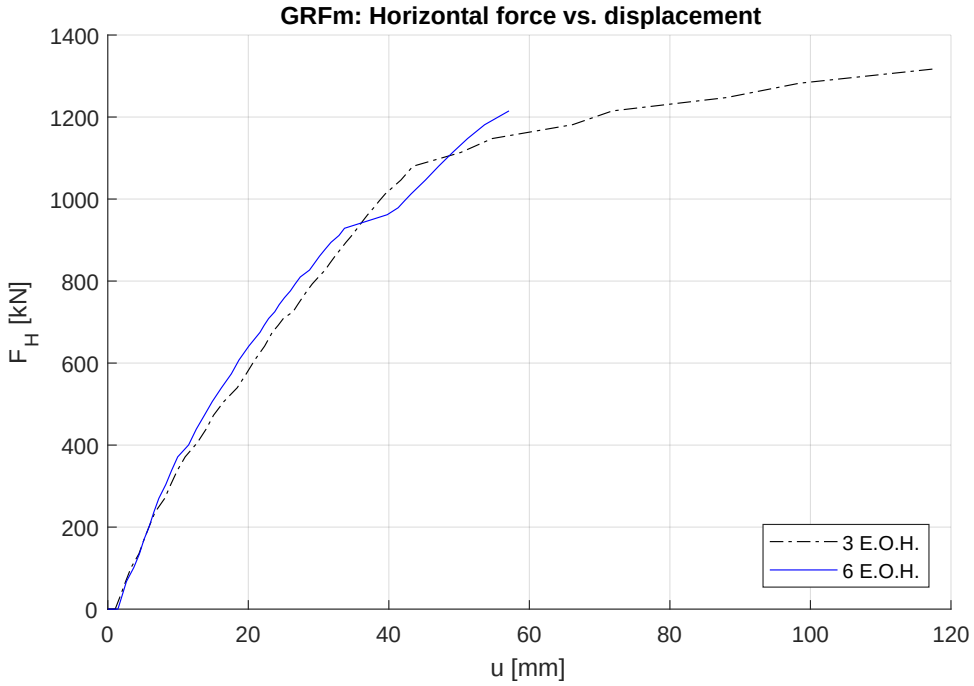

Figure 3.20: Horizontal force, F_H, vs. horizontal displacement, u, of the top right corner of the frame for GRFm analyses of load history 7. Includes the results from analyses with a mesh of 3 and 6 elements over the height (E.O.H.) of column cross sections. Load sequence 1 is left out for clarity which causes the small initial shift from the origin.

3.7 Results from nonlinear analyses of load histories

Nonlinear analyses were performed on the model described in section 3.2.2 with the material parameters stated in Section 3.5. The structural behaviour, e.g. load-displacement relations and cracking of concrete, is presented in the following subsections. The load-displacement relations and the development of crack patterns are presented in three groups of load histories depending on the initial loading sequence. This is followed by a summary of which parts of the reinforcement that are yielding at failure and by a control of the concrete failure in the right corner. The section is concluded with a presentation of the global capacities from analyses and the estimated design capacity of each safety format method for all of the load histories.

Most of the load histories have load sequences where either the vertical or horizontal force remain unchanged. These sequences are left out of the corresponding load-displacement plots for clarity. The load sequence(s) left out is specified in the figure text. This causes a horizontal shift in the plots where sequences are left out. For load sequence reference see Fig. 3.16 or Eqs. (3.1) to (3.8). All curves are labeled with the respective safety format method analysis.

3.7.1 Structural behaviour - initial vertical loading

3.7.1.1 Cracking of the frame - initial vertical loading

The three load histories with initial vertical loading, LH1, LH4 and LH7, are identical for the first two load sequences until characteristic loading is reached. The first cracks occur right beneath the vertical load at a 20-35% of characteristic vertical load, and within few load steps, cracks appear on the inside of the supports and on the outside of the frame corners. Throughout the application of the vertical load, the cracking of elements on the underside of the beam propagates towards the corners, and cracking propagates from both corners towards the mid span and supports along the outer edges of the frame. In addition, some additional cracks appear at the insides of the supports. The length of which the cracking propagates depends on tensile strength, the smaller the strength, the larger the propagation. For a visual illustration, please see the Fig. 3.6 as the pattern does not change significantly from the verification even with the updated parameter values.

When applying horizontal load, the cracks on the inside of the left support closes while propagation increases at the right support. At roughly 50% characteristic horizontal load, the outside of the left column is cracking along its entire height for all analyses. Cracking continues to propagate from the right corner and right support, while on the underside of the beam cracking mostly propagates towards the left corner. As for the cracking under vertical load, the crack pattern at the end of characteristic loading is indistinguishable from verification analyses, see Fig. 3.7.

When surpassing characteristic loads, the load histories are not equal. LH4, which only apply vertical load, experience mostly propagation of cracks on the underside of the beam in left and right directions. In addition, some propagation is seen in the right column, as cracking on the outside extends downwards from the right corner and on the inside extending upwards from the support. In the last sequence of LH4, the crack zones continue to merge in the right column and between mid span and both columns. An illustration of the crack pattern right before concrete failure of the top right corner can be seen in Fig. 3.21.

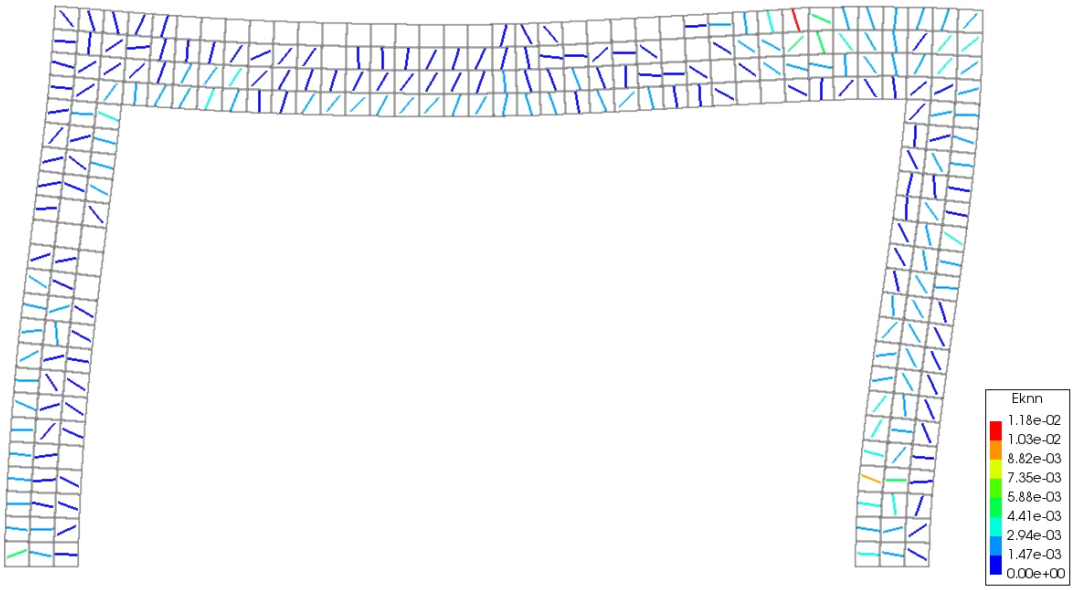

Figure 3.21: Crack pattern before concrete failure for load history 4. From mean ECOV analysis. Eknn is the crack strains perpendicular to the crack direction.

LH1 and LH7 are identical until loading reaches the design load level. The simultaneous loading from characteristic load level causes cracking to propagate on the underside of the beam towards the left corner, along the outside of the frame from the right corner towards both mid span and right support, upwards from inside the right support, and increased cracking of the outer part of the left column. From design load level, the crack pattern of LH1 remains virtually unchanged until concrete failure. The crack pattern of LH1 before failure is seen in Fig. 3.22. In contrast, LH7 experiences some cracking at the interior of the left corner and ends up with a crack pattern similar to that of LH4 before concrete failure.

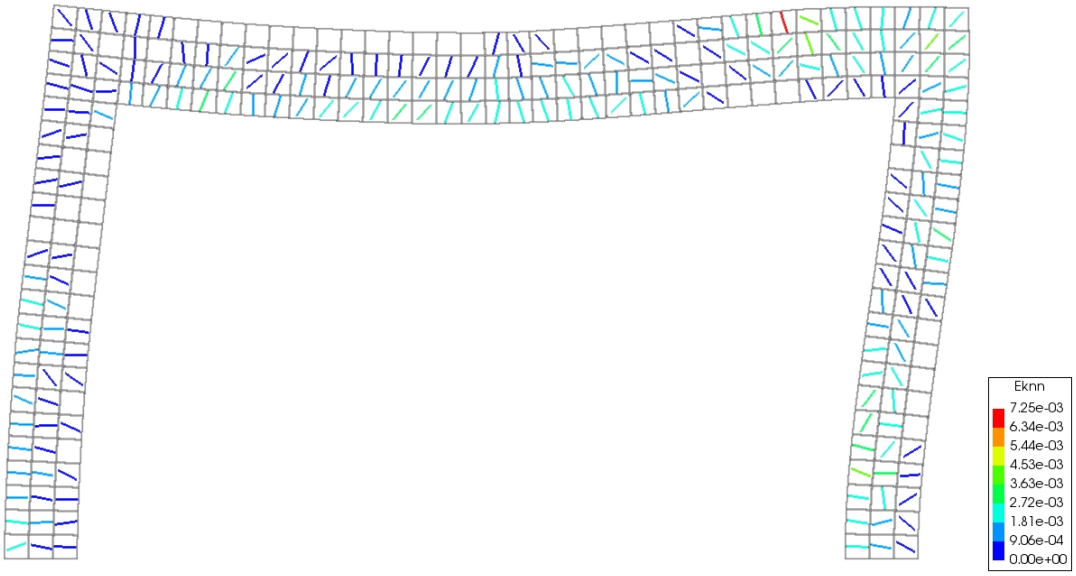

Figure 3.22: Crack pattern before concrete failure for load history 1. From mean ECOV analysis. Eknn is the crack strains perpendicular to the crack direction.

3.7.1.2 Loads and displacement - initial vertical loading

The initial stiffness of the frame shows a clear elastic behaviour. At the appearance of cracking, the stiffness gradually decreases during increased loading until more than half of the characteristic horizontal load is applied. From here, the cracking seems to have stabilized and the stiffness becomes more linear again. The stiffness undergoes one last great reduction at (or right before) concrete failure of the top right corner. All this is visible in the load-displacement curves given in Figs. 3.23 to 3.28. Note that the vertical displacement increases during load sequence 2. Although the vertical load-displacement plot of LH7 is almost identical to LH4, it is included to show the PSFm curve does not reach design load levels, as it diverges at 1026 kN.

Because the vertical load of LH4 and LH7 does not increase above design loading, the load-displacement plots have been restricted to the load sequences where vertical load is increasing. The resulting changes in vertical displacement is therefore not visible in the Figs. 3.25 and 3.27. In LH4, the vertical displacement remains constant or experience a slight increase for all analyses as horizontal load is increased above characteristic loading. During load sequence 4, PSFm diverges before design values are reached, and vertical displacement for GRFm does not change before local failure, but increases after failure. For the mean ECOV analysis, vertical displacement is reduced when horizontal load exceeds design level which continues until global failure. The total reduction amounts to roughly 15% compared to the displacement at design load level. Meanwhile, characteristic ECOV displacement does not change until global failure.

Above design load level, LH7 experienced similar behaviour as LH4, and mean ECOV analysis experienced a displacement reduction of roughly 14%. In addition, PSFm analysis did not reach design levels, characteristic ECOV analysis retained a constant vertical displacement, and GRFm analysis failed locally in the right corner before increasing the vertical displacement.

For the load histories with initial vertical loading, all safety format methods except the GRFm diverged when the interior of the top right corner failed in concrete compression. An illustration of such a crushing can be seen in Fig. 3.29. The divergence of the PSFm and characteristic ECOV analysis for LH1 stands in contrast to the verification analyses, where the same analyses did not diverge at first concrete failure. The more brittle behaviour does not affect the PSFm capacity to a significant degree compared to the verification analyses, however, the stiffness is greatly increased due to a large increase of the stiffness modulus of steel and concrete. Meanwhile, the characteristic ECOV capacity is slightly reduced compared to the verification analyses as a result of the tensile strength of concrete and ultimate strain of reinforcement being reduced.

As the GRFm analyses do not diverge at the concrete failure of the right corner, the capacity is increased due to a redistribution of forces. At failure, the right hand corner becomes a plastic hinge and looses some of its strength. Consequently, the load effects must be carried by other parts of the frame. The vertical loading is being carried by the beam which now more represents a simply supported beam which increases the compressive stresses in the mid span. Likewise, the horizontal load is carried to a greater extent by the columns which acts more like counter lever beams fixed at the supports. As the loading continues, the stress increase at the supports is significant. This redistribution increases the global capacity with roughly 20%. Illustrations are given in Fig. 3.30 which show the principal compressive

stresses for the GRFm analysis of LH1 right before compressive failure, and Fig. 3.31 which show the principal compressive stresses from the same analysis right before global failure.

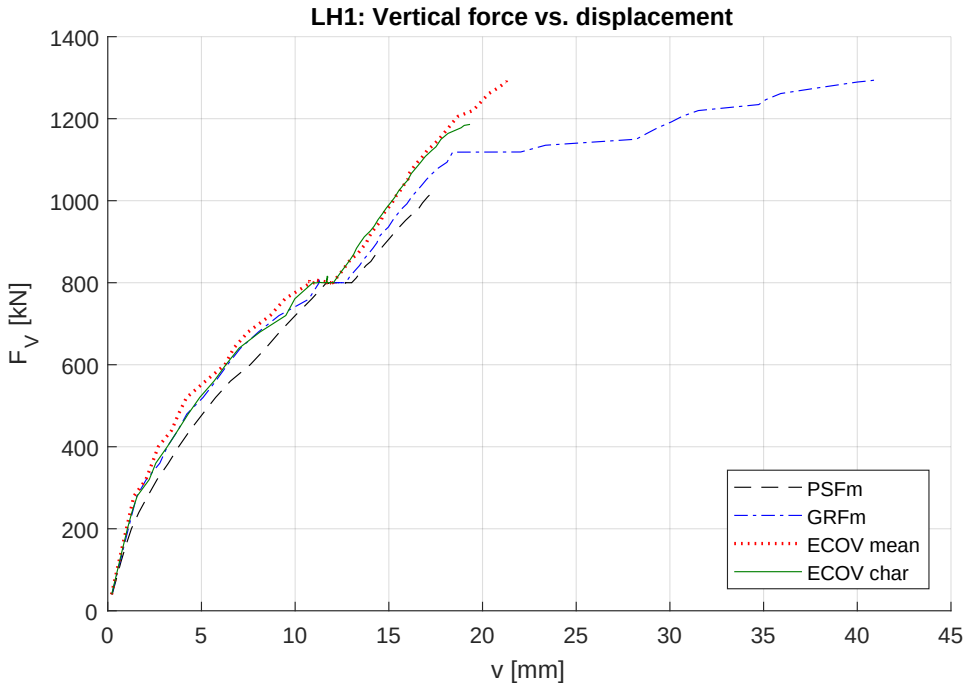

Figure 3.23: Vertical force, F_V, vs. vertical displacement, v, in mid span of the frame for all NLFEA (see legend) of load history 1. Load sequence 2 is left out for clarity which causes the horizontal shift at 800 kN.

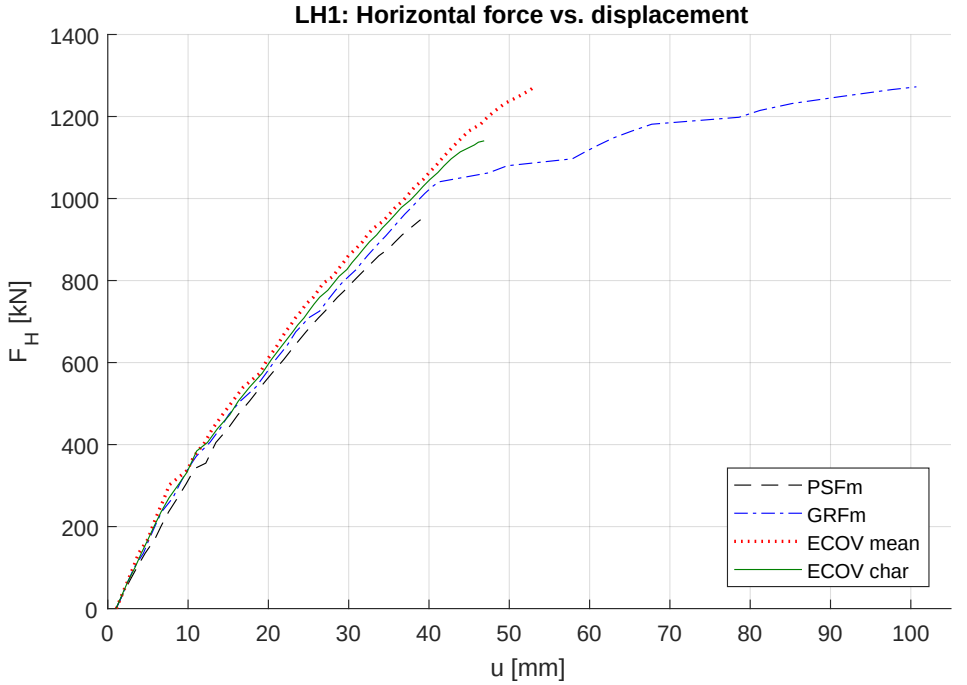

Figure 3.24: Horizontal force, F_H, vs. horizontal displacement, u, of the top right corner of the frame for all NLFEA (see legend) of load history 1. Load sequence 1 is left out for clarity which causes the small initial shift from the origin.

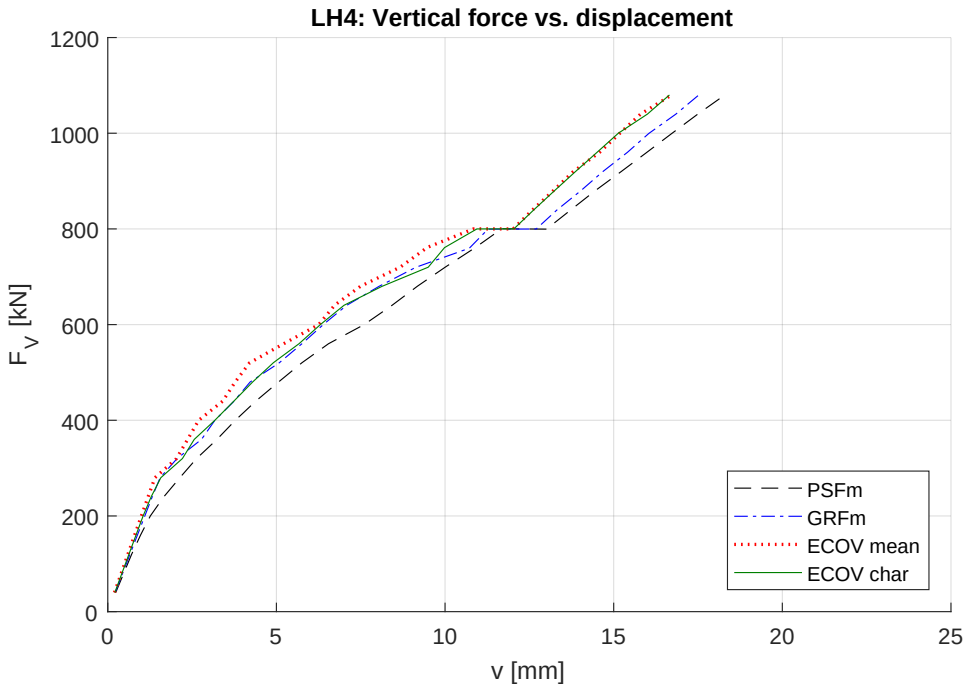

Figure 3.25: Vertical force, F_V, vs. vertical displacement, v, in mid span of the frame for all NLFEA (see legend) of load history 4. Load sequence 2 and 4 is left out for clarity which causes the horizontal shift at 800 kN and the cut off at 1080 kN respectively.

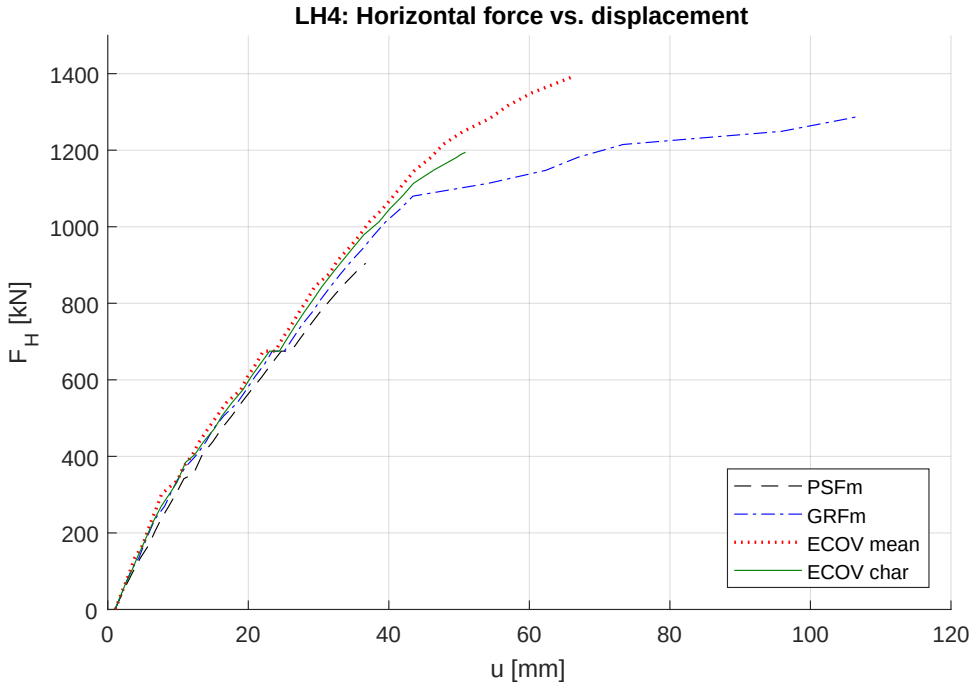

Figure 3.26: Horizontal force, F_H, vs. horizontal displacement, u, of the top right corner of the frame for all NLFEA (see legend) of load history 4. Load sequence 1 and 3 is left out for clarity which causes the small initial shift from the origin and the horizontal shift at 675 kN respectively.

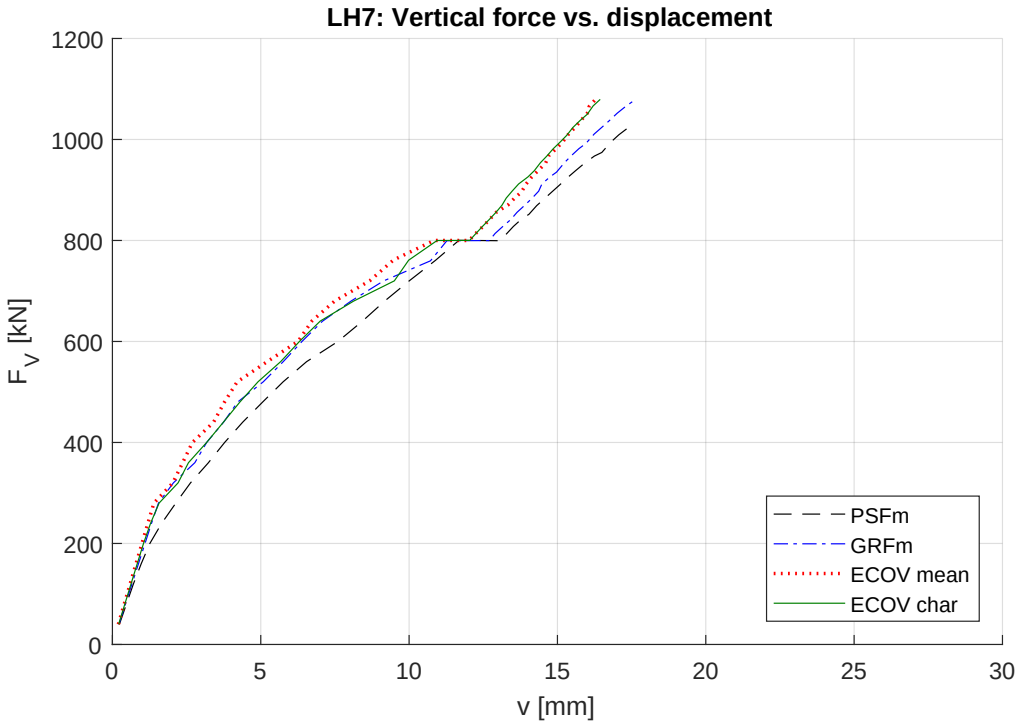

Figure 3.27: Vertical force, F_V, vs. vertical displacement, v, in mid span of the frame for all NLFEA (see legend) of load history 7. Load sequence 2 and 4 is left out for clarity which causes the horizontal shift at 800 kN and the cut off at 1080 kN respectively.

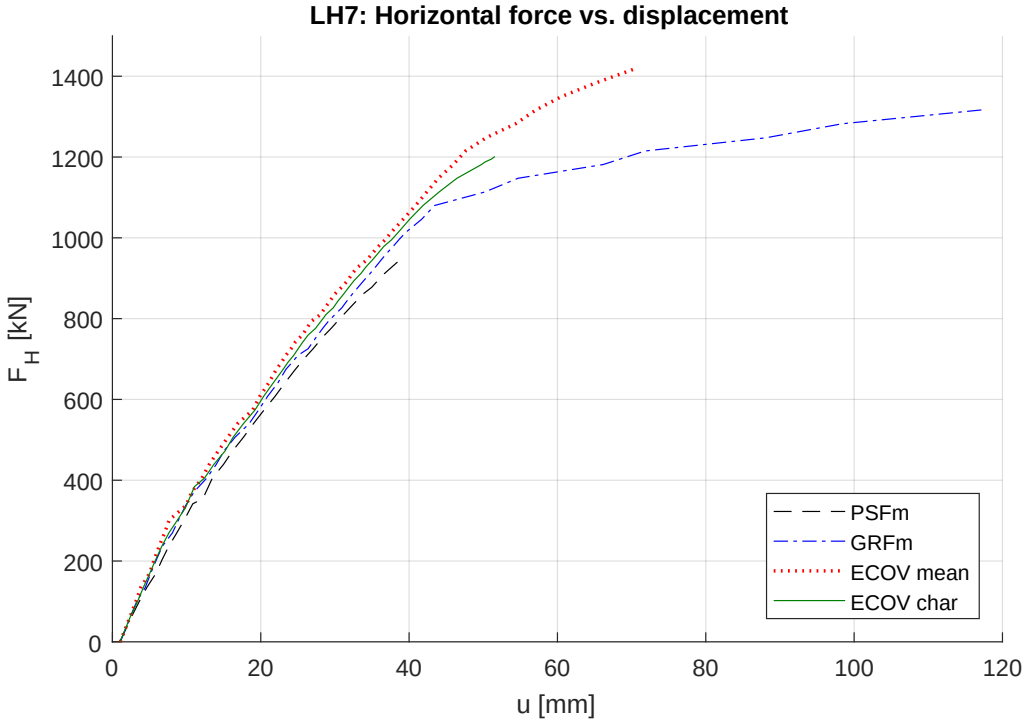

Figure 3.28: Horizontal force, F_H, vs. horizontal displacement, u, of the top right corner of the frame for all NLFEA (see legend) of load history 7. Load sequence 1 is left out for clarity which causes the small initial shift from the origin.

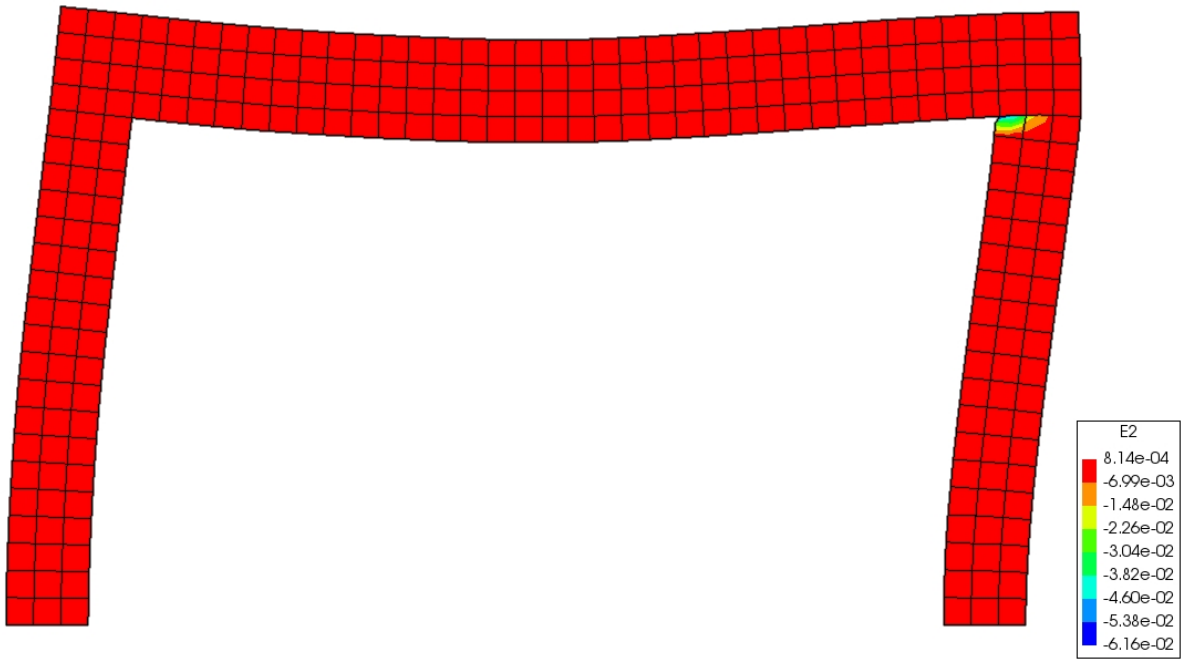

Figure 3.29: Illustration of concrete compressive failure in the column at the right frame corner. From GRFm analysis for load history 1. The figure show the principal compressive strains ε_2 (E2 in figure) at a time after compressive failure of the top right frame corner.

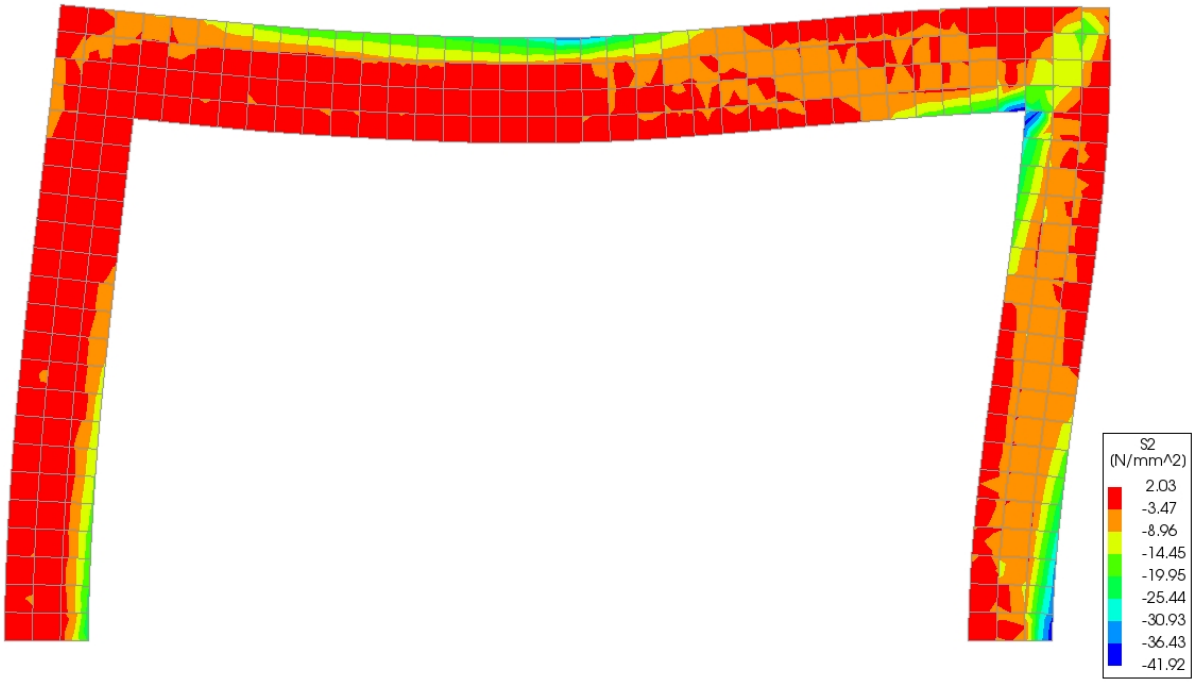

Figure 3.30: Illustration of principal concrete compressive stresses (S2, measured in MPa) in the frame right before concrete failure of the top right corner. From GRFm analysis for load history 1.

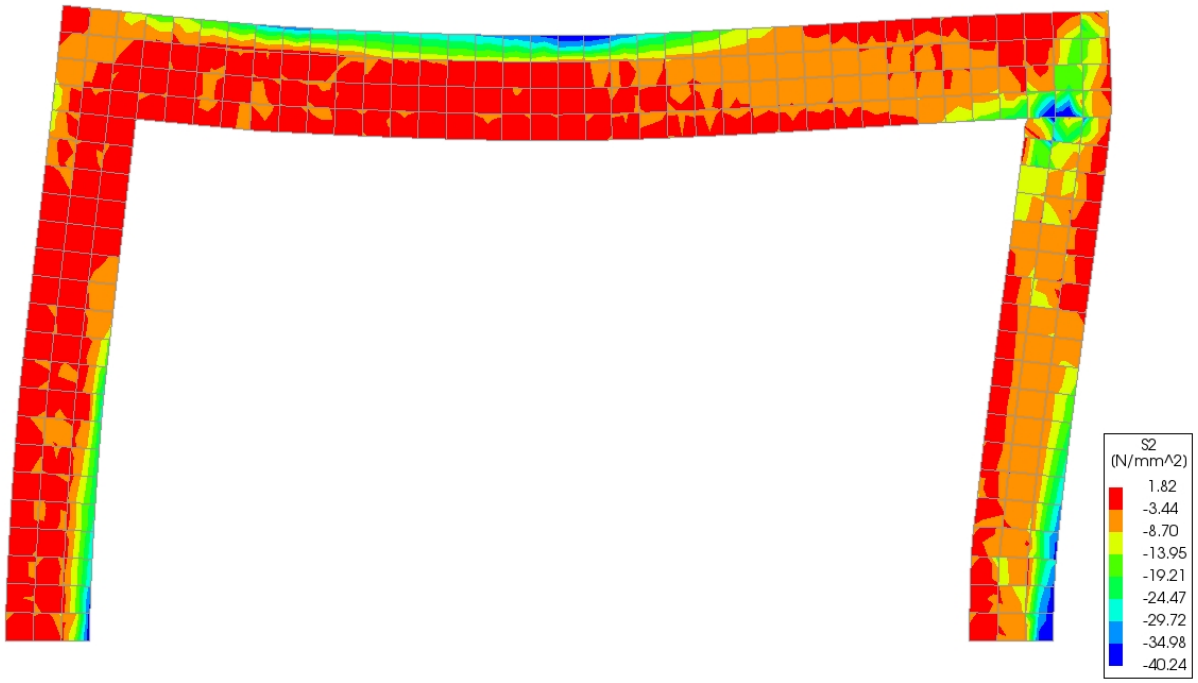

Figure 3.31: Illustration of principal concrete compressive stresses (S2, measured in MPa) in the frame right before global failure. From GRFm analysis for load history 1.

3.7.2 Structural behaviour - initial horizontal loading

3.7.2.1 Cracking of the frame - initial horizontal loading

As for histories with initial vertical loading, the load histories with initial horizontal loading are identical until characteristic load levels. These are LH2, LH5 and LH8. From characteristic levels, LH2, LH5 and LH8 are respectively identical to LH1, LH4 and LH7.

For these histories with initial horizontal loading, the first cracks appear in the column on the inside of the top left corner, and at the left side of the support of both columns. This occur for 15-20% of characteristic horizontal loading and contributes to a significant change in structural stiffness, more on that later. The cracking propagates upwards from the supports and downward from the left corner as loading increases. Next to crack is the outside of the top right corner, which then proceeds to spread toward the mid span and towards the support at increased loading. When horizontal load reaches characteristic values, the crack pattern is identical to Fig. 3.8 of the verification analyses. When vertical load is applied, cracking almost exclusively propagates from inside the top left corner and into the beam. Some additional propagation happens at the right corner, but this is relatively small in comparison. At characteristic loads, the crack pattern is identical to the pattern seen in Fig. 3.9.

During loading from characteristic to design values, there were no difference between cracking even though LH5 differs from LH2 and LH8. The crack pattern remained mostly unchanged with the exception of some propagation in the upper and lower part of the right column and right half of the beam. For loading above design levels, all histories experienced additional propagation of cracking in both columns and right half of the beam, and the cracked sections merge together into a completely cracked frame. Before concrete failure

of the right corner, most of the elements were cracked. The crack patterns before failure of mean ECOV analysis for LH2 and LH5 can be seen in Figs. 3.32 and 3.33.

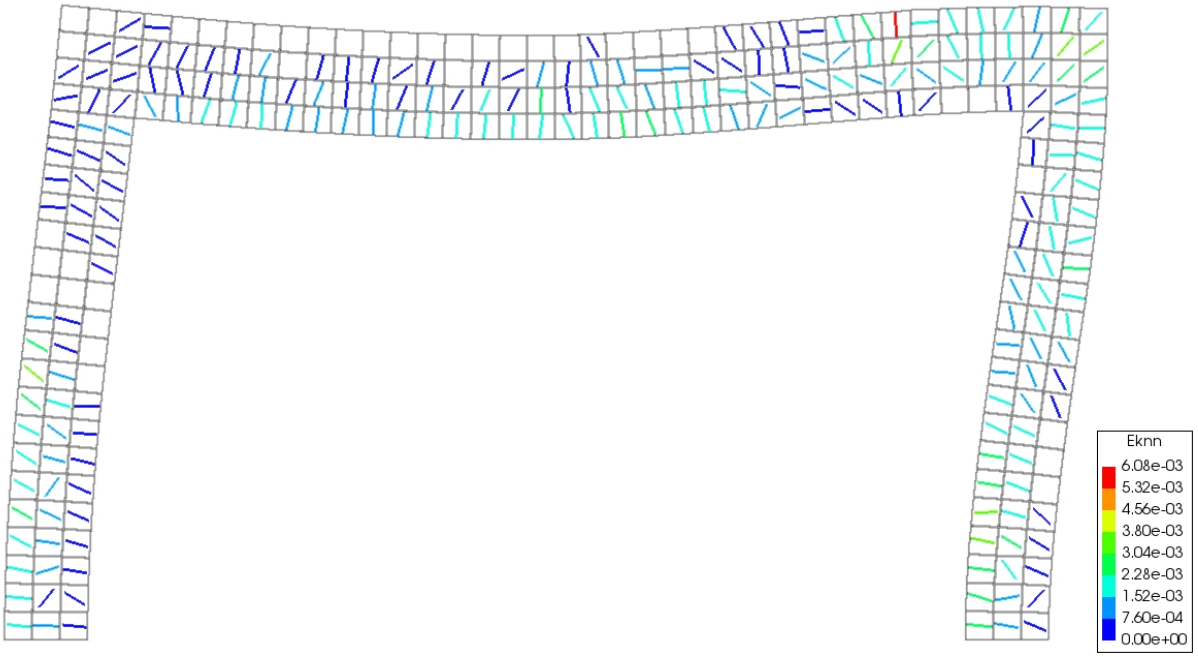

Figure 3.32: Crack pattern immediately before failure for load history 2. From mean ECOV analysis. Eknn is the crack strains perpendicular to the crack direction.

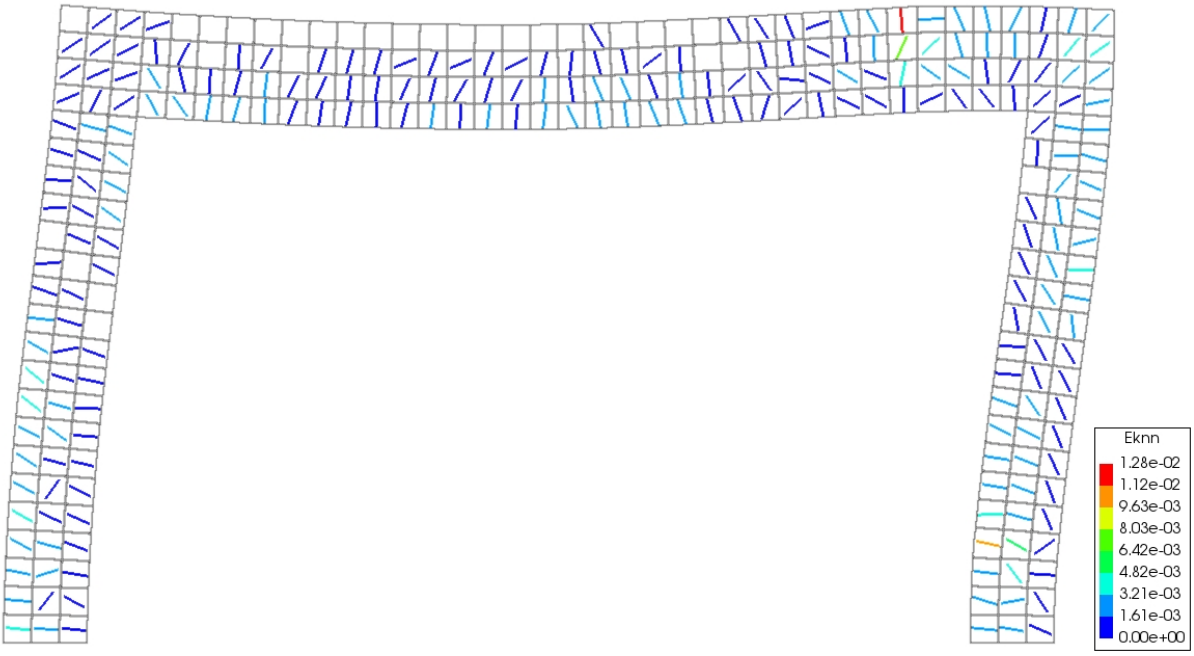

Figure 3.33: Crack pattern immediately before failure for load history 5. From mean ECOV analysis. Eknn is the crack strains perpendicular to the crack direction.

3.7.2.2 Loads and displacement - initial horizontal loading

The structural stiffness is elastic for an initial horizontal load smaller than 25% of characteristic load, where it is significantly reduced due to cracking. The new reduced stiffness remain fairly constant until half way into load sequence 2 and vertical loading. Then there is another stiffness reduction as the top beam is cracking. Note that the horizontal displacement now is reduced due to characteristic vertical loading, while the vertical displacement was increased by horizontal loading. The load-displacement curves are visible in Figs. 3.34 to 3.39. The vertical load-displacement plot for LH8 is provided as the PSFm analysis did not diverge at concrete failure of the right corner, else the plot is very similar to the plot of LH5. There is a deviance in the GRFm curve of Fig. 3.37 close to divergence, and this is assumed to be a numerical error as it clearly exceeds the applied loading. When thoroughly checking the analysis, there was found to be some spurious stresses in one of the elements at the left support which caused the spike in recorded loading.

For loading above characteristic level, the behaviour is very similar to the group of histories with initial vertical loading. There is a slight stiffness increase for vertical load-displacements, which is easier to see for the load histories with initial horizontal loading. The behavior of the different safety methods does not seem to differ between the two groups of histories for loading above design loads. The only exception is the now ductile behaviour of PSFm, where the analyses experience concrete failure at smaller loads, but does not diverge. The analyses then benefit from the capacity increase caused by redistribution of forces. However, this strength increase is not as substantial as it is for GRFm, and PSFm analyses diverge before reaching design load level.

The mean ECOV analyses of LH5 and LH8 experienced a reduction in vertical displacement for loading above design load level. This is the same behaviour as mean ECOV analyses showed for LH4 and LH7. The reduction is 15% and 20% for LH5 and LH8 respectively. No further reduction was observed for the other analyses though vertical displacement increased for GRFm after concrete failure of the right corner.

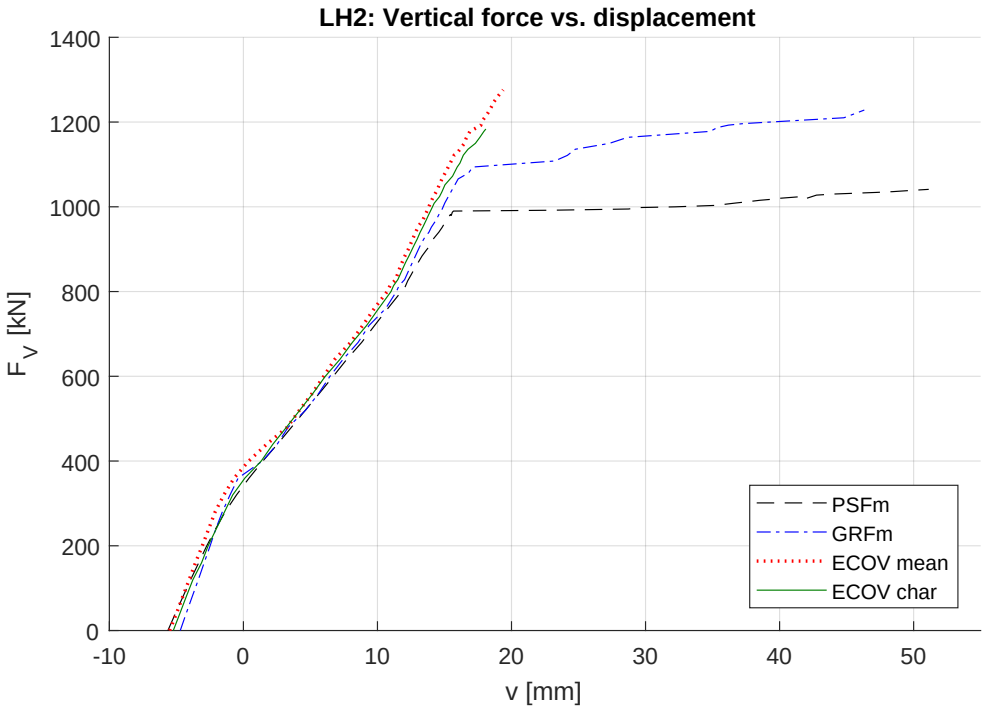

Figure 3.34: Vertical force, F_V, vs. vertical displacement, v, in mid span of the frame for all NLFEA (see legend) of load history 2. Load sequence 1 is left out for clarity which causes the initial shift from the origin.

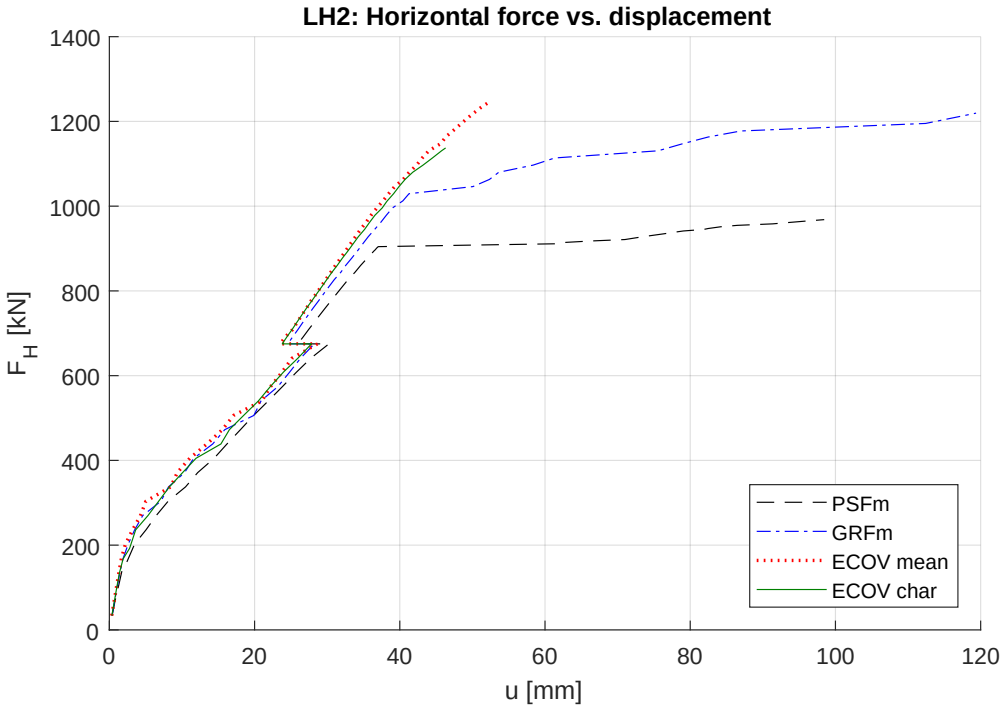

Figure 3.35: Horizontal force, F_H, vs. horizontal displacement, u, of the top right corner of the frame for all NLFEA (see legend) of load history 2. Load sequence 2 is left out for clarity which causes the horizontal shift at 675 kN.

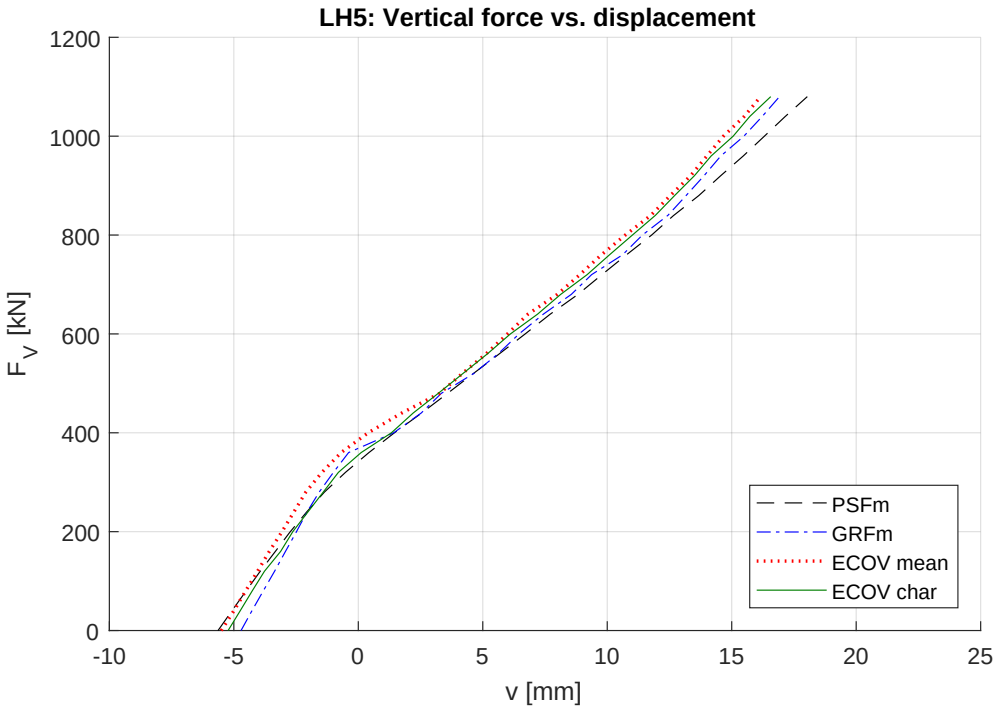

Figure 3.36: Vertical force, F_V, vs. vertical displacement, v, in mid span of the frame for all NLFEA (see legend) of load history 5. Load sequence 1 and 4 is left out for clarity which causes the initial shift from the origin and the cut off at 1080 kN respectively.

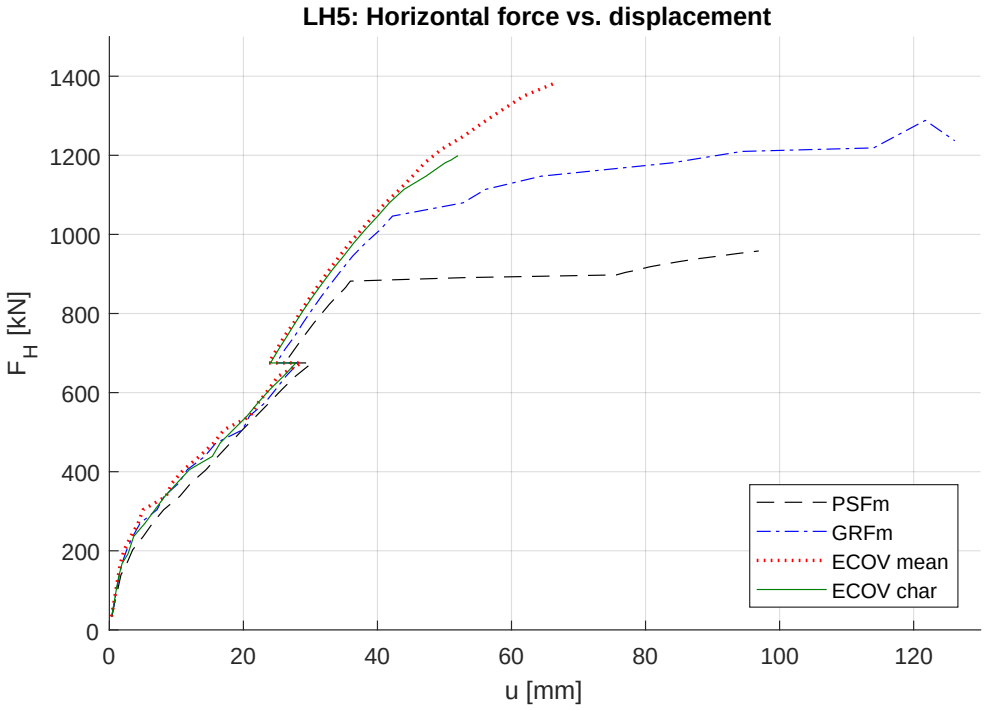

Figure 3.37: Horizontal force, F_H, vs. horizontal displacement, u, of the top right corner of the frame for all NLFEA (see legend) of load history 5. Load sequence 2 and 3 is left out for clarity which causes the horizontal shift at 675 kN.

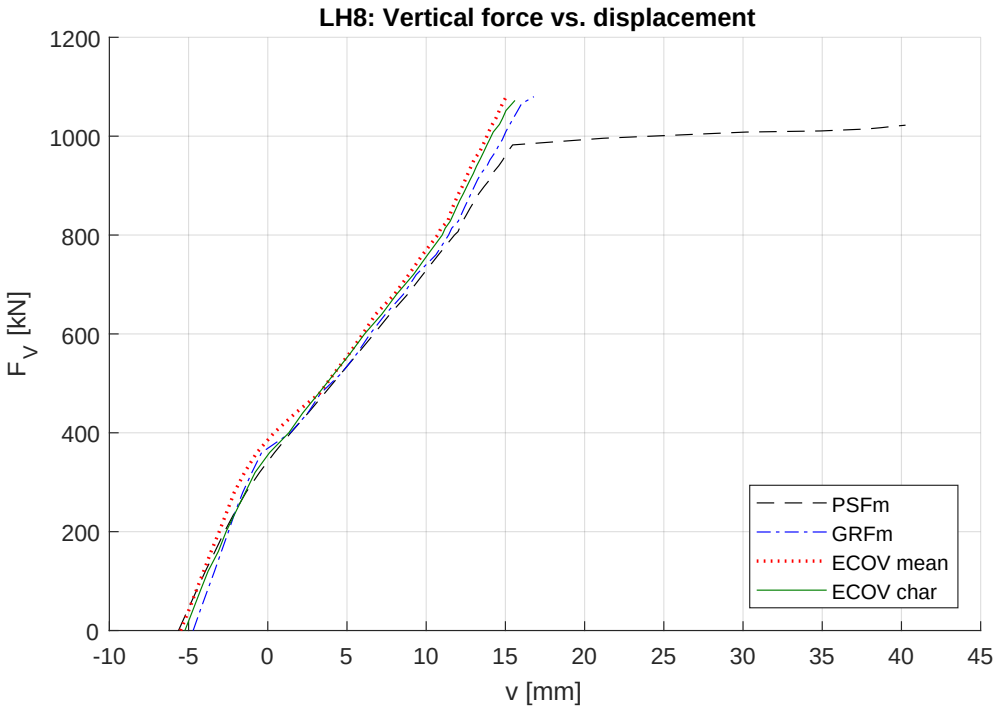

Figure 3.38: Vertical force, F_V, vs. vertical displacement, v, in mid span of the frame for all NLFEA (see legend) of load history 8. Load sequence 1 and 4 is left out for clarity which causes the initial shift from the origin and the cut off at 1080 kN respectively.

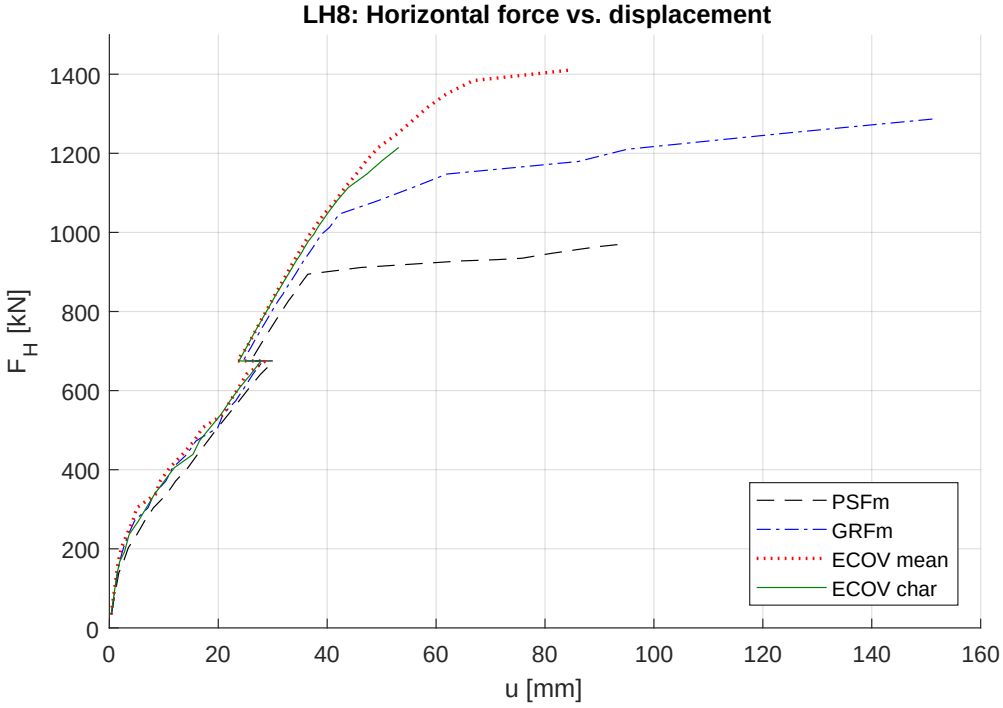

Figure 3.39: Horizontal force, F_H, vs. horizontal displacement, u, of the top right corner of the frame for all NLFEA (see legend) of load history 8. Load sequence 2 is left out for clarity which causes the horizontal shift at 675 kN.

3.7.3 Structural behaviour - initial simultaneous loading

3.7.3.1 Cracking of the frame - initial simultaneous loading

The last group of load histories contains LH3 and LH6. These histories have an initial loading of both vertical and horizontal load. Due to the relative loading of LH6 from zero to design load level , it will not obtain a characteristic load level. Though the load histories have small differences, the behaviour of the frame is very similar for both histories. The first cracks appear for loading between 15-25% of characteristic loads depending on the safety format method. Cracks appear almost simultaneously at the left side of both supports, on the underside of the beam in mid span, and on the outside of the right frame corner. The cracking propagates to both sides from the initial cracks. That is left and right in the beam, left and down from the right corner, and upwards from the supports. The crack pattern for LH3 at characteristic load level is presented in Fig. 3.40. Increasing the loading above characteristic values caused some additional propagation in the top and bottom halves of the right column and in the beam towards the left corner. At design values the crack patterns are close to identical and the pattern for LH6 is seen in Fig. 3.41.

As the loading above design levels are different, the patterns start to differ as well. The pattern for LH3 barely changes until concrete failure, just a few additional cracks in the beam and the right column, see Fig. 3.42. Meanwhile, a lot of cracking occur for LH6 in the left corner and in the top of the left column. Some additional propagation is also visible in the right column. Fig. 3.43 shows the pattern before global failure occur for LH6.

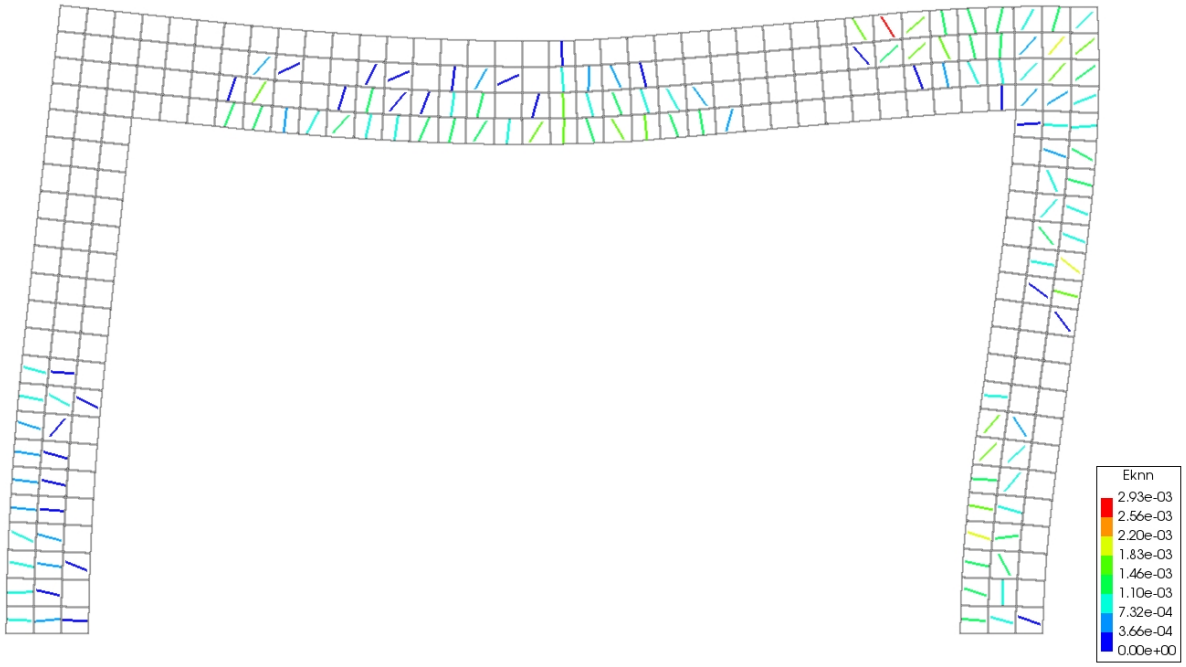

Figure 3.40: Crack pattern at characteristic loading for load history 3. From mean ECOV analysis. Eknn is the crack strains perpendicular to the crack direction.

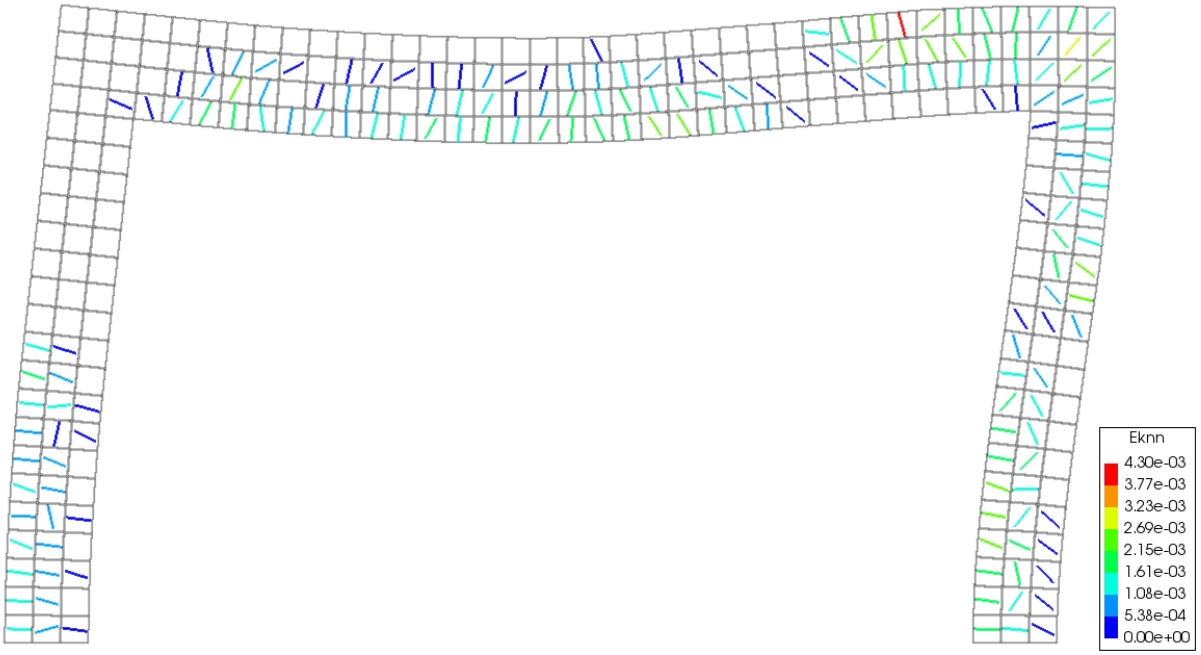

Figure 3.41: Crack pattern at design loading for load history 6. From mean ECOV analysis. Eknn is the crack strains perpendicular to the crack direction.

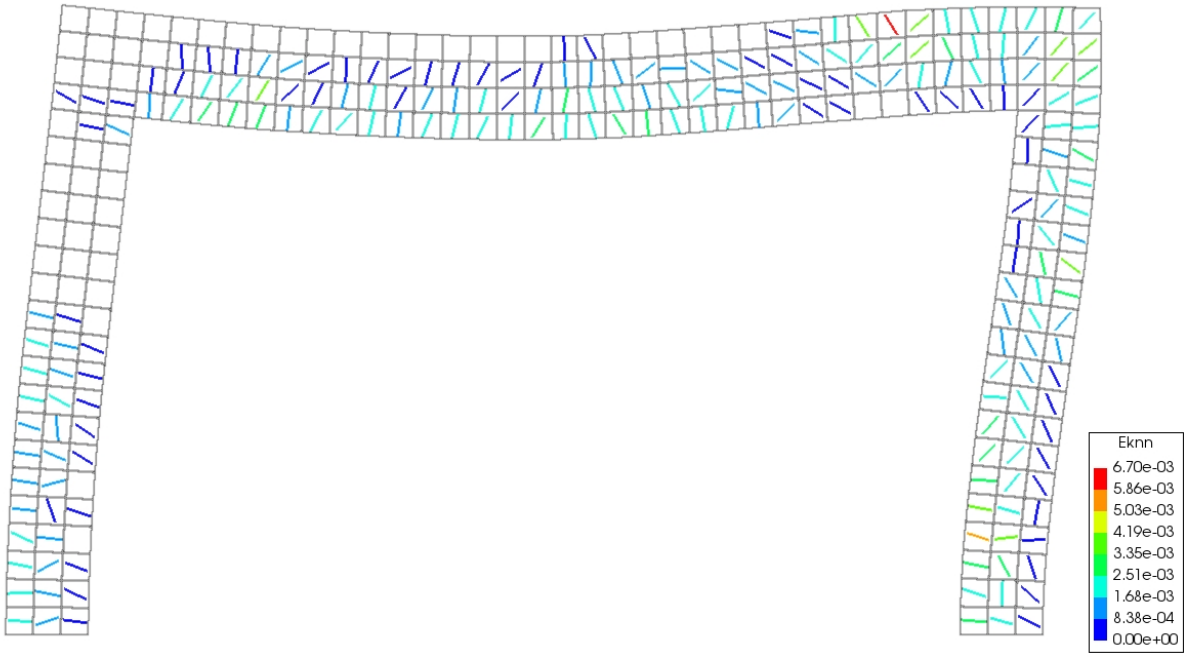

Figure 3.42: Crack pattern close to global failure for load history 3. From mean ECOV analysis. Eknn is the crack strains perpendicular to the crack direction.

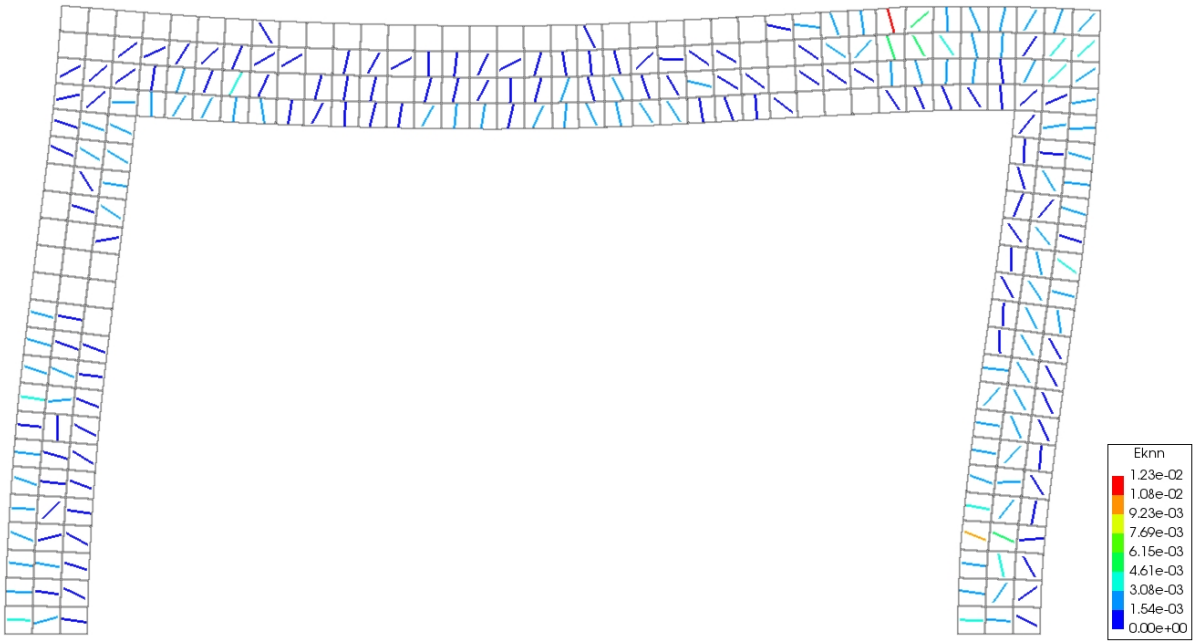

Figure 3.43: Crack pattern close to global failure for load history 6. From mean ECOV analysis. Eknn is the crack strains perpendicular to the crack direction.

3.7.3.2 Loads and displacement - initial simultaneous loading

Similar to the earlier load histories, the initial structural behavior is linear. At the appearance of cracking, the stiffness is reduced but then remain constant during loading up to design load level. The stiffness does not change when exceeding characteristic load, only changing when the frame is close to concrete failure. The load-displacement curves for LH3 and LH6 are seen in Figs. 3.44 to 3.47. Note that the PSFm analysis for LH6 diverges at concrete failure but does not for LH3, while neither of the two PSFm analyses ever reach design load level. Furthermore, the post failure capacity increase of GRFm and PSFm for LH3 is the smallest of such increases out of all the load histories that were analyzed.

For LH6, when the horizontal load is increased above design level, the vertical displacement is reduced in the mean ECOV analysis. The reduction before global failure occurs is about 17%. No other analysis of LH6 experience this reduction before failure. This behaviour is therefore seen in all the load histories where only horizontal load is applied beyond design load level.

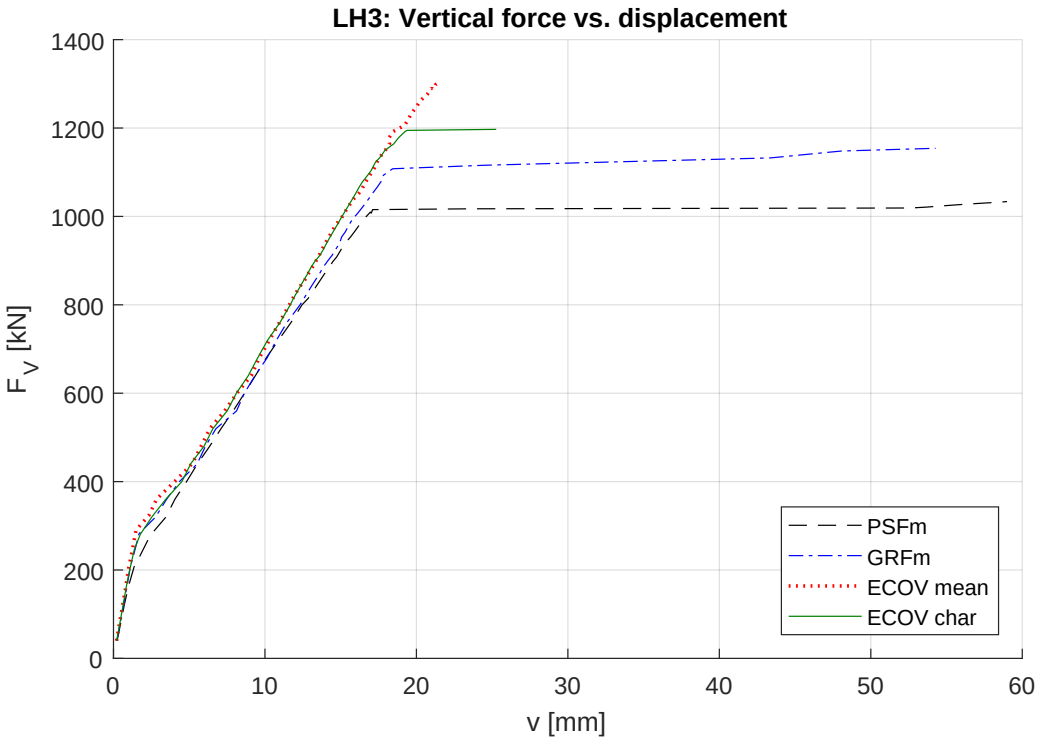

Figure 3.44: Vertical force, F_V, vs. vertical displacement, v, in mid span of the frame for all NLFEA (see legend) of load history 3.

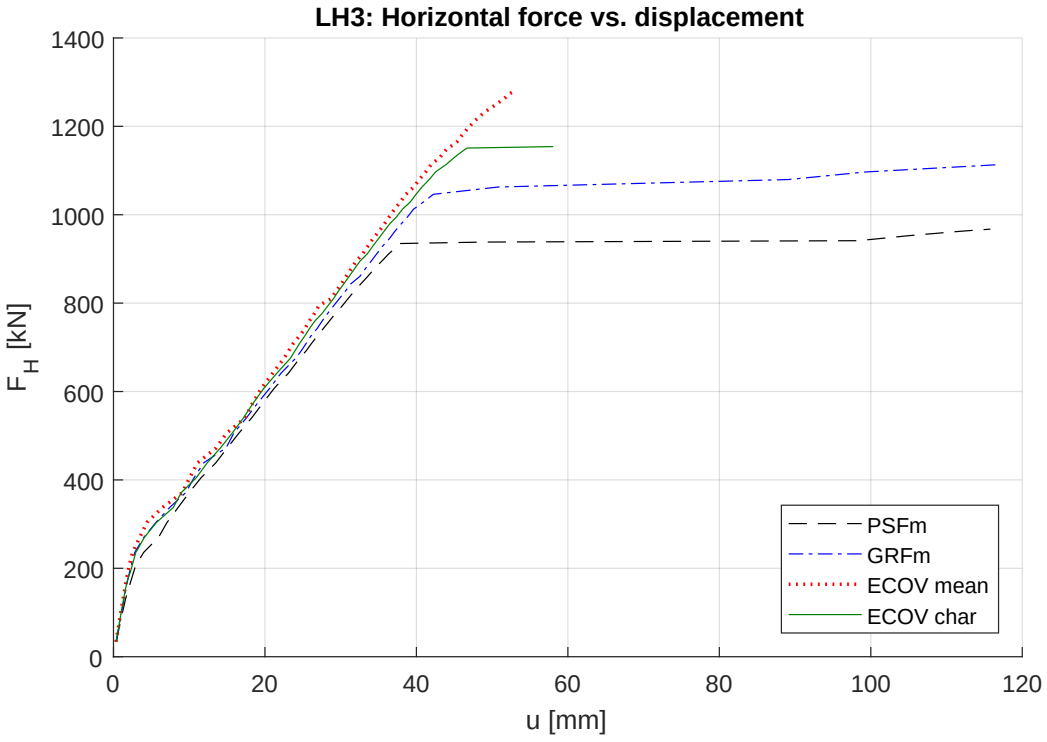

Figure 3.45: Horizontal force, F_H, vs. horizontal displacement, u, of the top right corner of the frame for all NLFEA (see legend) of load history 3.

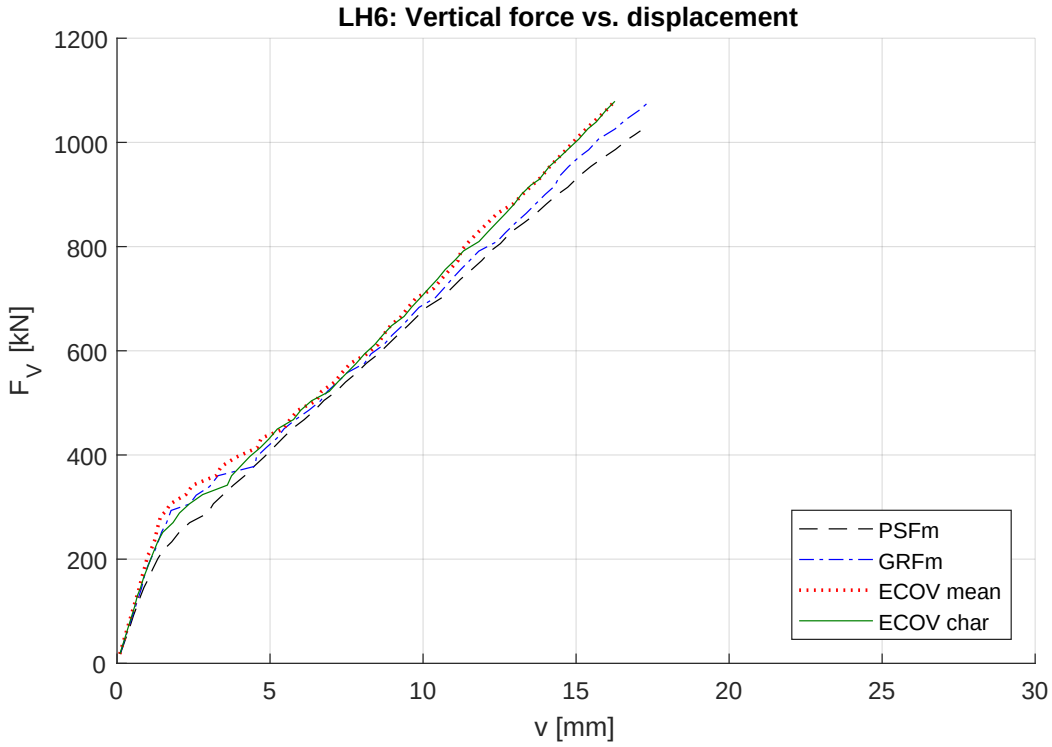

Figure 3.46: Vertical force, F_V, vs. vertical displacement, v, in mid span of the frame for all NLFEA (see legend) of load history 6. Load sequence 2 is left out for clarity which causes the cut off at 1080 kN.

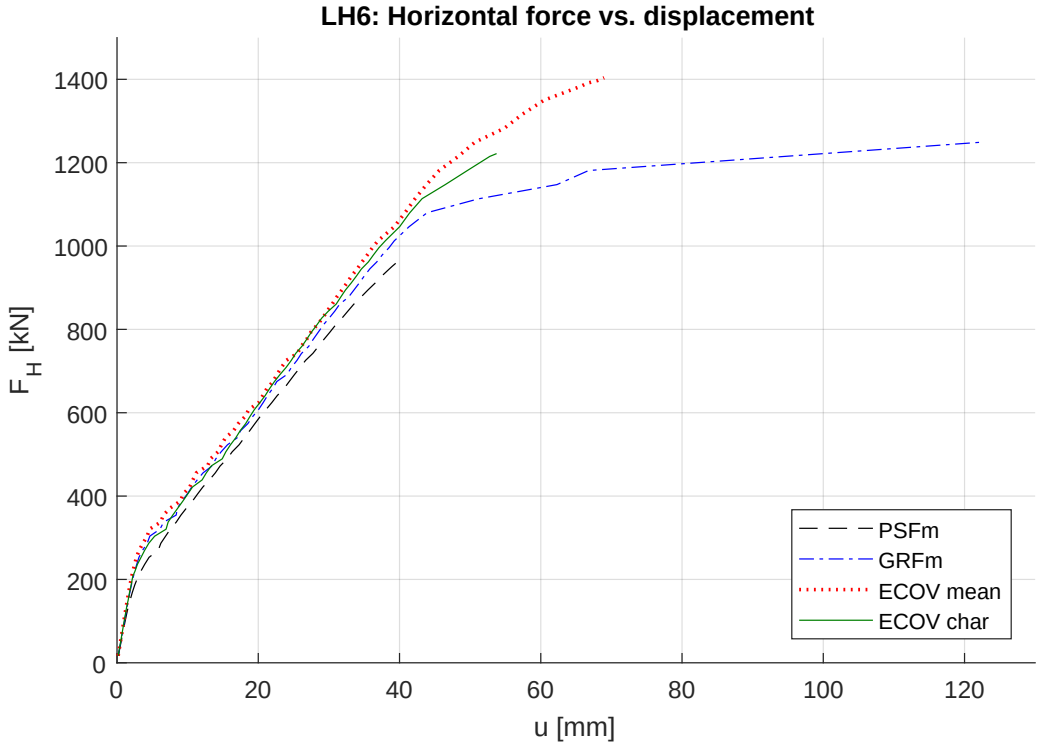

Figure 3.47: Horizontal force, F_H, vs. horizontal displacement, u, of the top right corner of the frame for all NLFEA (see legend) of load history 6.

3.7.4 Yield of reinforcement

By looking at the crack plots from the analyses before global failure, the strains across some cracks clearly reveal yielding of the reinforcement. This causes structural stiffness reduction in the frame prior to concrete failure by introducing sections with localized yield of reinforcement. This change can be observed before concrete failure occur by studying the curves of the load-displacement plots in Sections 3.7.1 to 3.7.3. An illustration of the reinforcement stresses prior to failure of the characteristic ECOV analysis of LH1 is presented in Fig. 3.48. The figure also includes numerated zones for later reference. For some analyses that survived the local concrete crushing of the right frame corner, the redistribution of forces would cause yielding in additional sections of the frame while previously yielding sections had their reinforcement stresses reduced. This is most noticeable for the longitudinal reinforcement in zone (6) of Fig. 3.48. The only occurrence of yield in compression was in zone (7).

For the undetermined frame to achieve a global failure, it would need to fail in several points in order to create a mechanism of failure. This does not imply that the capacity will increase after local concrete failure of the right corner. If the concrete failure causes a reduction of the corner's load bearing capacity to such an extent that load effects on other parts of the frame exceed their capacity, then global failure would occur. Before global failure, the reinforcement yields in several places for all analyses, and Table 3.13 summarizes the yielding of the longitudinal reinforcement with yield zone references to Fig. 3.48. In addition, yield of reinforcement stirrups are given in parentheses. The table gives information about PSFm and GRFm from two separate load steps. These are the moment before local failure of the right frame corner denoted as 'local' and the moment before global failure denoted as 'global'. If the local and global failure for PSFm is the same exact failure, e.g. for LH1, then the 'local' column is marked with an * and the yield zones are stated in the 'global' column instead. As the analyses with the ECOV method reach global failure at the first compressive concrete failure, the table does not separate the yielding as for the other methods, however, it does separate the characteristic and mean analyses.

From the results seen in Table 3.13, it appears that the ratio of yield stress divided by compressive strength causes a change in behaviour for the frame. The analyses of methods with the largest ratio, the PSFm and GRFm, show an early compressive failure with very little reinforcement yield prior to failure. Then, a redistribution of forces causes an increase in capacity and the frame starts yielding in several locations before experiencing a global failure. Meanwhile, for mean and characteristic ECOV which have a smaller yield stress to compressive strength ratio, the frame is yielding in many additional sections at the time the right corner fails in concrete compression. The number of sections yielding in ECOV analyses is almost as great as for the ductile failures of the GRFm. This may explain why ECOV analyses diverge at the first concrete failure, and that there are no post failure capacity increase by redistributing load effects as seen in GRFm analyses.

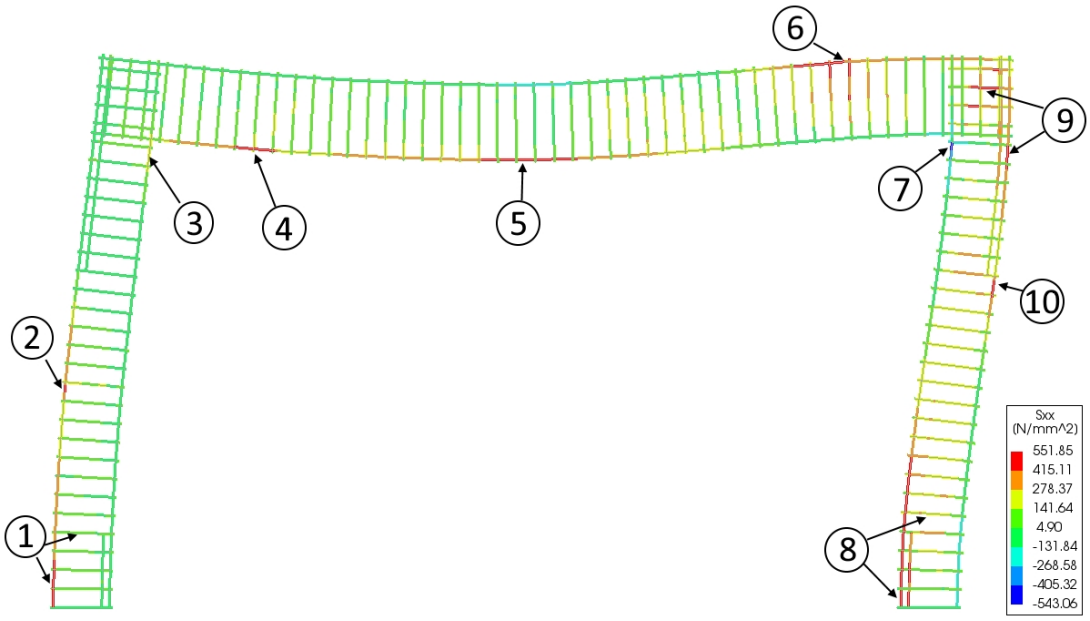

Figure 3.48: Reinforcement yield zones of the frame. Illustration from the mean ECOV analysis for load history 1. The figure show the Cauchy total stresses (Sxx, in MPa) at integration points in relation to the local reinforcement axes. Yielding for the illustrated analysis occur at zones 4, 6, 7, 8 and 10, with other zones being close to yielding.

Table 3.13: Yield zones of reinforcement at global failure for NLFEA. Zones given in Fig. 3.48. Yield of stirrups given in parentheses. In addition, yielding at local concrete failure is given for GRFm and PSFm. Where local and global failure for PSFm occur at the same time, the local column is marked with *.

Load	ECOV		GRFm		PSFm	
history	mean	char	Local	Global	Local	Global
LH1	4,6,7,8,10	4,6,7,8	6	1,2,4,5,7,8,9 (4,8,9)	*	4,6,7,8 (9)
LH2	2,6,7,8,10	6,7,8,10 (9)	7	1,2,4,5,7,8,9 (8)	10	1,2,4,5,7,8,9 (2,9)
LH3	2,4,6,7,8,10 (6,9)	2,4,6,7,8,9,10 (9)	6,7	1,2,4,5,7,8,9 (4,8)	6 (9)	1,2,4,5,7,8,9 (4,8)
LH4	4,6,7,8,10	1,2,4,6,7,8,10 (6)	6	1,2,4,5,7,8,9 (4,8,9)	*	6,7 (9)
LH5	1,2,4,6,7,8,10	2,6,7,8,10 (9)	6,7	1,2,3,4,5,7,8,9 (4,8)	7,10	1,2,4,5,7,8,9 (4,8)
LH6	1,2,4,6,7,8,10 (6)	2,4,6,7,8,10 (9)	6,7	1,2,3,4,7,8,9 (4,8)	*	6,8 (9)
LH7	1,2,4,6,7,8,10 (6)	4,6,7,8,10	6	1,2,4,7,8,9 (4,8,9)	*	4,6,7,8 (9)
LH8	1,2,4,6,7,8,10	2,6,7,8,10	7	1,2,4,5,7,8,9 (8)	10	1,2,4,5,7,8,9 (2,9)

3.7.5 Control of concrete failure

The concrete elements in the top right corner are of interest for two reasons. One, the principal compressive stresses exceeded the compressive strength of concrete for every analysis before these elements were crushed. And two, the failure should be the cause of load effects and not spurious strains.

The largest compressive principal stress in the right corner of the frame exceeded the compressive concrete strength by about 10% in all of the analyses before failure occurred. To examine the strength gain and verify that the failure is a result of compressive failure in concrete, the principal stress-strain relation of the most stressed element is studied. The stress-strain relation of the reinforcement in this element is examined as well. The element studied was the element located on the interior side of the right column adjacent to the corner (the concrete element located at reinforcement zone (7) from Fig. 3.48). The stresses are sampled at Gauss integration points. The two Gauss points examined in the concrete element are the point closest to the interior of the frame corner (from now called Gauss point 9), and the Gauss point to its right (Gauss point 8). Gauss point 9 should be the first to experience failure, and due to its placement it should not experience excessive confinement. The reinforcement stresses are sampled at the Gauss point of the longitudinal reinforcement that is located closest to the frame corner corner (at zone (7)) in close proximity to Gauss point 8. The stress-strain relations from characteristic ECOV analysis of LH3 can be seen in Fig. 3.49. The stresses are normalized in relation to the uni-axial compressive strength. The

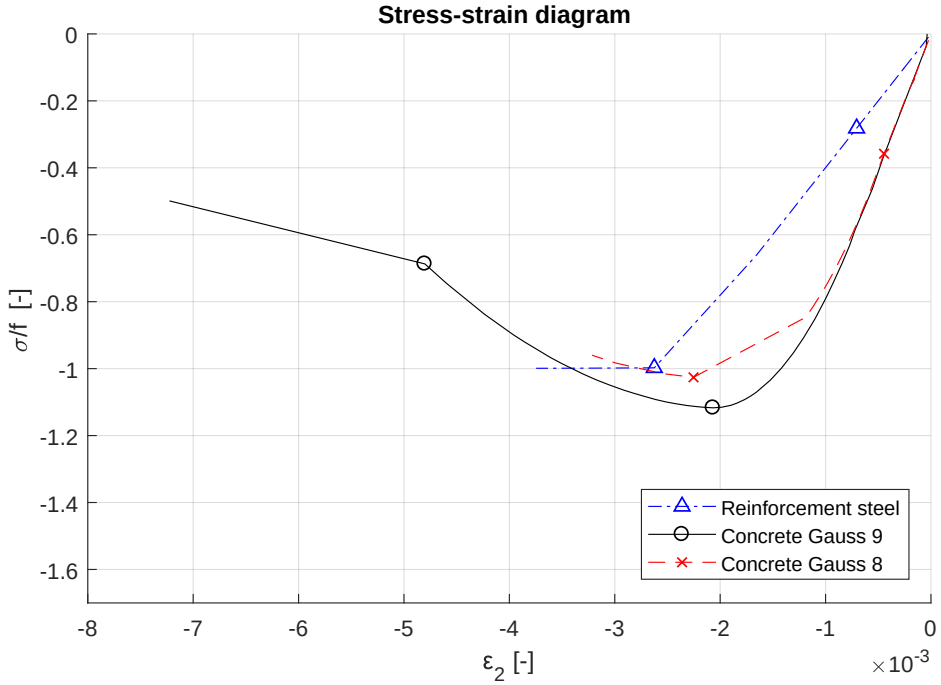

Figure 3.49: Principal stress-strain relations of reinforcement steel and concrete element located at the interior part of the top right corner. Relations are given for load steps right until compressive failure. The results are retrieved from characteristic ECOV analysis of load history 3. Stresses are normalized with relation to characteristic strength of concrete and yield strength of reinforcement. The curves are marked for two load steps, the first marker for when maximum concrete stress in Gauss point 9 is reached and the second for when reinforcement yields. Gauss point 9 is located closest to the interior of the corner.

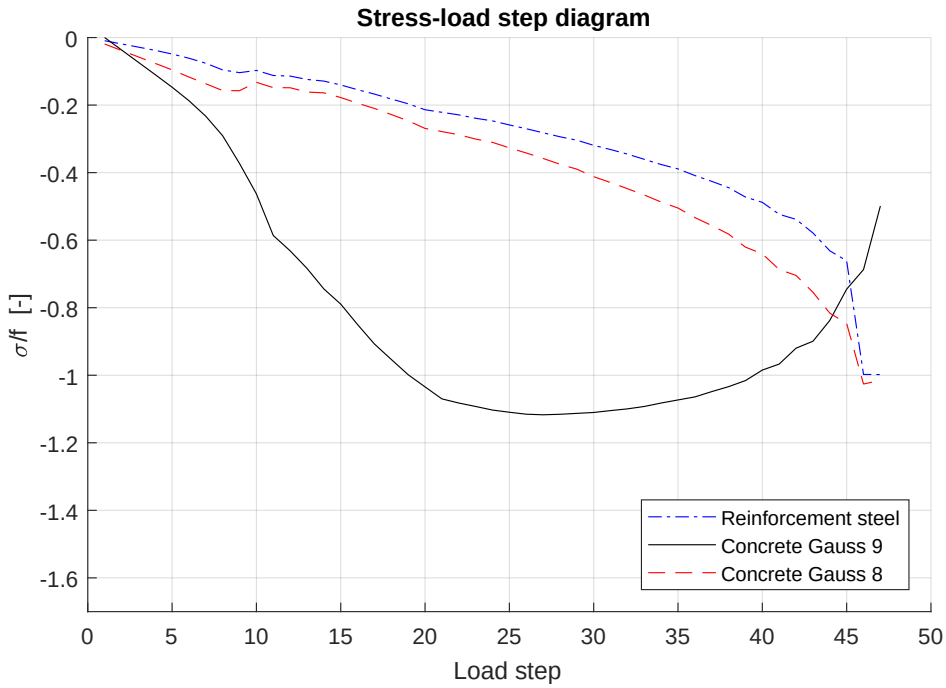

Figure 3.50: The figure illustrates the normalized principal stresses in relation to the loading (load steps) for the concrete element located at the interior part of the top right corner and the reinforcement in this element. Relations are given for load steps right until compressive failure. The results are retrieved from characteristic ECOV analysis of load history 3. Stresses are normalized with relation to characteristic strength of concrete and yield strength of reinforcement.

figure shows that the concrete and reinforcement stresses match the material models given in Table 3.7. The markers in Fig. 3.49 are given for the same load step. The first marker of each curve indicates the load step at which Gauss point 9 experienced maximum stress, and the second marker indicates the load step at which the reinforcement starts to yield. It is clear from the figure that the concrete initiates the failure close to the corner in Gauss point 9, and when load effects are redistributed to Gauss point 8 and to the reinforcement, the concrete element is visibly crushed.

Fig. 3.50 shows the normalized stresses in the concrete element Gauss points and the reinforcement Gauss point in relation to the load steps of the characteristic ECOV analysis of LH3. This gives a better picture of the force redistribution in the most stressed element during the loading of the frame.

3.7.6 Ultimate loading

Most of the load steps in the analyses reached convergence, often within 50 iterations, however, there were instances of non-converged load steps. The steps where the convergence criteria was not reached experienced either the first major instances of cracking or the local failure of concrete in the top right corner. Initial cracking and concrete crushing are instances with large changes to the structural stiffness and therefore would require more iterations to converge, although sometimes 200 iterations were not enough. All non-converged steps that were deemed satisfactory were followed by converged load steps.

Design values of the ECOV format were calculated using the method by Engen et al. (2017) which determine the global resistance factor γ_R with material, geometry and model uncertainty, see Eqs. (2.22) to (2.24). The coefficient of variation of geometry is assumed $v_G = 0.05$ according to Pimentel et al. (2014) which assumes a large structure insensitive to 2nd order effects. The coefficient of variation and mean value of modelling uncertainty are selected from Hendriks et al. (2017b). The values assume a failure mode of bending and get the respective values $v_\theta = 0.04$ and $\theta_m = 0.97$ for the coefficient of variation and mean model uncertainty.

The global capacities and design resistances of the first three load histories, LH1-LH3, are given in Table 3.14. The measurement used is a sum of the total loading on the frame as used in Blomfors (2014) and the earlier verification of the solution strategy. The ultimate capacities and design resistances for LH4-LH8 are presented in Table 3.15. The measurement used for these histories was the load factor for horizontal load, LF_H. The load factor for the vertical load was assumed to be constant and equal to 1.35 at global failure.

Most estimates of design capacities from the nonlinear analyses did not exceed the design loads the frame was initially designed for, there were only two exceptions for GRFm. In analogy to Blomfors (2014), this would mean the NLFEA safety formats are conservative compared to the design code. Therefore, similar structures that are designed by using either of the NLFEA safety formats should have a probability of failure that is smaller than the target probability of failure determined by the building code, e.g. Eurocode 2.

Table 3.14: Design resistances R_d for load histories 1-3 calculated according to the three safety formats from Model Code 2010 (fib, 2013). Global resistance factor γ_R for ECOV calculated according to Eq. (2.23).

Load History		R_m [kN]	R_k [kN]	v_M	v_R	γ_R	γ_{Rd}	R_d [kN]
LH1	ECOV	2 562	2 327	0.0582	0.0865	1.341	-	1 910
	GRFm	2 568	-	-	-	1.20	1.06	2 019
	PSFm	-	-	-	-	-	-	1 976
LH2	ECOV	2 525	2 321	0.0510	0.0819	1.322	-	1 909
	GRFm	2 438	-	-	-	1.20	1.06	1 917
	PSFm	-	-	-	-	-	-	2 013
LH3	ECOV	2 587	2 354	0.0570	0.0857	1.338	-	1 933
	GRFm	2 282	-	-	-	1.20	1.06	1 794
	PSFm	-	-	-	-	-	-	2 012

Table 3.15: Design load factor for horizontal load $LF_{H,d}$ for load histories 4-8 calculated according to the three safety formats from Model Code 2010 (fib, 2013). Global resistance factor γ_R for ECOV calculated according to Eq. (2.23).

Load History		$LF_{H,m}$	$LF_{H,k}$	v_M	v_R	γ_R	γ_{Rd}	$LF_{H,d}$
LH4	ECOV	2.060	1.770	0.0920	0.1121	1.449	-	1.421
	GRFm	1.910	-	-	-	1.20	1.06	1.502
	PSFm	-	-	-	-	-	-	1.350
LH5	ECOV	2.050	1.776	0.0868	0.1079	1.431	-	1.433
	GRFm	1.876	-	-	-	1.20	1.06	1.475
	PSFm	-	-	-	-	-	-	1.419
LH6	ECOV	2.080	1.810	0.0843	0.1058	1.422	-	1.463
	GRFm	1.851	-	-	-	1.20	1.06	1.455
	PSFm	-	-	-	-	-	-	1.430*
LH7	ECOV	2.100	1.787	0.0978	0.1169	1.471	-	1.428
	GRFm	1.952	-	-	-	1.20	1.06	1.535
	PSFm	-	-	-	-	-	-	1.410*
LH8	ECOV	2.091	1.800	0.0908	0.1111	1.445	-	1.447
	GRFm	1.856	-	-	-	1.20	1.06	1.459
	PSFm	-	-	-	-	-	-	1.439*

* The vertical load factor at failure is less than the assumed constant value of 1.35

There are differences in how conservative the formats are and how they are affected by the load histories. For the first set of load histories, LH1-LH3, the PSFm and ECOV methods give very consistent design capacities and are not as affected by the differences in the load histories. The ECOV method gives only a slightly larger capacity when loads are initially applied simultaneously compared to an initial individual loading. Meanwhile, PSFm gives a slightly reduced design capacity when initial loading begins with an individual vertical load. The analyses from the first set of histories show that the GRFm is most affected by the loading history. For GRFm, initial individual vertical loading gives the greatest estimated capacity while initial simultaneous loading gives the smallest capacity. The difference between the two capacities is 13%. The last capacity for initial horizontal loading is about mid way between the two extremities.

For the second set of load histories, LH4-LH8, the two instances where design capacity exceeded the design value (LF_H = 1.5) occurred for the GRFm analyses of LH4 and LH7. However, compared to the first set of histories, the difference in estimated design capacity for GRFm was smaller, about 6% as opposed to 13%. GRFm achieved the largest average capacity of the three methods for the second set of histories compared to the smallest average for the first set. The largest capacities with GRFm were obtained for LH4 and LH7, where both histories initiates with an individual vertical loading, repeating the trend seen in the first set. Moreover, the smallest capacity was obtained for LH6 with simultaneous loading. Estimated design capacities for the ECOV method remain consistent with about a 3% maximum difference. The second set of histories confirms the behaviour seen in the first set, and the largest capacity is given for LH6 with initial simultaneous loading. Likewise, the smallest capacities are given for LH4 and LH7, both with initial vertical loading. One notable change with the exchange of capacity measurement is the coefficient of variation of material

parameters in ECOV almost doubling. This is mostly due to the change of measurement, as the difference between mean and characteristic capacity is divided by a smaller total which makes the relative difference larger.

Several of the PSFm analyses of the second set of load histories did not reach a vertical loading equal to the assumed design load factor of 1.35. This makes it difficult to compare the histories where the vertical load factor did reach 1.35 (LH4 and LH5) with those that did not (LH6, LH7 and LH8). In addition, as respectively LH7 and LH8 are equal to LH1 and LH2 for loads below design level, the PSFm analyses of LH7 and LH8 did not generate any additional information. Nonetheless, the estimated capacities are found to be greatest for load histories that start with individual horizontal loading, and second largest for histories with initial simultaneous loading.

The GRFm and ECOV methods behaved consistently in regard to divergence. All GRFm analyses survived concrete failure of the top right corner and all of the ECOV analyses did not. Characteristic ECOV analysis of LH3 survived the first load step of the failure, but did not survive the entire failure before the analysis diverged. The PSFm analyses did not end with the same type of global failure. Half of the analyses failed with the compressive concrete failure of the right corner while the other half survived and obtained some increased capacity due to the redistribution of load effects in the frame.

It should be noted that the design capacities presented in this section are limited to the load histories, load combinations and load measures used. For other compositions of loads, load histories and measures, additional analyses must be performed and resistances calculated. It is also worth noting that the element model, solution strategy and material parameters as well as the method of estimating the safety factor of the ECOV format will influence the obtained design values.

4. Discussion

As mentioned in the introduction, a reason for performing a NLFEA is to improve the accuracy of structural analyses in order to gain environmental and/or financial benefits. This is why it is important to understand how NLFEA works and which possibilities and drawbacks it may include. As the safety aspect is often the most decisive condition when designing structures, a safety format could be used to simplify a complex, and sometimes difficult, reliability analysis in order to ensure that a target probability of failure is satisfied. Some factors may influence the results from these analyses, for example load history, and the factors are discussed below.

4.1 Modelling and solution strategy

The solution strategy that is used when performing NLFEA include a large number of considerations and choices that can affect the analysis results. These choices are not always trivial to make, especially for those with inadequate experience, but there also exist disagreements between professionals in this field. It is therefore important for engineering that good and relevant guidelines for executing accurate NLFEA are developed. There already exist a few, like the one by Hendriks et al. (2017a), however, there may be some difficulties developing a general guideline that is accurate enough for NLFEA to be applicable to all types of structures.

The accuracy of the solution strategy should be addressed. There are many choices that are based on guidelines, however, some variables were determined through a verification analysis. In this work, the strategy was compared to a calibrated NLFEA strategy and not a physical experiment. Furthermore, that NLFEA strategy was only calibrated against one physical experiment. One is apt to recognize the possible statistical implications this may have on the obtained results, more on this in Section 4.5. If there are too many variables that need calibrating, one might experience the problem of overfitting the solution strategy, where the strategy works well on the cases used in calibration, while most likely performing worse elsewhere (Engen, 2017). Also, there is a possibility of overfitting if only one physical experiment is used for calibration.

One of the variables that were calibrated was the mesh size. 3-4 E.O.H. gave reasonable results for all formats, with an average design capacity close to the capacities of Blomfors (2014). Some analyses were performed with a finer mesh, and they provided smaller capacities on average compared to the coarse mesh. As the coarse mesh already averaged smaller capacities compared to Blomfors (2014), the coarse mesh was used. In addition, as seen in the mesh sensitivity tests presented in Section 3.6, results with 6-8 E.O.H. showed a more accurate behaviour of PSFm and a good estimate of the design capacity, though the GRFm and the ECOV methods did not perform nearly as well. Even though all analyses survived initial crushing of the right corner with a finer mesh, the design capacities were greatly influenced. Meanwhile, for the coarser mesh, all ECOV and most of the PSFm analyses diverged at the first compressive failure of a concrete element. It was seen from Blomfors (2014) that after the failure of the right corner, the expected gain in capacity

for the ECOV analyses was minimal. Regardless of the early divergence, the coefficient of variation of material uncertainty obtained for ECOV remained very consistent for the analyses. Consequently, the choice was made to prioritize accuracy in capacity for all methods, rather than ensuring all analyses survived initial crushing.

The choice of using a 2D element model was based on a reduction in computation time and on the assumption that no failure modes or forces were expected to occur orthogonal (in the z-direction) to the frame's major axes (x- and y-axis). The latter fixes stresses in z-direction to a constant zero value in any point of the frame at all times, disregarding any possible support actions or concrete confinement by shear reinforcement stirrups. It also assumes a uniform stress distribution across the whole width of the cross sections which would be appropriate for narrow cross sections. As the cross sectional height to width ratio is equal to or less than 2:1, this is arguably not representing the true stress distribution in the designed frame. One should expect a larger degree of confinement in the center of the frames thickness compared to the edges, and thus expect a larger strength increase due to concrete confinement and possibly a larger failure load. The load capacities in general were found to be smaller for the 2D analyses of this work than for the 3D analyses performed in Blomfors (2014). This reduction due to dimension change should be taken into consideration when establishing an element model because results from this work show a slight difference of affection between safety format methods. Due to dimension changes, GRFm and ECOV have a significantly reduced capacity for initial vertical loading, while PSFm have a significant reduction in capacity for initial horizontal loading, see Tables 3.5 and 3.6. However, further 3D analyses would be required to determine if this effect holds for the updated material parameters used in the main analyses of this work.

The convergence and accuracy of a nonlinear analysis is highly dependant on the convergence criteria. There is no consensus on what tolerance to use, therefore, the criteria used was the one suggested in the guidelines of Hendriks et al. (2017a). Convergence was assumed if either the tolerance for the unbalanced force norm or the energy norm was satisfied. Simultaneous satisfaction was not required, as typically, when one norm was satisfied, the other norm was close to satisfactory as well. The only visible exception was the second to last load step for the GRFm analysis of LH5, where the force norm was considerably off due to spurious stresses in the left support. Meanwhile, there were only a few instances of unconverged load steps though no more than one at the time. According to the guidelines, unconverged steps can be admissible, provided they are followed by converged load steps and that a plausible explanation for the non-convergence is provided. For the analyses performed, all of the unconverged steps were followed by converged steps, and they occurred for the initial cracking and at the concrete failure of the corner. Both situations cause large changes to the structural stiffness and would require additional iterations to reach convergence. The unconverged load steps are therefore not considered to have influenced the results to any significance.

The guidelines of Hendriks et al. (2017a) do not recommend the use of a constant shear retention model when using fixed crack models of concrete. If a constant model is used, it should be accompanied with a post-analysis check for spurious tensile stresses. There were registered principal tensile stresses exceeding the tensile strength of concrete, some were recorded close to double the tensile strength, but there were no recording of principal tensile stresses in the problematic areas near or around the top right corner of the frame. In addition, the areas of exceeding tensile stresses were small in comparison to frame dimensions, often covering less than half the area of a single mesh element. Based on this,

it is assumed the constant shear retention model used had little influence on the estimated capacity. This is further proved in Section 3.7.5 where the failure was found to be caused by a gradual concrete compressive failure with lateral confining compressive stresses.

4.2 Load history and measures

The safety format methods in this study are used to estimate the design capacity of structures. However, Mode Code 2010 (fib, 2013) does not specify what measure of capacity to use, leaving it to the analyst to decide a reasonable measurement. For the load histories studied in this paper, there were two different measures used. However, the choice of these measures where not trivial. There were a few load aspects that needed to be taken into consideration.

There's a concern with the measure of total loading as used in LH1 trough LH3. First, the measure does not take into account that the loads are applied in different directions or at different locations of the frame. Even if the load situation of the frame is very simple, this could make the measure dependant on load ratios. For example, the ratio is determined by the scaling of the loads past the design load level. In the analyses, loads are scaled relative to the difference from characteristic to design load values. This will cause the ratio between horizontal and vertical loading to change with a change in total loading. If the loads would instead be increased relative to zero loading and the design load level, the ratio would remain constant for loads above design level. None of the obtained literature gives any further specification regarding the handling of the load ratio and was not researched any further. This aspect would not have been of a concern if the loads were applied at the same point and in the same direction, as any ratio would give the same capacity. Besides, the best example available for comparing load ratios is the PSFm analyses of LH3 and LH6. LH3 has a slightly larger capacity compared to LH6 in addition to a larger load ratio (vertical/horizontal). This may point to horizontal load being more critical to the total capacity, though further analyses would be required.

For LH4-LH8, the horizontal load factor was used as the measure of capacity. In these analyses, the vertical load was restricted to its design value. This may implicate that the vertical load is more predictable than the horizontal load. As stated in Section 3.4, the origin of the loads was not emphasized in order to increase the number of load histories which included another measurement. The main focus is not on the origin of such a load history, but on the effect it may have on the safety formats and the calculated design capacity. In comparison to the first measure of capacity, the load ratio would also change with increasing loads, meaning the effect of a changing load ratio can not be quantified here. Nevertheless, this may be the reason that measurements are not specified in literature, as the chosen measurement would need to vary based on the load histories or loading in general.

There may be another possible unwanted effect of fixing the vertical load. Even though the design loads calculated for LH4-LH8 are fairly equal, the failure capacities from the analyses are not. This will cause the utilization of the frame to vary between the analyses of the different methods. For example, the utilization of the frame when design loads are applied will be different for the PSFm compared to the ECOV method. As no PSFm analyses ever reached design levels, this would give an utilization factor above 1.0, but a mean ECOV analysis might only be at 0.8. The remaining utilization of 0.2 of the ECOV analysis is then reached by only increasing the horizontal load. This problem loops back to the consideration

Table 4.1: Design capacity of all load histories and safety formats. Capacities given in kN for load histories 1-3 and with the load factor for horizontal load, $LF_{H,d}$, for load histories 4-8.

	ECOV	GRFm	PSFm
LH1	1 910	2 019	1 976
LH2	1 909	1 917	2 013
LH3	1 933	1 794	2 012
LH4	1.421	1.502	1.340
LH5	1.437	1.470	1.420
LH6	1.463	1.454	1.420*
LH7	1.419	1.533	1.405*
LH8	1.444	1.454	1.440*

* The vertical load factor is less than the assumed constant value of 1.35

of the load ratio, as the load ratio would be very different at global failure for PSFm and ECOV. The possible implications of this discrepancy would require further research.

The calculated design capacities are presented in Table 4.1 for all load histories and safety format methods. The results indicate that the load history has some effect on the estimated design capacity, though some of the load histories used may be more realistic than others. As stated in Section 3.4, the assumption of self weight being applied first was not implemented in all load histories. The results from the analyses of this work show that there are in fact differences in the design capacities primarily based on the initial loading sequences which also establish the majority of the cracking of the structure. On this basis, one should seek to use load histories that closest represent the actual loading that is expected to occur or have occurred. However, it is important to include all load histories that have a realistic chance of occurring. To improve the realism further, load histories should include loading from construction as well as the loads after completion.

The analyses performed in this work do not take the construction loads into account as the loading is very simplified. Furthermore, as some histories only apply horizontal load in the initial load sequence, the realistic part of generating load histories are not included either. The results from LH4-LH8 clearly show the initial loading has the largest impact on design capacity. The specific impact is discussed in the next sections. The most realistic load histories would initiate with a vertical self weight before experiencing very large horizontal forces. This would benefit some methods and disadvantage others, i.e. GRFm capacity is increased and ECOV capacity is reduced. Note that this is true for the analyses performed here, and should not be assumed to be true for any other situations without further research.

One aspect of loading that has not been treated in this work is the possibility of cyclic loading. This could be caused by traffic loads, wind loads and most other kinds of live loads. In this case, horizontal loads may reach characteristic loads before being reduced several times before a design case occurs. This could create several new histories with identical initial loading situations. Additionally, this could include studying effects of material fatigue.

4.3 Reinforcement layout

The frame was designed using LFEA and a post processor which optimized the reinforcement layout based on input variables. As seen the reinforcement scheme in Fig. 3.3, this causes the longitudinal reinforcement of the columns to change cross sectional area several times in the same reinforcement layer. In the columns and the beam this occur up to three times over a length of 6 and 10 meters respectively, and often in different sections for reinforcement located on the inside and outside of the frame. This leads to several stiffness changes in the columns and beam over a relatively short distance. This would not be factored into a LFEA, but would be affecting a NLFEA as the concrete cracks and sections of varying stiffness interact with each other. In some areas of the frame, the change in reinforcement area is very significant, e.g. in zone (10) of Fig. 3.48, where the change in reinforcement area is greater than a factor of 4. This is not common practice, and should be reevaluated in any further analyses. A more realistic layout would include one continuous layer with an additional layer where it is needed, e.g. the 7Φ28 of the outer part of the columns could have stretched the entire column height with an additional layer at the top.

The reinforcement layout influences the cracking of the columns as well. In the areas around the reinforcement where the change is great, the tensile strains accross the concrete cracks are large compared to adjacent elements (see top of the beam in Fig. 3.7). This may greatly reduce the shear retention locally and contribute to possible shear failure. This was dealt with by using a constant shear retention model even though it is not advised which caused additional checks to be performed post analysis (see the discussion at the end of Section 4.1). These strains could also become problematic for serviceability limit state checks, but this is not the focus of this thesis.

4.4 Performance of the PSFm format

A reason to perform a NLFEA is to check the reliability of a complex structure that otherwise would be hard to do with e.g. LFEA. As stated in Section 2.3.1, Model Code 2010 states the Partial factor method may be used for a safe estimate in absence of a more refined solution (fib, 2013). Meanwhile, it assumes a weakness in every point of the structure which is not realistic and may lead to a different failure mode. In the analyses performed, there was no major deviance in structural behaviour or the failure mode compared to the other methods, which should make the PSFm applicable. If the use of the PSFm should be justified, it should give safe estimates that are not too conservative. This applies to all of the safety format methods.

Because the estimated capacity from PSFm is obtained directly from the analysis, it may prove difficult to determine the effects from changes in load histories close to or above the design load level. Safe estimates would return a capacity below the designed load level, which reduces the number of comparable histories from the second set of load histories. The second set assumes a vertical loading equal to design value at global failure. When the analyses fail for the three load histories LH6-LH8 before the vertical load reaches the design level, they can not be directly compared to LH4 and LH5. Furthermore, this causes LH7 and LH8 to be duplicates of LH1 and LH2 respectively, and they do not generate any new information.

The analyses showed that the PSFm is affected by the initial loading sequences. The obtained capacity is slightly reduced with initial vertical loading compared to initial horizontal or

simultaneous loading. As the initial vertical loading caused the analyses to diverge when concrete failed in the right frame corner, those histories could not benefit from a ductile failure. This might be improved by a change in solution strategy, however, as seen in the test for mesh sensitivity, Figs. 3.17 and 3.18, the method provides less conservative estimates with a slightly different element model. In addition to no global failure due to divergence at first instance of concrete failure, the total loading of LH3 and LH7 with the finer mesh model are close to identical. Furthermore, as the resulting capacity is just below design level, LH7 is still equivalent to LH1. Consequently, the finer mesh only makes a slight change to the influence of initial loading effects on the PSFm as the capacity is still slightly smaller for initial vertical loading but less when compared to a coarse mesh.

4.5 Performance of the ECOV format

The ECOV analyses performed consistent and diverged when concrete failure occurred in the top right corner. This simplified the determination of the failure capacity as there were typically no unconverged steps before divergence. This failure capacity was determined with greater ease compared to GRFm analyses, which may have improved the accuracy of the coefficient of variation of material uncertainty that remained fairly consistent in the two sets of load histories. When the margin of error in determining the capacities becomes significant compared to the difference in mean and characteristic analysis capacity, the influence of a single load step converging or not may have large consequences on the estimated coefficient. The decision of reducing the load increments close to failure was based on reducing the possible effect of load steps on the relatively small difference between mean and characteristic capacities. Consequently, one can argue that a change in design capacity would be the result of load history effects and not the error in determining the coefficient of variation of material parameters.

The failure mode is more brittle than expected compared to the ductile failure mode as seen from the GRFm analyses or from the ECOV analyses of Blomfors (2014). The brittle failure is also seen in half of the PSFm analyses where the resulting capacity is slightly smaller than for the ductile mode. As none of the ECOV analyses experienced a ductile behaviour, it could be assumed that the capacities obtained are more conservative for both the mean and characteristic capacities, however, it is not as intuitive for design capacity. This is because the design capacity is more dependant from the variation of the two analyses. Nevertheless, the results should still include the the effects of the load histories.

A change in mesh size would cause the analyses to survive the concrete failure and result in a ductile failure mode. A problem in this case was the resulting coefficient of variation of material parameters becoming negative if using Eq. (2.19). This shows an unfortunate effect from depending on two capacities for determining the design capacity of the structure. Furthermore, it shows the need to calibrate the solution strategy with physical experiments in order to minimize modelling error. As seen in the analyses of this work, it might be easier when the failure mode is brittle and the capacities have clearly separate values compared to the overlapping seen in Fig. 3.19.

The design capacity of the ECOV method was not calculated according to Mode Code 2010 for load histories with updated material properties. Instead it was based on a method suggested in Engen et al. (2017) which combines material uncertainties and model uncertainty into one global resistance factor instead of two. An advantage of this, is that

it gives the opportunity of adjusting the resistance factor with a model bias. In this way, the solution strategy may be calibrated based on behaviour rather than capacity, and then the average bias (or mean uncertainty) adjusts for capacity when calculating the resistance factor. A possible disadvantage is that the coefficient of variation would need to include variation of model uncertainty as well as material variation, and thus the material variation could be overwhelmed by a much larger variation of model uncertainty. It is therefore important to use model uncertainties that best represent the failure modes that occur in the analysis, as the variance may vary greatly between the different types of modes as seen in Hendriks et al. (2017b). This may increase the number of calibration analyses needed to create an accurate estimate, however, it has the opportunity of being less conservative than the GRFm while giving a realistic representation of the structural behaviour.

The mean value of modelling uncertainty, θ_M, and the coefficient of variation of modelling uncertainty, v_θ, was obtained from Hendriks et al. (2017b) for concrete failure in bending. Though Hendriks et al. (2017b) utilizes a finer meshing than what was used and the verification experiments were done on beams in bending, there were no reasonable substitute values to be obtained at this time. The values could have been calibrated as stated above, though this would have required several more studies in order to provide values of statistical certainty. It should be noted that θ_M and v_θ for bending modes from Hendriks et al. (2017b) are obtained from three case studies and that the statistical significance of those parameters is questionable, yet they still have a better statistical significance than the values that can be calculated from this paper.

Similarly to the PSFm format, the load histories with initial simultaneous or horizontal loading result in slightly greater design values than histories with initial vertical loading. The most notable difference is in the second set of histories with LH6 resulting in the greatest design capacity and LH7 resulting in the smallest capacity. All design capacities are still considered safe as they do not exceed the original design values.

The inclusion of model uncertainty in the design calculations of the ECOV method did not influence the initial loading effects on the ECOV method. Initial vertical loading would still be giving the smallest design values if the procedure described in Model Code 2010 (fib, 2013) were to be used. The inclusion did however, slightly reduce the differences in design capacities due to the addition of variance originating from geometric and modelling uncertainty. This is important because it preserves the importance of using the correct load history in order to obtain the most realistic estimate of the design capacity.

4.6 Performance of the GRFm format

Of the three methods studied, the GRFm was the most affected by load history changes. It is not clear why it is the most affected, though it might be connected to the increase in capacity as the frame experiences the ductile deformations after concrete failure in the top right corner. Typically the load steps did not converge when the local concrete failure occurred and may have caused the analysis software to overestimate the reactions of the frame. Even though the load steps were followed by several converged load steps, the measure of unbalance in the norms varied a lot. Some steps were almost converged, others could be off by a factor of 30 or more (i.e. force norm of 30% or more at cancellation). In addition, the analyses often contained several unconverged load steps before divergence occurred.

All GRFm analyses experienced the most ductile behavior as expected for the frame in concrete bending failure. The capacity increase was also notable for all analyses. The reason for the early concrete failure was due to the reduced compressive strength of concrete and a high yield strength of the reinforcement steel compared to the ECOV analyses. As seen for ECOV in Fig. 3.50, the concrete fails locally in the element before the reinforcement yields. This occurs at smaller loads for GRFm, and because the reinforcement is capable of withstanding the large loads when concrete fails compared to the other methods, the failure is more gradual and the capacity increase due to redistribution of load effects is significantly larger than what is seen for the PSFm. However, one could question the probability of this failure, as it probably is significantly more ductile than reality.

The capacity was found to be impacted by mesh size just like the ECOV method (see Fig. 3.20), and for a fine mesh the behaviour became less ductile. Consequently, the design capacity was greatly reduced. Without the possibility to correct for a generally low estimate in contrast to ECOV, the GRFm method is more dependant on an adapted solution strategy to provide less conservative yet safe estimates.

The large effects on the GRFm method are not necessarily caused by the load history. In the thesis of Blomfors (2014), there were no difference in GRFm design capacities between LH1 and LH2. Note that the material input parameters were notably different and used different solution strategies. This could imply that solution strategy or the calculation of material parameters have just as much influence on safety formats as the load history does. As the material parameters in Blomfors (2014) do not coinside with the parameters calculated according to Mode Code 2010 as presented in Hendriks et al. (2017a), and with the solution strategy being different, it is not possible to determine the origin of this difference in affection without further analyses.

As stated in the beginning of this section, the GRFm method was the most affected by changes in the load history. Nevertheless, there were another remarkable difference in the affection. The effects on the GRFm design capacities were opposite than those of the ECOV method, despite both methods being part of the same global resistance safety format. The estimated design capacity was greater for initial vertical loading and smallest for initial simultaneous loading. It is not clear what causes this inverse correlation within the format, however, it emphasizes the importance in the choice of safety format method. An accurate NLFEA should use a method that predicts the real effects of loading on a structure. For example, in the case of the reinforced frame, if the real behaviour from physical experiments shows an increased capacity for initial vertical loading compared to initial horizontal loading, then the GRFm method could be the method of choice. Furthermore, when the method is chosen, it is important to use the realistic load history when designing new structures.

5. Conclusion

The application of nonlinear finite element analysis (NLFEA) for design or control purposes may be justified if it can provide more accurate estimates and better information of structural behaviour than common practice with linear finite element analysis. When adapting a NLFEA for this purpose, it is important to consider the effects on the estimated design capacity by the load history for a complex set of loads.

This work have shown that the order of which a horizontal and a vertical load is applied to an undetermined reinforced concrete frame will influence the estimated design capacity estimated by using NLFEA safety formats from Mode Code 2010 (fib, 2013). Furthermore, the results show the difference in capacity depends the most on the initial loading, i.e. for loads smaller than the expected characteristic loads. Because the estimated design capacities change based on initial loading, only the load histories that may physically occur should be included when designing structures using NLFEA.

Furthermore, the results show that the partial safety factor method (PSFm) and the method of estimation a coefficient of variation of resistance (ECOV) both provide the smallest capacities for load histories with an initial individual vertical load, while they provide the greatest capacities for load histories that included an initial simultaneous application of both loads or an individual horizontal load. The global resistance factor method (GRFm) provided capacities with an inverse correlation compared to the former two methods, even though it originates from the same safety format as ECOV. It provides the greatest capacities when initial loading consists of an individual vertical load and the smallest capacity for an initial simultaneous loading.

The safety format methods were not influenced to the same degree by the load histories. The GRFm was influenced the most, while the PSFm was the least affected. It is therefore important to consider which format to use when designing a structure. One should use the method that best represents the effects of loading on the true capacity in order to reduce modelling uncertainty and achieve the least conservative but still safe design estimates. However, this work can not conclude which method is fitting for a specific purpose or structure. This would require additional research to be performed.

There were problems with comparing some results from PSFm analyses, as the method is inherently conservative and design capacity in obtained directly from the analysis. Due to global failure occurring before loading could reach expected design loads, some load histories with a variation in loading close to the design load level could not be compared. This reduced the available results which show that the PSFm is not suited for exploring the effects from changes in loading close to design level using NLFEA.

6. Suggestions for further research

To fully understand how the load history affects the estimates of design capacity of established safety formats, more research is required. It is suggested to work on understanding which effects causes the behaviour seen in this thesis and how load histories might effect other structures. To justify the use of NLFEA, the safety formats should be able to produce estimates which are less conservative and more accurately describe the true behaviour of a structure than LFEA while still retaining a certain target reliability. The different suggestions are given below.

It is suggested to examine the possible effects that load histories have on other failure modes, i.e. shear or punching shear failure. These are more brittle failure modes compared to concrete in bending and might be more susceptible to differences in initial loading and the development of crack patterns. Another suggestion is to examine more complex structures in bending with or without a more complex loading scheme.

Guidelines provide some information on what loads to apply in initial order, but when developing realistic load histories, it is also desired that the future guidelines for NLFEA give better advice on what measures to use when determining the capacity in a NLFEA. This is essential for load conditions that may not be easily simplified, e.g. loads acting in different directions, at different points of attachment and/or with different origins. Also, it is desired that the future guidelines or other regulations provide information on what loads to increase when the loading exceeds the target design values.

As the analyses indicate the initial loading have the largest influence on the estimated design capacity, it is suggested that further work is to be done on the effects of more complex loading schemes which include loads during construction or the effects of cyclic loading. An analogy for the latter can be structures exposed to large horizontal loads, e.g. wind, for thereby to calculate the design capacity for vertical loads, e.g. snow.

As the uncertainty of elastic and plastic stiffness of reinforcement steel is typically less than for the material strength, it is desirable that the design codes specify what values to be used in the existing safety formats. It could be dealt with in the same fashion as concrete stiffness, however, a specification is needed.

Furthermore, it is suggested to examine the influence of meshing on the NLFEA safety formats. In addition to meshing, it would also be of interest to examine the significance of 2D vs. 3D modelling. As uncovered in this work, the mesh influenced some formats more than others, and 2D modelling seemed to reduce the quality of convergence at concrete crushing. This could be performed as a study of model uncertainty.

Bibliography

ANSYS (2014). ANSYS Mechanical 14.5. ANSYS inc., Canonsburg, USA. Available from: <http://www.ansys.com/Products/Simulation+Technology/Srtuctural+Analysis/ANSYS+Mechanical>.

Blomfors, M. (2014). Global Safety Assessment of Concrete Structures using Nonlinear Finite Element Analysis. Master's thesis, Chalmers University of Technology, Pub. No. 163, Gothenburg, Sweden.

Brekke, D.-E., Åldstedt, E., and Grosch, H. (1994). Design of Offshore Concrete Structures Based on Postprocessing of Results from Finite Element Analysis (FEA): Methods, Limitations and Accuracy. Proceedings of the fourth International Offshore and Polar Engineering Conference, April 1994.

CEN (2002). *EN 1990:2002 Eurocode: Basis of structural design.* European Committee for Standardization, Brussels.

CEN (2004). *EN 1992-1-1:2004 - Design of concrete structures. General rules and rules for buildings.* European Committee for Standardization, Brussels.

Cook, R., Malkus, D., Plesha, M., and Witt, R. (2002). *Concepts and applications of finite element analysis.* John Wiley & Sons, inc., 4th edition.

DIANA FEA (2014). *DIANA FEM-software release 9.4.4.* DIANA FEA BV, Delft, The nederlands. Available at <https://dianafea.com/content/DIANA> (28.11.2017).

DIANA FEA (2017a). *DIANA FEM-software release 10.1.* DIANA FEA BV, Delft, The nederlands. Available at <https://dianafea.com/content/DIANA> (28.11.2017).

DIANA FEA (2017b). *DIANA User's Manual release 10.1.* DIANA FEA BV, Delft, The nederlands. Available at <https://dianafea.com/manuals/d101/Diana.html> (28.11.2017).

Engen, M. (2017). *Aspects of design of reinforced concrete structures using non-linear finite element analyses. Solution strategy, modelling uncertainty and material uncertainty.* PhD thesis, NTNU; 2017:149.

Engen, M., Hendriks, M., Øverli, J., and Åldstedt, E. (2014). Application of NLFEA in the Design of Large Concrete Stuctures. Proceedings of the XXII Nordic Concrete Research Symposium, Reykajavik, Iceland.

Engen, M., Hendriks, M., Øverli, J., and Åldstedt, E. (2017). Reliability assessment of a large concrete structure making use of non-linear finite element analyses. The Second Concrete Innovation Conference, paper no. 34, 6.-8. March, 2017, Tromsø, Norway.

fib (2013). *fib Model Code for Concrete Structures 2010.* Ernst & Sohn GmbH & Co, Hoboken, New Jersey.

Hendriks, M. A. N., de Boer, A., and Belletti, B. (2017a). *Guidelines for Nonlinear Finite Element Analysis of Concrete Structures.* , Rijkswaterstaat Center for Infrastructure, Report RTD:1016-1:2017, Delft, The Netherlands.

Hendriks, M. A. N., de Boer, A., and Belletti, B. (2017b). *Validation of the Guidelines for Nonlinear Finite Element Analysis of Concrete Structures. Part: Review of results.* , Rijkswaterstaat Center for Infrastructure, Report RTD:1016-2:2017, Delft, The Netherlands.

Hinton, E. (1992). *NAFEMS Introduction to Nonlinear Finite Element Analysis.* National Agency for Finite Element Methods & Standards, Glasgow, Great Britain.

JCSS (2001). *Probabalistic Model Code. Part 1: Basis of Design.* Joint Committee on Structural Safety, Delft, The Nederlands.

Melchers, R. (1999). *Structural Reliability : Analysis and Predication.* John & Sons Ltd, Chichester, England, 2nd edition.

Norwegian Standard (2012). *NS 3576-3:2012 Steel for the reinforcement of concrete. Dimensions and properties. Part 3: Ribbed steel B500NC.* Standard Norge, Lysaker, Norway.

Norwegian Standard (2016). *NS-EN 1990:2002 Eurocode: Basis of structural design*, volume A1:2005+NA:2016. Standard Norge, Lysaker, Norway.

Pimentel, M., Brüwiler, E., and Figueiras, J. (2014). Safety examination of existing concrete structures using the global resistance safety factor concept. *Engineering Structures*, 70:130–143.

Reddy, J. (2004). *Introduction to Nonlinear Finite Element Analysis.* Oxford University Press.

Rijkswaterstaat (2012). *Guidelines for Nonlinear Finite Element Analysis of Concrete Structures.* Rijkswaterstaat Technisch Document (RTD), The Nederlands.

Schlune, H. (2011). *Safety Evaluation of Concrete Structures with Nonlinear Analysis.* PhD thesis, Chalmers University of Technology, Gothenburg, Sweden.

Seraj, S., Kotsovos, M., and Pavlovic, M. (1995). Application of the compressive-force path concept in the design of reinforced concrete indeterminate structures: A pilot study. *Structural Engineering and Mechanics*, 3(5):475–495.